**MAIMÓNIDES BIOMEDICAL RESEARCH INSTITUTE OF CÓRDOBA**

**REINA SOFÍA UNIVERSITY HOSPITAL**

**UNIVERSITY OF CÓRDOBA**

# MOLECULAR SUBTYPES OF COLORECTAL CANCER:

# MECHANISMS INVOLVED IN TUMOR PROGRESSION AND IMMUNE EVASION

**Rafael Mena Osuna**

**Córdoba, Spain**

**2021**

TITULO: *MOLECULAR SUBTYPES OF COLORECTAL CANCER: MECHANISMS INVOLVED IN TUMOR PROGRESSION AND IMMUNE EVASION*

AUTOR: *Rafael Mena Osuna*

---


Campus de Rabanales
Ctra. Nacional IV, Km. 396 A
14071 Córdoba

https://www.uco.es/ucopress/index.php/es/
ucopress@uco.es

---

# MOLECULAR SUBTYPES OF COLORECTAL CANCER: MECHANISMS INVOLVED IN TUMOR PROGRESSION AND IMMUNE EVASION

## SUBTIPOS MOLECULARES DE CÁNCER COLORRECTAL: MECANISMOS IMPLICADOS EN LA PROGRESIÓN TUMORAL Y EN LA EVASIÓN INMUNE


Report presented by

**Rafael Mena Osuna**

Graduate in Biochemistry, to apply for

**PhD in Biomedicine**


Doctoral thesis conducted under the supervision of Dr. Antonio Rodríguez Ariza, Dr. Enrique Aranda Aguilar, and Dr. Silvia Guil Luna at the Maimónides Biomedical Research Institute of Córdoba (IMIBIC)

PhD student,

MENA OSUNA RAFAEL - 45885977B

Firmado digitalmente por MENA OSUNA RAFAEL - 45885977B
Fecha: 2021.06.14 11:28:19 +02'00'

Rafael Mena Osuna

Director,

RODRIGUEZ ARIZA ANTONIO - 30482007S

Firmado digitalmente por RODRIGUEZ ARIZA ANTONIO - 30482007S
Fecha: 2021.06.14 11:59:30 +02'00'

Dr. Antonio Rodríguez Ariza

Co-director,

ARANDA AGUILAR ENRIQUE - 30424970H

Firmado digitalmente por ARANDA AGUILAR ENRIQUE - 30424970H
Fecha: 2021.06.14 11:59:07 +02'00'

Dr. Enrique Aranda Aguilar

Co-director,

GUIL LUNA SILVIA - 30980844M

Firmado digitalmente por GUIL LUNA SILVIA - 30980844M
Fecha: 2021.06.14 11:42:35 +02'00'

Dr. Silvia Guil Luna

**TÍTULO DE LA TESIS:**

**Molecular subtypes of colorectal cancer: mechanisms involved in tumor progression and immune evasion**

**DOCTORANDO/A: Rafael Mena Osuna**

## INFORME RAZONADO DEL/DE LOS DIRECTOR/ES DE LA TESIS

D. Rafael Mena Osuna presenta un trabajo original en el que se investigan los distintos mecanismos involucrados en la progresión tumoral y en la evasión inmune en los diferentes subtipos moleculares de cáncer colorrectal, especialmente en relación con el "budding" tumoral y la expresión de la enzima denitrosilasa GSNOR/ADH5. Para ello se han analizado muestras clínicas y también xenoinjertos derivados de pacientes como modelos preclínicos relevantes. Asimismo, se han utilizado técnicas avanzadas de edición génica (CRISPR-Cas9) para profundizar en los mecanismos moleculares. Los resultados obtenidos indican un estrecho vínculo entre el "budding" tumoral y un microambiente inmunosupresor que promueve la invasión tumoral. Además, este estudio también demuestra que los modelos PDXs pueden constituir una sólida plataforma preclínica para el desarrollo de terapias dirigidas contra el "budding" tumoral. Por otro lado, se demuestra también la reprogramación metabólica inducida por una alterada desnitrosilación como un nuevo mecanismo de adquisición de fenotipos agresivos e inmunoevasores en cáncer colorrectal. Parte de los resultados obtenidos en esta tesis han sido ya publicados en una revista de reconocido prestigio internacional (**Frontiers in Medicine**) y el resto se encuentran en fase de redacción para su publicación. La tesis doctoral presentada se enmarca dentro de las líneas de investigación de nuestro grupo de investigación.

Finalmente, cabe destacar la excelente formación técnica y científica alcanzada por el doctorando, con la realización de una estancia en un centro internacional de reconocido prestigio (*Institute of Cancer Research*, Londres), por lo que se presenta la tesis con Mención Internacional.

Por todo ello, se autoriza la presentación de la tesis doctoral.

Córdoba, a 14 de junio de 2021

Firma de los directores

RODRIGUEZ ARIZA ANTONIO - 30482007S
Firmado digitalmente por RODRIGUEZ ARIZA ANTONIO - 30482007S
Fecha: 2021.06.14 13:05:38 +02'00'

Fdo: Antonio Rodríguez Ariza

ARANDA AGUILAR ENRIQUE - 30424970H
Firmado digitalmente por ARANDA AGUILAR ENRIQUE - 30424970H
Fecha: 2021.06.14 13:05:08 +02'00'

Fdo: Enrique Aranda Aguilar

GUIL LUNA SILVIA - 30980844M
Firmado digitalmente por GUIL LUNA SILVIA - 30980844M
Fecha: 2021.06.14 11:42:02 +02'00'

Fdo: Silvia Guil Luna

*“Toda ciencia empieza como filosofía y acaba como un arte”*

*Will Durant*

***A mi familia***

# *Agradecimientos*

***Esta tesis doctoral no habría sido posible sin la ayuda, el apoyo, el tiempo y los consejos de todos los que habéis compartido conmigo este largo camino que comenzaba en 2016, así que por todo ello y mucho más: ¡¡Muchas Gracias!!***

A pesar de la gran satisfacción y emoción que siento por acabar la tesis y por ver que me deparará el futuro, se me hace raro que termine esta etapa la cual he disfrutado y he sufrido a partes iguales y de la que guardo un cariño especial por todos los momentos vividos.

En general, y pido disculpas si me olvido de alguien, estos agradecimientos van dirigidos a todos los que de una forma u otra han estado ahí mostrándome su apoyo incondicional, su ayuda y su cariño.

En primer lugar, quisiera mostrar mi gratitud a mis directores de tesis, **Antonio Rodríguez** y **Enrique Aranda**, por su ayuda y por la confianza depositada en mí. A Enrique agradecerle su cercanía, amabilidad y por haberme introducido en el apasionante mundo de la investigación en oncología. A Antonio, del que he tenido la suerte de aprender mucho durante estos años, le agradezco profundamente que me brindara la gran oportunidad de formar parte del grupo y de realizar esta tesis doctoral. Sin sus consejos y su tiempo esta tesis no hubiese sido posible. Gracias.

A continuación, me gustaría dar las gracias al gran equipo humano que forma parte del IMIBIC, que ha sido mi segunda casa, en la que hemos pasado muchas horas, y donde he podido crecer tanto personal como profesionalmente. En concreto me gustaría agradecer a la tercera planta del IMIBIC, mi segunda familia aquí, deciros que sois unas personas increíbles.

A mi grupo de laboratorio me gustaría dedicarle unas palabras de agradecimiento por todo el tiempo que habéis invertido en mí, por vuestro esfuerzo y por escucharme y apoyarme en todo momento. A **Silvia Guil**, que aparte de una co-directora de tesis excelente, ha sido mi compañera de fatigas y de cafés durante todo este tiempo, decirle que sin su ayuda y sus consejos esta tesis tampoco hubiese sido posible, y que no solo ha demostrado ser una investigadora increíble si no que también ha sido una buena amiga y consejera. A **Marta Toledano**, mi compi de tesis, darle las gracias por su amabilidad y generosidad, porque pese a no haber compartido poyata juntos, ha sido un gran apoyo durante todo este camino de tesis, en el que hemos "entrado y salido de la nube", hemos compartido incertidumbres, agobios, éxitos y finalmente estamos viendo la luz al final de camino, camino que no ha hecho nada más que empezar y que espero nos traiga muchos

éxitos y felicidad. A mis pollitos, **Ana** y **Carmely**, que fueron unas excelentes aprendices, darles las gracias por todo lo que han hecho por mí, por su tiempo y ayuda, por nuestras horas de cultivos con la música a toda leche, por nuestros canturreos y por otros miles de momentos dentro y fuera del laboratorio que se quedaran para siempre. Ahora empieza vuestro camino y os deseo toda la suerte del mundo y estoy seguro de que lo vais a hacer genial. A **Mariví**, la nueva incorporación del grupo, agradecerle todo lo que me ha enseñado durante estos años, y todo su tiempo y su apoyo en ésta última etapa. A **Ángeles** y **Dani**, mostrarle mi gratitud por estar siempre disponibles para cualquier cosa que he necesitado en el laboratorio, por su ayuda y compresión y por las palabras de ánimo en todo momento. También me gustaría agradecer a personas que, aunque ya no están en el grupo, han formado parte de él en algún momento, y de los cuales he aprendido mucho durante este tiempo. En concreto a **Jon, Laura, Vane** y **Paco**, por vuestro tiempo en enseñarme tanto de laboratorio, por guiarme en el camino de la investigación, por vuestros consejos y experiencia. Gracias.

También quisiera dar las gracias a mi **Ana Blanca**, que tiene un gran corazón y vale mucho, por dar todo lo que tiene y ayudar en todo momento al que lo necesita, gracias por tus consejos, por esas risas en el despachito y por cederme un huequito para encontrar la inspiración en la última etapa de la Tesis.

A nuestros vecinos "los Epigenéticos", que aunque la gran mayoría ya no están aquí en el IMIBIC, han sido parte de nuestro grupo con el que hemos compartido desayunos, cumpleaños, ferias, comidas del IMIBIC y muchos momentos especiales que guardo con gran cariño. A **Teresa**, darle la gracias porque más que compañera ha sido como una madre, que me ha aconsejado y me ha ayudado mucho cuando no tenía ni idea de lo que significada la palabra CRISPR. Por todas esas tardes dedicadas al diseño de primers y PCRs y por ser tan buena conmigo y preocuparte tanto por mí, ¡muchas gracias! A **Jara, Ivan y Macarena**, dar las gracias por hacerme sentir como en casa, por ser tan buenas personas y por vuestra ayuda con toda la parte técnica del CRISPR. Y por último a **Maribel**, la nueva incorporación del los epigenéticos, que pese a que he compartido poco tiempo con ella, siempre tiene palabras de ánimo, es buena consejera y es un buen ejemplo de tesón, esfuerzo y perseverancia. Tenemos pendiente una buena cata de vinos de Jerez.

No quisiera olvidarme de agradecer a todos los que forman parte de la unidad de apoyo a la investigación "*los UCAIB*" por la ayuda prestada durante estos años. A **Edu Chicano** por estar disponible siempre que lo he necesitado en proteómica. A **Esther Peralbo** por su inestimable ayuda en citometría sin la cual no hubiese podido generar las líneas celulares *knockout* que han sido la base de todos mis ensayos *in vitro*. A **Gema García** por enseñarme tanto de microscopía y ayudarme con el análisis y la microscopía

confocal, gracias por esas fotos de la portada. Y para finalizar a **Pilar Rubín** y a **Alvaro Jiménez** de la unidad de genómica por estar siempre dispuestos para ayudarme en todo lo que he necesitado tanto dentro como fuera del laboratorio, por su alegría y por ese buen rollo que siempre transmiten en la tercera planta del IMIBIC.

Y como todo no es el IMIBIC, también quería agradecer a mi familia y amigos todo el apoyo emocional que me han dado, porque ellos también han estado ahí en los momentos buenos y en los malos, y porque han disfrutado y sufrido conmigo durante todo este camino de tesis. A mis bochornos (Paula, Jose, Nacho, Amparo, Paloma, Dela, Pablo y Adri) que los quiero muchísimo y siempre habéis estado ahí cuando he necesitado un hombro en el que desahogarme, un consejo o simplemente despejarme, relajarme y disfrutar de una buena charla o cerveza. ¡Gracias por estar ahí siempre!

Dar las gracias también a mis amigos del cole y del instituto (Lidia, Naza, Jesús, Mari, Marina y Gabi) por ser como sois y estar ahí siempre después de tantos años. A mis Biolocos (Hermi, María, Carlos, Pablo, Viole y Fran) por tantas risas y buenos momentos durante la carrera y después de ella. A mis festivaleros preferidos (Inma, María, Rafa, Cristina, Cristian y Almudena) por ser un gran apoyo y estar ahí siempre que los he necesitado, qué ganas de un nuevo viaje con vosotros. A mis karaokeños con los que he compartido ensayos, cervezas, risas, nervios, actuaciones y muchos momentos increíbles.

Y por último, darle las gracias a toda mi familia, porque han sido un pilar muy importante para mí durante esta etapa y me han levantado siempre tras cada tropiezo. En especial agradecer a mis tíos Manolo y Mari Carmen por ser tan generosos y cariñosos. A mis cuñados que son como unos hermanos para mí. A mis hermanos Andrés y Lola que los quiero con locura pese a que nunca lo demuestre y que siempre están ahí alegrándose de cada éxito y animándome en cada fracaso. A mis sobrinos que son un rayito de luz y alegría y que los quiero muchísimo. Y a mis padres Rafael y Lola que sin ellos no habría podido llegar hasta aquí, por ser unos padres excelentes que me han inculcado buenos valores, que me han ayudado y apoyado en todo momento y han confiado en que era capaz de conseguirlo. ¡¡Os quiero mucho!!

A mi abuela, mi amigo Luis y a Tango, mi rubio peludo, dedicarle esta tesis, porque allá donde estén me cuidan y protegen, y seguro que están contentos y orgullosos de este logro. ¡¡Os quiero!!

Muchas Gracias a TODOS

Rafa

# INDEX

# *I. ABBREVIATIONS*

| | |
|---|---|
| **2DG** | 2-Deoxy-D-glucose |
| **5-FU** | 5-Fluorouracil |
| **ADH5** | Alcohol dehydrogenase 5 (Class III) |
| **AIC** | Akaike information criterion |
| **APC** | Adenomatous polyposis coli |
| **bFGF** | Basic fibroblast growth factor |
| **BSA** | Bovine serum albumin |
| **CDX2** | Caudal type homeobox 2 |
| **cGMP** | Cyclic guanosine monophosphate |
| **CIMP** | CpG island methylator phenotype |
| **CIN** | Chromosomal instability |
| **CMS** | Consensus molecular subtypes |
| **CRC** | Colorectal cancer |
| **CRCSC** | International CRC subtyping consortium |
| **CRISPR-Cas9** | Clustered regularly interspaced short palindromic repeats |
| **CSC** | Cancer stem cell |
| **CSNO** | S-nitrosocysteine |
| **CTLA4** | Cytotoxic T-lymphocyte Antigen 4 |
| **DAB** | 3,3-diaminobenzidine |
| **DFS** | Disease-free survival |
| **Drp1** | Dynamin-related protein 1 |

| | |
|---|---|
| **EGF** | Epidermal growth factor |
| **EGFR** | Epidermal growth factor receptor |
| **EMT** | Epithelial-to-mesenchymal transition |
| **eNOS** | Endothelial nitric oxide synthase (*NOS3*) |
| **FAP** | Familial adenomatous polyposis |
| **FBS** | Fetal bovine serum |
| **FDA** | Food and drug administration |
| **FFPE** | Formalin fixed paraffin embedded |
| **GCs** | Guanylate Cyclase |
| **GFR** | Growth Factor Reduced |
| **GSNO** | S-nitrosoglutathione |
| **GSNOR** | S-nitrosoglutathione reductase |
| **HER2** | Epidermal growth factor receptor 2 |
| **H&E** | Hematoxylin and eosin |
| **HR** | Hazard ratio |
| **HRP** | Horseradish peroxidase |
| **ICIs** | Immune checkpoint inhibitors |
| **IHC** | Immunohistochemistry |
| **iNOS** | Inducible nitric oxide synthase (*NOS2*) |
| **ITBCC** | International tumor budding consensus conference |
| **LDA** | Limiting dilution assay |

| | |
|---|---|
| **mCRC** | Metastatic CRC |
| **MDSCs** | Myeloid-derived suppressor cells |
| **MMR** | Mismatch repair |
| **MSI** | Microsatellite instability |
| **MSI-H** | High microsatellite instability |
| **MSI-L** | Low microsatellite instability |
| **MSS** | Microsatellite stability |
| | |
| **NO** | Nitric oxide |
| **NOD-SCID mice** | Nonobese diabetic-severe combined immunodeficiency mice |
| **NOS** | Nitric oxide synthase |
| **nNOS** | Neural nitric oxide synthase (*NOS1*) |
| | |
| **OPA1** | Optic atrophy 1 |
| **OS** | Overall survival |
| | |
| **PD1** | Programmed cell death protein 1 |
| **PDL1** | Programmed cell death protein 1 ligand 1 |
| **PDX** | Patient derived xenograft |
| **PFS** | Progression-free survival |
| | |
| **RIN** | RNA integrity number |
| **RLU** | Relative light unit |
| **RPL13** | Ribosomal protein L13 |
| **RT** | Room temperature |

| | |
|---|---|
| **SCNA** | Somatic copy number alterations |
| **SD** | Standard deviation |
| **sgRNA** | Sequence guides RNA |
| **SNO** | S-nitrosothiol |
| **SNO-LMW** | Low molecular weight thiols |
| **SNO-proteins** | S-nitrosoproteins |
| **TAM** | Tumor-associated macrophages |
| **TAN** | Tumor-associated neutrophils |
| **TGF-β** | Transforming growth factor-beta |
| **TLRs** | Toll-like receptors |
| **TNM** | Tumor, Node, Metastasis |
| **Treg** | Regulatory T cells |
| **Trx/TrxR** | Thioredoxin/thioredoxin reductase system |
| **TTBS** | Tween tris-buffered saline |
| **VEGF** | Vascular endothelial growth factor |
| **VEGFR** | Vascular endothelial growth factor receptor |
| **WT** | Wild type |

## *II. ABSTRACT*

Molecular classification of colorectal cancer (CRC) has led to the identification of four Consensus Molecular Subtypes (CMS), with different immune microenvironments linked to distinct prognosis and therapeutic responses. Recently, tumor budding has been found to be of prognostic significance for several cancers, including CRC. Still, the association between tumor budding and the different CMS subtypes of CRC and distinct immune profiles has not been fully elucidated. On the other hand, S-nitrosoglutathione reductase (GSNOR) is a highly evolutionarily conserved denitrosylase enzyme, which is coded by *ADH5* gene in humans and its impaired expression has been associated with different pathologies, including cancer. However, it is unknown the potential role of GSNOR/*ADH5* in the pathogenesis of CRC and its relationship with the distinct CMS subtypes and tumor immune microenvironment. Therefore, the main objective of this thesis was to investigate the mechanisms involved in tumor progression and immune evasion in the different CMS subtypes, and particularly in relation with tumor budding and GSNOR/*ADH5* expression.

We first studied clinical CRC samples with different grades of tumor budding and their corresponding patient derived xenografts (PDXs) models, by analyzing gene expression signatures of immune checkpoints, toll-like receptors (TLRs), and chemokine families. We found that CMS subtypes and tumor budding grade were reliably reproduced in early passages of PDXs, and that high-grade tumor budding was intimately related with the poor-prognosis CMS4 mesenchymal subtype. In addition, an upregulation of negative regulatory immune checkpoints (*PDL1*, *TIM-3*, *NOX2*, and *IDO1*), TLRs (*TLR1*, *TLR3*, *TLR4*, and *TLR6*), and chemokine receptors and ligands (*CXCR2*, *CXCR4*, *CXCL1*, *CXCL2*, *CXCL6*, and *CXCL9*) was detected in high-grade tumor budding in both human samples and their corresponding xenografts. We also found a remarkable overexpression of

the endothelial nitric synthase isoform (eNOS) in both the poor prognosis CMS4 subtype as well as in tumor with high-grade tumor budding, suggesting that the immunosuppressive capacity of nitric oxide (NO) may also facilitate tumor bud formation. Therefore, our data support a close link between high-grade tumor budding in CRC and a distinctive immunosuppressive microenvironment promoting tumor invasion, which may have a determinant role in the poor prognosis of the CMS4 mesenchymal subtype. In addition, our study also demonstrates that PDX models may constitute a robust preclinical platform for the development of novel therapies directed against tumor budding in CRC.

We next investigated the significance of GSNOR/*ADH5* in CRC, and the immunohistochemical and gene expression analyses showed that low levels of this denitrosylase enzyme were associated with the CMS4 aggressive CRC type, worse prognosis and poor survival in CRC patients. Besides, analysis of immune cell gene expression revealed an immunosuppressive microenvironment in GSNOR/*ADH5*-low tumors, with a marked reduction in T cell gene expression signature, downregulation of genes related to cytotoxicity (*GNLY*, *GZMA*, *CXCR6*, *CD3D* and *TARP*), and up-regulation of genes known to inhibit anti-tumor immunity (*ITGA2*, *LGALS3* and *CD46*). CRISPR-Cas9–mediated *ADH5* gene knockout (KO) in CRC cells confirmed that GSNOR/*ADH5* deficiency confers higher tumorigenic capacity. Thus, in comparison with parental cells, *ADH5*-KO cells possessed greater ability to generate tumorospheres and tumor spheroids, and initiated tumors with higher efficiency in immunodeficient mice. Moreover, *ADH5*-KO cells had a lower expression of the intestinal differentiation marker CDX2 and a higher expression of the immune checkpoint protein PDL1, indicating enhanced immunoevasive capacity. Importantly, the higher tumorigenic potential of *ADH5*-KO cells was associated to a metabolic switch from oxidative phosphorylation to aerobic glycolysis, as indicated by decreased

ATP content, higher 2-deoxyglucose sensitivity and increased lactate production. It is known that fragmentation of the mitochondrial network, which is accompanied by increased aerobic glycolysis and lactate production, occurs during cell dedifferentiation, malignant transformation, and cancer immune evasion. Significantly, mitochondrial network analysis confirmed that, compared to parental cells, *ADH5*-KO cells had a higher number of mitochondria per cell and a smaller mitochondrial diameter, which is consistent with a higher rate of mitochondrial fission and glycolytic reprogramming. Therefore, our results support that metabolic rewiring induced by impaired denitrosylation constitutes an important novel mechanism contributing to the acquisition of aggressive and immune evasive phenotypes in CRC. This new role of NO in the metabolic reprogramming of tumors may help explain some of the puzzling aspects of signaling mediated by NO in cancer, which may suggest new therapeutic approaches in this disease.

**Key words:** Colorectal cancer, Consensus molecular subtype, tumor budding, GSNOR/*ADH5*, immune microenvironment

La clasificación molecular del cáncer colorrectal (CCR) ha conducido a la identificación de cuatro Subtipos Moleculares de Consenso (CMS), con diferentes microambientes inmunes vinculados a distintos pronósticos y respuestas terapéuticas. Recientemente, se ha descubierto que el *budding* tumoral tiene relevancia pronóstica en varios cánceres, incluido el CCR. Aun así, no se ha dilucidado por completo la asociación entre el *budding* tumoral y los diferentes subtipos CMS de CCR y los distintos perfiles inmunes. Por otro lado, la S-nitrosoglutatión reductasa (GSNOR) es una enzima denitrosilasa altamente conservada evolutivamente, que está codificada por el gen *ADH5* en humanos y cuya expresión alterada se ha asociado con diferentes patologías, incluyendo el cáncer. Sin embargo, no se conoce la relevancia de la GSNOR/*ADH5* en la patogénesis del CCR y su relación con los distintos subtipos CMS y el microambiente tumoral inmune. Por tanto, el principal objetivo de esta tesis fue investigar los mecanismos involucrados en la progresión tumoral y en la evasión inmune en los diferentes subtipos CMS de CCR, especialmente en relación con el *budding* tumoral y la expresión de GSNOR/*ADH5*.

En primer lugar, se estudiaron muestras clínicas de CCR con diferentes grados de *budding* y sus correspondientes modelos de xenoinjertos derivados de pacientes (PDXs), mediante el análisis de firmas de expresión génica de puntos de control inmune, receptores *toll-like* (TLRs), y familias de citoquinas. Significativamente, los distintos subtipos CMS y el grado de *budding* tumoral fueron fielmente reproducidos en los primeros pases de PDXs. Además, el alto grado de *budding* tumoral estuvo estrechamente asociado con el subtipo mesenquimal CMS4 de mal pronóstico. En los tumores con alto grado de *budding* se observó una sobreexpresión de reguladores negativos de puntos de control inmune (*PDL1*, *TIM-3*, *NOX2*, and *IDO1*), TLRs (*TLR1*, *TLR3*, *TLR4*, and *TLR6*), receptores de quimioquinas y sus ligandos (*CXCR2*, *CXCR4*, *CXCL1*, *CXCL2*,

*CXCL6*, and *CXCL9*), tanto en las muestras clínicas como en sus correspondientes modelos PDXs. También se encontró una notable sobreexpresión de la isoforma endotelial de la sintasa de óxido nítrico (eNOS), tanto en los tumores CMS4 de mal pronóstico como en aquellos con un alto grado de *budding* tumoral, lo que sugiere que la capacidad inmunosupresora del óxido nítrico (NO) también puede facilitar la formación de *buds* tumorales. Estos resultados indican un estrecho vínculo entre el alto grado de *budding* tumoral en CCR y un microambiente inmunosupresor distintivo que promueve la invasión tumoral, y que puede tener un papel determinante en el subtipo mesenquimal CMS4 de mal pronóstico. Además, este estudio también demuestra que los modelos PDXs pueden constituir una sólida plataforma preclínica para el desarrollo de nuevas terapias dirigidas contra el *budding* tumoral en CCR.

A continuación, se investigó la importancia de la denitrosilasa GSNOR/*ADH5* en CCR, y los análisis inmunohistoquímicos y de expresión génica mostraron que los niveles bajos de esta enzima se asociaron con el tipo agresivo CMS4 de CCR, con características clínicas de peor pronóstico y con una baja supervivencia en pacientes de CCR. Además, el análisis de expresión génica del perfil inmune reveló un microambiente inmunosupresor en tumores con niveles bajos de GSNOR/*ADH5*, con una marcada reducción en la firma de expresión génica de células T, una menor expresión de genes relacionados con citotoxicidad (*GNLY, GZMA, CXCR6, CD3D y TARP*), y una mayor expresión de genes que inhiben la inmunidad antitumoral (*ITGA2, LGALS3 y CD46*). La eliminación del gen *ADH5* (KO) mediante tecnología CRISPR-Cas9 en células de CCR confirmó que la deficiencia de GSNOR/*ADH5* confiere una mayor capacidad tumorigénica. Así, en comparación con las células parentales, las células *ADH5*-KO demostraron una mayor capacidad para generar tumorosferas y esferoides tumorales, e iniciaron tumores con mayor eficacia en ratones inmunodeficientes. Además, las células

*ADH5*-KO mostraron una menor expresión del marcador de diferenciación intestinal CDX2 y una mayor expresión de la proteína del punto de control inmune PDL1, indicando una mayor capacidad inmunoevasiva. Es importante destacar que la mayor tumorigenicidad de las células *ADH5*-KO se asoció con una reprogramación metabólica desde la fosforilación oxidativa hacia un aumento de la glucólisis aerobia, con un menor contenido basal de ATP, una mayor sensibilidad a la 2-desoxiglucosa y una mayor producción de lactato. Se sabe que la fragmentación de la red mitocondrial, que conduce a un aumento de la glucólisis aeróbica y de la producción de lactato, se produce durante la desdiferenciación celular, la transformación maligna y la evasión inmune en cáncer. De manera significativa, el análisis de la red mitocondrial confirmó que, en comparación con las células parentales, las células *ADH5*-KO mostraron un mayor número de mitocondrias por célula y un diámetro mitocondrial más pequeño, lo que es consistente con una mayor tasa de fisión mitocondrial y reprogramación glucolítica. Por lo tanto, estos resultados apoyan que la reprogramación metabólica inducida por una alterada desnitrosilación constituye un importante nuevo mecanismo que contribuye a la adquisición de fenotipos agresivos e inmunoevasores en CCR. Este nuevo papel del NO en la reprogramación metabólica en cáncer puede ayudar a explicar algunos de los aspectos desconcertantes de la señalización mediada por el NO en cáncer, y puede sugerir nuevas aproximaciones terapéuticas en esta enfermedad.

**Palabras clave:** Cáncer colorrectal, subtipos moleculares de consenso, budding tumoral, GSNOR/*ADH5*, microambiente inmune

# *III. INTRODUCTION*

## 1. Etiology and epidemiology of colorectal cancer (CRC)

Colorectal cancer (CRC) remains a leading cause of death in worldwide despite the advance in the recent years in the development of new therapeutic targets and deeper understanding of molecular mechanisms[1]. According to World Health Organization GLOBOCAN 2020 database, CRC is the second most common diagnosed cancer and the second leading cause of cancer death worldwide, comprising 10% of all cancer diagnoses, with 1.93 million new cases and 935,180 deaths in 2020. Rates are substantially higher in males than in females[2]. In Spain, the CRC incidence has been estimated in 44,200 new cases in 2020, with a 19% increment in the number of new cases in comparison with 2018[3]. Besides age and gender, other factors associated with higher CRC risk include alcohol intake, high consumption of red and processed meat, obesity, smoking and inflammatory bowel disease[4,5]. Moreover, the number of affected relatives and the age at diagnosis are strong risk factors for familial CRC (20% of CRC patients)[6]. As in other malignancies, metastatic disease is the main cause of deaths in CRC, where approximately 25% of the patients have metastases at initial diagnosis and almost 50% of them will develop them, contributing to the high mortality rates reported for this malignancy, with a 5-year survival rate approaching the 60%[7]. Therefore, this increasingly evolution makes crucial a deeper knowledge of the underlying mechanisms of CRC progression as well as the identification of new therapeutic targets.

## 2. Molecular pathogenesis of CRC

CRC is traditionally divided into familial (hereditary) CRC, which represents around 20% of cases, and sporadic cases which are the majority of the CRC patients. The most common inherited CRC syndromes are Lynch syndrome,

familial adenomatous polyposis (FAP), and certain hamartomatous polyposis conditions[8]. Lynch syndrome occurs in approximately 2.5% of CRC cases and is characterized by germline mutations in mismatch repair (MMR) genes (*MLH1*, *MSH2*, *MSH6* and *PMS2* genes). MMR-deficient tumors are characterized by a high rate of mutations that accumulate in repetitive DNA sequences known as microsatellites, which is commonly referred to as microsatellite instability (MSI). However, MSI is not specific for Lynch syndrome, and approximately 15% of sporadic CRC cancers also demonstrate MSI status. The second most common CRC inherited condition is FAP, which is caused by a defect in the adenomatous polyposis coli gene (*APC* gene). FAP is characterized by the development of many tens to thousands of adenomas and a 100% risk to develop CRC, being responsible of around 1% of all CRC cases. Finally, the hamartomatous polyposis syndromes are a group of disorders which have in common the development of polyps in the gastrointestinal tract causing an increased risk for CRC[9,10].

Three different pathways of genomic instability have been implicated in the development of CRC tumors: chromosomal instability (**CIN**), **MSI** and CpG island methylator phenotype (**CIMP**) pathway[11]. These genomic instability pathways are involved in the two sequences of progression from normal colon to CRC that have been identified[12] (**Figure 1**). The classical **CIN pathway** begins with de mutations in *APC* tumor suppressor gene, which is the primary event that acts as precursor lesion. This is followed by activating mutations in *RAS/RAF* genes and loss of *p53* function during the subsequent malignant transformation, along with changes in tumor characteristics in the classical adenoma-carcinoma pathway described by Fearon and Vogelstein in 1990[13]. CIN tumors constitute the 84% of sporadic tumors and also include hereditary cases (FAP) associated with mutations in *APC* gene[14]. The **MSI pathway** is responsible for a hypermutable phenotype caused by the loss of DNA MMR activity and it is detected in about

15% of all CRCs[15], while the other 12% are caused by sporadic, acquired hypermethylation of the promoter of the *MLH1* gene, which occurs in tumors with the CpG island methylator phenotype[15]. The **CIMP pathway** is distinguished by hypermethylated promoters of tumor suppressor genes (e.g. *MGMT* and *MLH1*), being this hypermethylation process associated with *BRAF* mutations and MSI. CIMP-positive tumors typically show serrated adenomas as precursor lesions[16] and most of them are characterized by MSI and lack of CIN[17] (**Figure 1**).

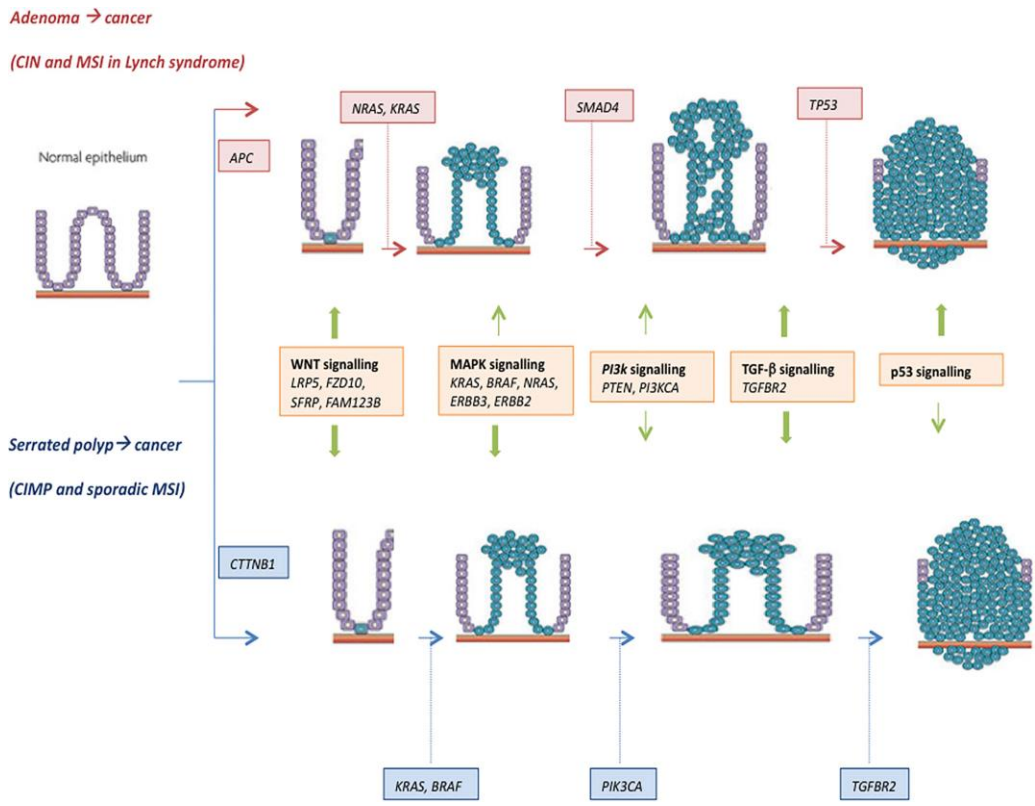


**Figure 1. Multistep progression sequences of CRC.** Two CRC progression sequences have been identified. The classical pathway (top) involves the development of tubular adenomas which progress to adenocarcinomas after loss of *APC* gene function. For each pathway, the genes mutated or epigenetically altered are indicated. During tumorigenesis, genes sequentially acquire epigenetic alterations or mutations, some are shared among pathways and others are unique, such as *BRAF* mutations and CIMP phenotype that only arises in the serrated pathway (bottom). Figure from Dickinson et al, 2015[12].

Apart from the different genomic instability pathways, multiple dysregulated pathways are implicated in the tumor progression of this malignancy. The most common dysregulated signaling pathways in CRC includes the EGFR/RAS/RAF/MAPK, PI3K/AKT/mTOR, WNT-APC-β-CATENIN, TGF-β/SMAD, and p53 pathways[18].

The WNT-APC-β-CATENIN signaling pathway is an evolutionarily conserved cell-cell communication system that plays a critical role in controlling processes such as stem cell renewal, cell proliferation, cell differentiation, cell cycle arrest and apoptosis, both during embryogenesis and during adult tissue homeostasis, and its dysregulation contributes to a wide variety of human diseases[19,20]. Over 90% of CRC tumors have mutations that activate the WNT pathway and up to 70% of sporadic CRC tumors harbor *APC* inactivating mutations[21]. Remarkably, *APC* gene mutation is a key and early event in this malignancy and its frequency is constant during tumor progression[22]. The *APC* mutations occurring in germline linage lead to the inherited disorder FAP, which normally results in the progression to CRC[23].

Epidermal Growth Factor Receptor (EGFR, also known as ErbB1 or HER1) is a cell-surface receptor which binds to various ligands and cytokines leading to cell division via RAS/RAF/MAPK tyrosine kinase cascade[24]. The *EGFR* gene appears abnormally expressed or upregulated in about 50–80% of CRC patients[24,25] and is also responsible for the transduction of signals via PI3K/AKT/mTOR pathway which triggers crucial steps for cell growth and survival[24]. Monoclonal antibodies (mAbs) which block EGFR preventing ligand-binding have been developed as drugs for the treatment of metastatic CRC[26]. A key component of the EGFR pathway is RAS protein, and roughly 45% of CRC tumors express a mutated form of *RAS* which results in the constitutive activation

of the pathway[27]. Consequently, those metastatic CRC patients with tumors harboring activating *RAS* mutations do not benefit from anti-EGFR mAb therapy[28].

Transforming growth factor-beta (TGF-β) signaling pathway plays critical roles in controlling tissue development, proliferation, differentiation, apoptosis, and homeostasis[29], and its disruption leads to several diseases including cancer. In epithelial cells TGF-β signaling regulates many target genes (either positively or negatively) in a context-dependent manner[30], promoting tumor cell progression in tissues with advanced cancer[31]. In addition to its effect on epithelial cells, TGF-β plays an important role suppressing intestinal immune cells in the stroma and inducing immune tolerance[32,33]. Therefore, disruption of TGF-β signaling in the colon prompts tumor progression not only via epithelial transformation but also via tumor-stromal interactions. TGF-β signaling causes epithelial-to-mesenchymal transition (EMT) in cancer cells, resulting in an aggressive phenotype, especially in advanced CRC, and, consequently, poor prognosis[34].

Finally, the p53 pathway is comprised of a gene network and their products that are targeted to respond to a wide variety of stress signals which impact upon cellular homeostatic mechanisms[35] and plays a key role in cell cycle where induces cell arrest, senescence or apoptosis[36]. The frequency of *p53* mutations is approximately 45-50% in sporadic CRC, occurring most of them in exons 5 to 8[37], highly conserved areas in the structural domains of the protein, and participate in the adenoma-carcinoma transition[13].

## 3. Tumor Heterogeneity in CRC

The tumor heterogeneity concept has been long recognized as an essential clinical determinant for the outcome of patients[38] and, as in other malignancies, it

has a great impact in the patient stratification in CRC[39]. Tumor heterogeneity, which can be classified as intertumoral and intratumoral, poses a considerable challenge to matching patients with the right treatment at the right time. Intertumoral heterogeneity refers to differences between synchronic primary tumors or between a primary tumor and its matched metastases developing in the same patient, as well as those differences found in primary tumors between patients. On the other hand, intratumoral heterogeneity refers to differences in the cell subpopulations within the same neoplasm[39]. It has been shown that morphologically diverse areas of a tumor might share the same genetic landscape, and this can be explained by nongenetic influences such as epigenetic regulation, post-translational modifications or by differences in the tumor microenvironment[39]. This intratumoral heterogeneity is considered a key factor that highly contributes to the lethal outcome of cancer, therapeutic failure, and drug resistance[40].

### 3.1 Molecular classification of CRC and consensus molecular subtypes

Due to the high heterogeneity of CRC, the establishment of an accurate classification is a key challenge which will impact in the diagnosis, treatment, and cancer progression prediction of the patients. In the past, tumor classification was established according to clinicopathological features such as anatomical location or tumoral histology since it was thought that distinct tumors with identical origin share the same pathological process[41]. This was the basis for the following CRC classification systems, as the **TNM (Tumor, Node, Metastasis) staging system** which classifies CRC by the size and extent of the primary tumor (T), involvement of regional lymph nodes (N), and the presence or absence of distant metastases (M), dividing patients into four groups (stages I to IV) with valuable prognostic and therapy response information[42,43], and supplemented in recent years by

evidence-based prognostic and predictive factors[44] **(Figure 2)**. However, CRC tumors with common mutations or similar histology differ significantly in the clinical outcomes and the treatment response with chemotherapy and/or biological therapy[45].

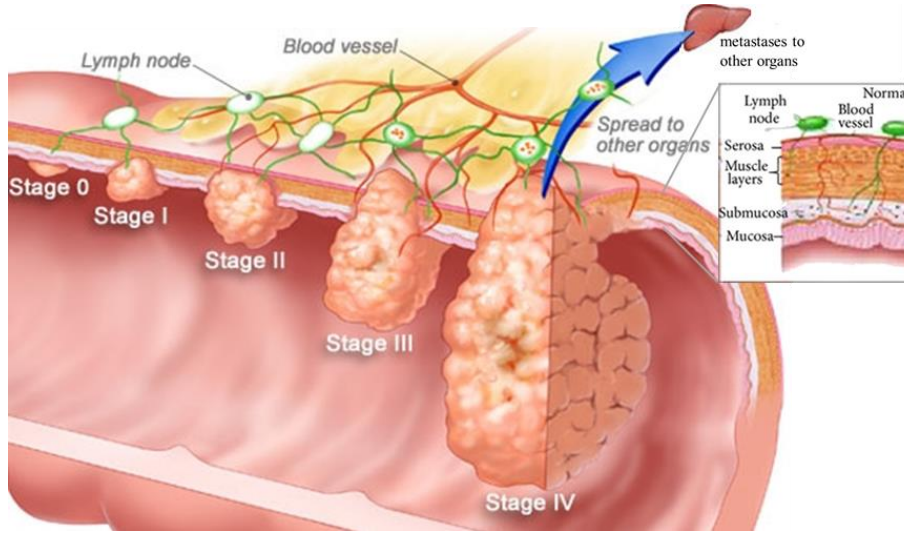


**Figure 2. The TNM staging system.** TNM classification has great importance in the diagnosis and the treatment of CRC depending on the patient stage at diagnosis. **Stage 0**: polyp or carcinoma *in situ* invading mucosa without contacting bowel wall; **Stage I**: tumor invades submucosa layer without affecting lymph nodes; **Stage II**: tumor invades the muscle layers without contacting pericolorectal tissues and lymph nodes; **Stage III**: tumor invading bowel wall into pericolorectal tissues and lymph nodes; **Stage IV**: tumor invades other tissues and spread to other organs. Figure modified from National Cancer Institute (https://www.nih.gov/research-training/advances-colorectal-cancer-research).

In an effort to generate a unified classification system, the International CRC Subtyping Consortium (CRCSC) was formed in 2014 to classify a large number of CRC samples into one of four main **Consensus Molecular Subtypes (CMSs)**. This study described by Guinney and colleagues[46] identified four subtypes each one with differentiating characteristics: CMS1 (MSI-immune), CMS2

(canonical), CMS3 (metabolic) and CMS4 (mesenchymal) subtypes **(Figure 3)**. The **CMS1** subtype (14% of CRC cases) is characterized by a hypermutation and MSI status due to a deficiency in the *MMR* genes (*MLH1*, *MSH2*, *PMS2*, and *MSH6* genes), hypermethylation (CIMP) and intense immune activation of cytotoxic and helper T lymphocytes, macrophages, and neutrophils[47]. The **CMS2** subtype (37%) displays high CIN by showing a high number of alterations in somatic copy number (SCNA) as well as hyperactivated WNT and MYC pathways, and increased oncogene expression such as *HER2, IGF-2* and *IRS2*[46,47]. The **CMS3** subtype (13%) shows a low immune activation level and metabolic reprogramming capacity, leading to a hyperactivation in glutaminolysis and lipogenesis. On the molecular level, these tumors frequently display mutations in *KRAS,* have an increase in metabolic pathways and are generally CIMP low. And finally, the **CMS4** subtype represents 23% of cases in early stages and is characterized by the activation of EMT pathway, as well as by the overexpression of proteins involved in extracellular matrix remodeling and angiogenesis[47]. This subtype also displays strong stromal cells infiltration, especially fibroblasts, and the worst relapse-free and overall survival (OS), matching with the previously described stem-like subtype[46].

| CMS1 MSI Immune | CMS2 Canonical | CMS3 Metabolic | CMS4 Mesenchymal |
|---|---|---|---|
| 14% | 37% | 13% | 23% |
| MSI, CIMP high, hypermutation | SCNA high | Mixed MSI status, SCNA low, CIMP low | SCNA high |
| *BRAF* mutations | | *KRAS* mutations | |
| Immune infiltration and activation | WNT and MYC activation | Metabolic deregulation | Stromal infiltration, TGFβ activation, angiogenesis |
| Worse survival after relapse | | | Worse relapse-free and overall survival |

**Figure 3. The Consensus Molecular Subtypes (CMS) classification of CRC.** The frequency and main molecular characteristics of the four CMS subtypes identified by Guinney and colleagues are shown. CIMP, CpG Island Methylator Phenotype; MSI, microsatellite instability; SCNA, somatic copy number alterations; TGF-ß, transforming growth factor-ß. Figure from Guinney et al, 2015[46].

The existence of these four distinctive molecular subtypes reinforces the potential of subtype-specific targeting regimens in order to develop more effective therapies[46]. Since publication of the CMS classification, numerous studies have explored how patients with different subtypes exhibit differential sensitivities to commonly used drugs contributing evidence to the clinical utility of CMS categorization[48].

Progress towards clinical application of the CMS subtypes has been achieved recently with an immunohistochemistry-based classifier to validate the predictive and prognostic value of molecular CRC subtyping in a multicenter study[49]. This classifier system has demonstrated high concordance with the main gene expression-based classification and has also confirmed the poor prognosis of the mesenchymal-like molecular subtype[49]. In addition, this tool has immediate clinical implication in the development of personalized therapies, improving the

clinical utility of the current molecular taxonomy and identifying a subset of patients of about 30%, who benefited from anti-EGFR therapy, improving its efficacy[49,50].

## 4. Immune system and tumor microenvironment of CRC

The tumor microenvironment, which includes molecular and cellular components of the immune system, is essential in modulating tumor progression and responses to cancer treatment, including immunotherapies. Although growing human solid tumors are infiltrated by immune cells, a complex set of molecular mechanisms is mounted by tumors to evade immune destruction[51]. One major mechanism deployed by tumor cells to evade T cell-mediated killing is the upregulation of immune checkpoints, which is a set of molecules that represses the activation and function of immune cells, including T cells[52]. Hence, immune checkpoint inhibitors (ICIs) have emerged as promising immunotherapeutic options for cancer, and their use has been approved for the treatment of a number of solid tumor malignancies, including advanced deficient MMR/MSI CRC[53].

### 4.1 CMSs and immune microenvironment

It is now evident that subdivision of CRC into CMS subtypes is not only driven by gene expression profiles derived from tumor cells, but it is highly influenced by the nature and composition of tumor microenvironment. Thus, Galon and colleagues first demonstrated the relevance of specific immune signatures in the prognosis of CRC through the determination of the "Immunoscore", which is a digital pathology-based assay based on the quantification of CD3+ and CD8+ lymphocytes at the tumor center and invasive margin[54,55]. The integration of the immune composition of the tumor microenvironment with the current consensus molecular CRC classification is

therefore critical. A number of studies have recently reported a correlation of CMS classification with distinct immune subtypes (**Figure 4**) thereby allowing a more precise categorization of patients[47,56,57].

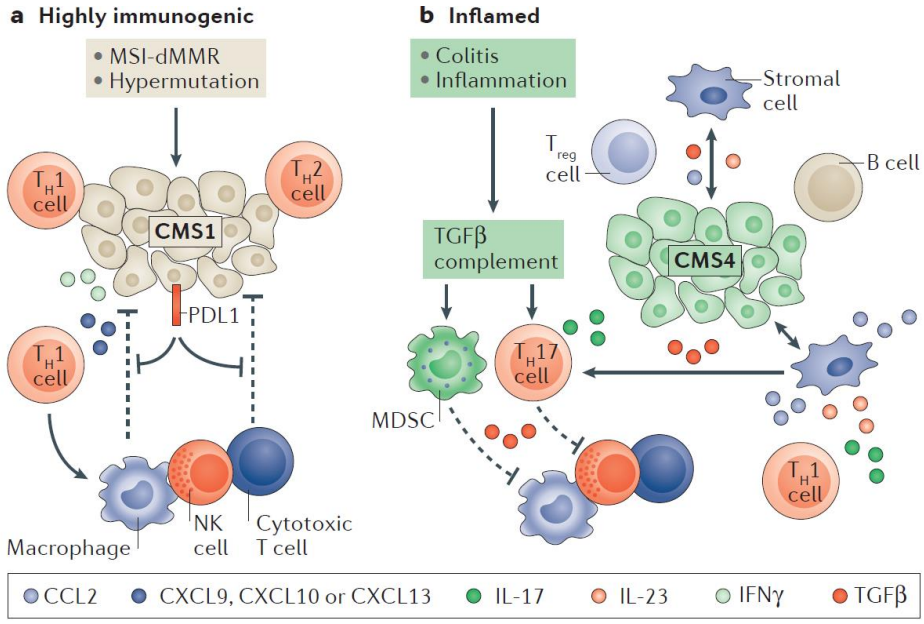


**Figure 4. Immune characterization of CMS CRC subtypes.** A) Highly immunogenic CMS1 MSI immune subtype, is infiltrated with adaptive cytotoxic cells and display a counterbalance of programmed cell death protein 1 ligand 1 (PDL1) expression. B) Chronic inflammation triggers an innate immune reaction that drives tumor growth by allowing cancer cells to evade immune attack. In the inflamed microenvironment of CMS4 mesenchymal subtype, stromal cells interact with cancer cells through immunosuppressive chemokines that inhibit cytotoxic immune cells and promote the proliferation of myeloid-derived suppressor cells (MDSCs), B cells and regulatory T (Treg) cells. Figure from Dienstmann et al, 2017[47].

This is especially apparent in CMS1, in which relatively high numbers of CD8+ cytotoxic lymphocytes, T helper 1 cells and natural killer cells infiltrate the tumor which is counterbalanced with upregulated expression of multiple immune checkpoints such as programmed cell death protein 1 ligand 1 (PDL1)[56,58,59].

However, the poor prognosis CMS4 subtype displays a different immune infiltration pattern. These tumors showed high TGFβ signaling, high expression of genes specific to Treg cells, myeloid-derived suppressor cells (MDSCs), monocyte-derived cells and specific chemokines (CXCL12, CCL2), promoting a more immunosuppressive microenvironment[56,59]. In contrast, tumors of CMS2 and CMS3 subtypes are characterized by poor infiltration by immune cells and are typically PDL1-negative which suggest that these tumors are poorly immunogenic[56].

### 4.2 Tumor budding

Tumor budding is other aspect of tumor microenvironment that plays an essential role in tumor progression, the metastasis cascade and that has been recently identified as an important prognosis factor for several malignancies including CRC[60,61]. Tumor budding is described as a single tumor cell or cell cluster of up to 4 cells at the tumor invasive front[62,63]. In 2016, the International Tumor Budding Consensus Conference (ITBCC) established a standardized scoring system which defined cut-offs to stratify budding grade into three groups (**Figure 5**): low (BD1, 0-4 buds), intermediate (BD2, 5-9 buds) and high (BD3, ≥ 10 buds)[64]. High-grade tumor budding has been recently established as an independent poor prognostic factor since it has been associated with shorter OS and disease-free survival (DFS) in several cancer types[63,65], and inversely correlated with the presence of cytotoxic immune infiltrate at the invasive margin. Accordingly, some studies have shown that the combination of tumor budding and immune cell score might be a stronger predictor of survival[66,67,68]. Moreover, although the biology of tumor budding is not totally understood, it has been demonstrated an overexpression of stem-cell related genes such as *ZEB1*, *ZEB2*, *DES* and *VIM*, and WNT and TGF-β signaling activation in tumor buds[69,70,71].

Recent studies have observed a close association of high-grade tumor budding with the poor prognosis CMS4 subtype of CRC which exhibits similar features of stem cell markers overexpression and TGF-β signaling activation, modulating immune evasion and the metastasis process[72]. However, the relationships between the immunosuppressive microenvironment of the poor prognosis CMS4 CRC subtype and tumor buds still remains unknown. The unraveling of the potential immunosuppressive mechanisms involved might help to better understand these processes and contribute to develop more effective personalized therapies.

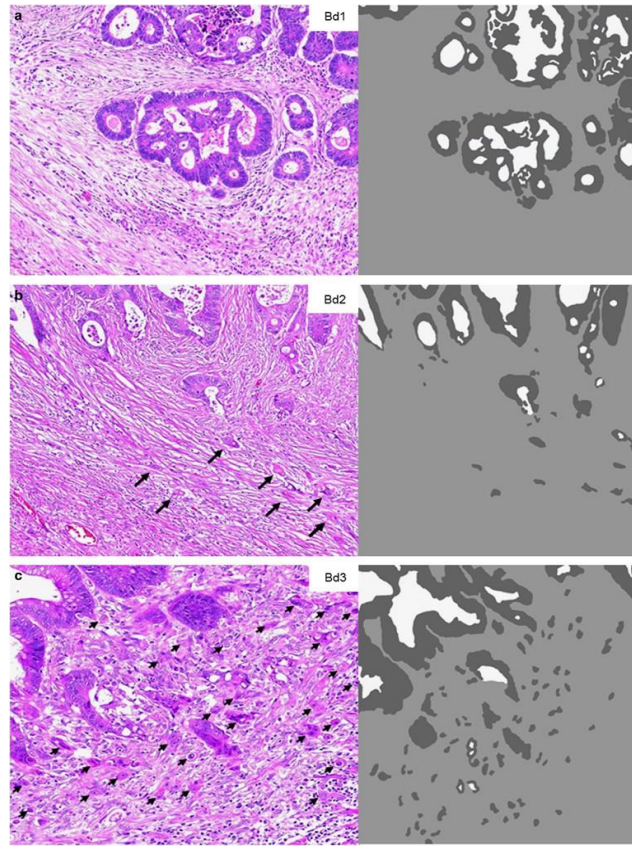


**Figure 5. Examples of different tumor budding grades at the invasive front of CRC based on the International Tumor Budding Consensus Conference 2016.** (a): BD1 (low), (b): BD2 (intermediate) and (c): BD3 (high). Figure from Lugli et al, 2017[62].

## 5. CRC Treatment

Despite all the progress and improvements achieved and the deeper understanding of CRC biology, in most of the cases the standard treatment regimen are surgery and chemotherapy. One of the most important chemotherapeutic agents is the fluoropyrimidine 5-Fluorouracil (5-FU), which is an antimetabolite drug that exerts its anticancer effects through inhibition of thymidylate synthase and incorporation of its metabolites into RNA and DNA. 5-FU is widely used for the treatment of cancer, and it is the basis of most chemotherapeutic regimens in advanced CRC patients[73,74,75]. This treatment can be administrated alone or in combination with the biomodulator leucovorin to increase its anticancer activity[76]. The Food and Drug Administration (FDA) also approved irinotecan, which is an inhibitor of topoisomerase I, as the second agent against CRC[73]. Thus, irinotecan and its derivate oxaliplatin, were used in combination with 5-FU as second-line therapy, to be later approved as first-line treatment against metastatic CRC (mCRC)[77,78,79]. Since then, the development of new molecules has been focused on targeting specific tumor-promoting signaling pathways to improve the therapeutic outcome in mCRC[80]. Among the targeted therapies for mCRC approved by the FDA are included mAbs such as bevacizumab (anti-VEGF therapy), and cetuximab and panitumumab (anti-EGFR therapy)[81]. Thus, bevacizumab in monotherapy has shown to be ineffective, but in combination with 5-FU has demonstrated to achieve a statistically significant and clinically improvement in mCRC patient survival[82,83]. The other relevant therapeutic target is the EGFR signaling pathway owing to its relationship with tumor progression and worse prognosis in mCRC[84,85]. Targeting EGFR has particularly been appealing due to the favorable efficacy benefits that mAbs such as cetuximab and panitumumab have demonstrated in clinic and development of

predictive biomarkers informing treatment decisions[86]. Both antibodies have proven to be clinically relevant alone in monotherapy and in combination with chemotherapy, nevertheless initial studies showed low efficacy in monotherapy, where 10-20% of mCRC patients responded favorably to anti-EGFR treatment[87], and this was related to the *KRAS* and *BRAF* mutational status in patients. Immunotherapy has recently emerged as one of the most encouraging fields in the search for targeted therapies with promising results in solid tumors[88]. In 2017, the FDA approved the use of the anti-PD1 immune checkpoint inhibitors nivolumab and pembrolizumab for the treatment of MSI-H mCRC patients or those harboring deficiencies in the MMR system (dMMR)[89,90], providing a new therapeutic option for patients with advanced disease[91]. Since then, combined therapy of nivolumab with low-dose ipilimumab (anti-CTLA4) has demonstrated even higher response rates, improving long-term clinical benefit compared to monotherapy. By contrast, these ICIs are ineffective in non-dMMR and microsatellite stablility (MSS) or MSI-L tumors. In this situation, low tumor mutation burden and low or null immune cell infiltration have been pointed as the immune resistance mechanisms, so new studies and approaches need to be done to overcome this therapeutical failures[92].

## 6. Nitric oxide and cancer

Nitric oxide (NO) plays an essential role as a signaling molecule in the regulation of a large number of important physiological processes, including vasodilation, platelet aggregation inhibition, neurotransmission and immune response[93]. In recent years, an increasing number of studies have shown that there is an important connection between this simple diatomic molecule and the pathogenesis of a significant number of diseases, including cancer[94,95,96,97]. The relationship between NO levels and biological response suggests a dual role of

NO in cancer pathogenesis, being cytotoxic or cytostatic at high levels whereas low levels can have the opposite effect promoting tumor growth[95,98]. Thus, low NO levels facilitate tumor progression, favoring pro-tumorigenic processes as angiogenesis stimulation and anti-apoptotic effects, while high NO levels exert inhibitory effects, oxidative and nitrosative stress, resulting in DNA damage, mitochondrial dysfunction, and increased apoptosis[95,96,97,98].

NO is synthesized through the metabolism of L-arginine to L-citrulline, in a complex reaction catalyzed by the enzyme nitric oxide synthase (NOS; EC1.14.13.39), of which there are three isoforms in mammals: neuronal NOS (nNOS or NOS1), inducible NOS (iNOS or NOS2), and endothelial NOS (eNOS or NOS3)[99]. These three isoforms differ in both specific biochemical requirements for their enzymatic activity and the levels of synthesized NO. Thus, NOS1 and NOS3, which are constitutively expressed in neural and endothelial cells respectively, produce low and transient levels of NO and their enzymatic activity is strongly regulated by intracellular calcium levels[100]. In contrast, NOS2 is calcium independent and can rapidly produce high local levels of NO after stimulation through inflammatory cytokines, endotoxin, hypoxia, and oxidative stress[95,101,102]. Abnormal NO production of the three NOS isoforms has been observed in different tumors[103,104,105], including CRC[106,107,108].

### 6.1 S-nitrosylation and denitrosylation of proteins: S-nitroglutathione reductase (GSNOR, ADH5)

NO is involved in cancer biology through the post-translational modification of key proteins affecting resistance to therapy, angiogenesis, apoptosis, invasion, and the development of metastases[95]. Many NO actions are mediated through a cyclic GMP (cGMP) dependent pathway by the stimulation of soluble guanylate cyclase (GCs), in which NO freely diffuses and binds to the heme group of GCs

which leads to the production of the second messenger cGMP, which acts on cGMP-dependent protein kinases, cGMP-gated cation channels, and phosphodiesterases, regulating among other processes neurotransmission or vascular tone[109]. However, NO-driven cell signaling is also mediated by the capacity of NO to modify other proteins than GCs. Hence, one key mechanism by which NO regulates the function of various target proteins is through the coupling of a nitroso moiety to the reactive thiol group (-SH) of a cysteine residue, leading to the formation of a S-nitrosothiol (SNO), a process commonly known as S-nitrosylation[109]. Protein S-nitrosylation is a key reversible modification that regulates enzyme activity, subcellular localization, protein complex formation, and protein degradation. Therefore, this NO posttranslational modification is considered as a regulatory process equivalent to protein phosphorylation[109,110]. An altered production of NO or an imbalance in the SNOs homeostasis leads to aberrant S-nitrosylation of proteins, which has been described in numerous pathophysiological contexts including cardiovascular, respiratory, hepatic, neurodegenerative and neoplastic diseases[95,101]. A key aspect in the maintenance of SNOs homeostasis is the activity of a particular group of enzymes termed denitrosilases.

S-nitrosylation occurs both in proteins, with the generation of S-nitrosoproteins (SNO-proteins), and in low molecular weight thiols (SNO-LMW), including glutathione and coenzyme A, generating **S-nitrosoglutathione (GSNO)** and S-nitroso-coenzyme A (SNO-CoA) respectively[109]. SNO-protein and SNO-LMW thiol levels are in equilibrium through transnitrosylation reactions, and are regulated by denitrosylation of the SNO group in proteins through the thioredoxin/thioredoxin reductase system (Trx/TrxR), as well as by denitrosylation of GSNO and SNO-CoA, through the enzymatic activity of the

enzymes **S-nitroglutathione reductase (GSNOR, *ADH5*)** and S-nitroso-Coenzyme A reductase (SCoR, AKR1A1), respectively[109,111] (**Figure 6**).

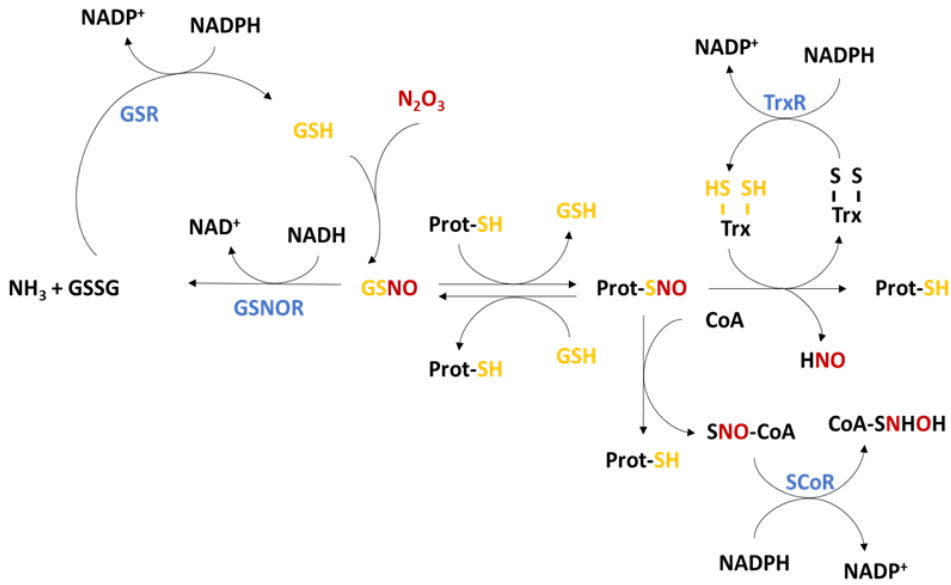


**Figure 6. Denitrosylase enzyme system and regulation of protein S-nitrosylation.** S-nitrosylated proteins (SNO-Prot) are directly denitrosylated by the action of the thioredoxin/thioredoxin reductase (Trx/TrxR) enzyme system. However, SNO-Prot levels are maintained in equilibrium by transnitrosylation reactions with the low molecular weight S-nitrosothiols S-nitrosoglutathione (GSNO) and S-nitroso-coenzyme A (SNO-CoA), which in turn are denitrosylated by the action of the denitrosylases GSNO reductase (GSNOR) and SNO-CoA reductase (ScoR), respectively.

The enzyme **GSNOR** or alcohol dehydrogenase III, is a highly conserved NADH-dependent enzyme, encoded by the ***ADH5* gene**, and it plays an important role in regulating SNOs homeostasis[112]. This enzyme metabolizes long-chain alcohols, but its main physiological function is the denitrosylation of GSNO. GSNO is an important NO reservoir in cells and, although there are other enzymes capable of metabolizing GSNO, the enzyme GSNOR shows the highest affinity for this substrate, and therefore it directly controls the homeostasis of SNOs and

the balance between SNO-LMW and SNO-proteins. This enzyme has been shown to be key to the maintenance of nitrosothiol homeostasis because ADH5$^{-/-}$ mice lacking GSNOR display high basal levels of GSNO and nitrosylated proteins[113]. Furthermore, our group demonstrated that the treatment with S-nitrosocysteine (CSNO) in human hepatocytes increased *ADH5* mRNA levels in a process transcriptionally regulated by the transcription factor Sp1[114]. Besides, our group also recently demonstrated that increased *ADH5* expression is significantly associated with higher survival rates in patients with HER2+ breast cancer, and that the antiproliferative action exerted by the anti-HER2 drug trastuzumab is suppressed when GSNOR activity is inhibited[115].

### 6.2 NO and immune evasion in the tumor microenvironment

Recent research has drawn attention to the important role of NO in the intricate relationships between tumor microenvironment and immune response, and in particular the participation of NO as an immunosuppressive mediator in the tumor microenvironment[96]. Moreover, NO directly facilitates a rewiring of metabolic pathways in tumor cells enabling their uncontrolled proliferation, and also modifies the tumor microenvironment to support cancer invasion and the escape from immune system-mediated recognition[97] (**Figure 7**).

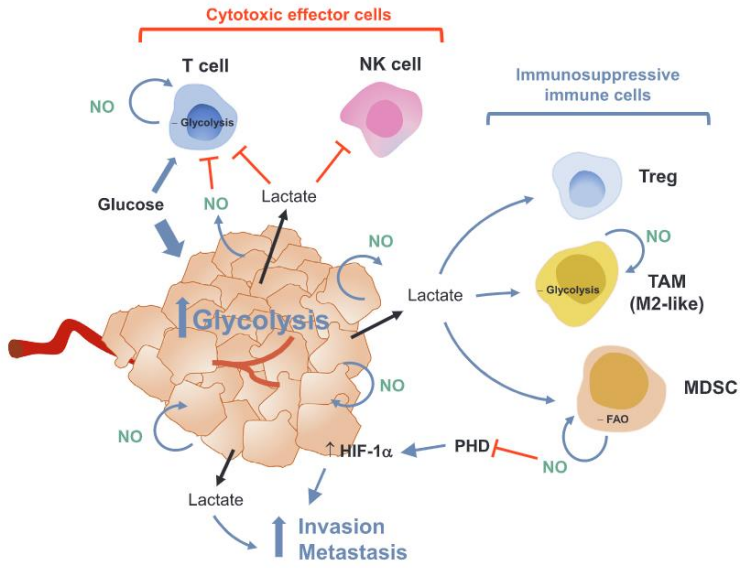


**Figure 7. Nitric oxide (NO) and the metabolic switch in the tumor microenvironment.** NO can directly facilitate the metabolic reprogramming in the tumor microenvironment by favoring aerobic glycolysis in tumor cells and lactate secretion in the tumor milieu. Tumor microenvironment acidification promotes immune escape by recruiting and activating immunosuppressive immune cells, while is unfavorable to infiltrating cytotoxic effector cells. Figure from Lopez-Sanchez et al, 2020[97].

Importantly, S-nitrosylation appears to be the main mechanism by which NO bioactivity may be transduced in the changes that cells undergo in the tumor microenvironment[96,97]. In this regard, different studies have shown that NOS3 is the isoform that contributes most significantly to the S-nitrosylation of proteins, being this enzyme responsible for 50-85% of the SNO-proteins identified in different tissues[116]. Moreover, recent studies in our group have demonstrated that NOS3 isoform is overexpressed in different scenarios related to intestinal tumor stem cells, including distinct CRC animal models, poorly differentiated aggressive adenocarcinomas and in worse prognosis mesenchymal CRC tumors (CMS4)[117]. However, no data is available to date about the importance of the

enzymatic systems that regulate SNO homeostasis in CRC. Specifically, it is important to know the role of the GSNOR enzyme in the different CRC subtypes and to elucidate possible mechanisms connecting the aberrant S-nitrosylation of proteins with the aggressive tumoral phenotypes and immune evasion in CRC.

## *IV. AIMS*

## General aim

The main objective of this study was to investigate the mechanisms involved in tumor progression and immune evasion in CRC, particularly in relation with the distinct CMS subtypes of this malignant disease.

## Specific aims

**1.-** To investigate the relationships between immune evasion and tumor budding in the different CMS subtypes of CRC and to unravel the potential immunosuppressive mechanisms involved.

**2.-** To explore the relevance of the major denitrosylase S-nitrosoglutathione reductase (GSNOR/*ADH5*) in the different CMS subtypes and to elucidate possible mechanisms connecting the aberrant S-nitrosylation of proteins with aggressive tumoral phenotypes and immune evasion in CRC.

# *V. MATERIALS AND METHODS*

# A. Study 1: Association between tumor budding, CMS subtypes and immune tumor microenvironment in CRC

## 1. Patients and inclusion criteria

For this study, a consecutive population-based series of forty-five patients over 18 years of age with resectable colon cancer submitted to Reina Sofia Hospital (Córdoba, Spain) was prospectively included. All rectal cancer patients were excluded in order to avoid the bias of neoadjuvant treated patients. The study was approved by the Reina Sofía Hospital ethical committee (Protocol number PI-0150-2017) in accordance with the Code of Ethics of the World Medical Association (Declaration of Helsinki). Informed consent was obtained from each patient, and clinicopathological information and follow-up was prospectively collected (**Table 1**).

**Table 1. Clinicopathological data of the patients included in the study 1.**

| **Patients characteristics (n=45)** | **All subjects, n (%)** |
|---|---|
| **Gender** | |
| Female | 15 (33%) |
| Male | 30 (67%) |
| **Age (mean ± SD)** | 73.8±10.1 |
| **Metastasis at the diagnosis** | |
| No | 40 (89%) |
| Yes | 5 (11%) |
| **Tumor size (cm, mean ± SD)** | 4.2±1.1 |
| **Tumor Histological grade** | |
| Low | 39 (87%) |
| High | 6 (13%) |
| **TNM Staging** | |
| 0 | 2 (4%) |
| I | 1 (2%) |
| II | 21 (47%) |

| | |
|---|---|
| III | 16 (36%) |
| IV | 5 (11%) |
| **Anatomical Location** | |
| Left | 20 (44%) |
| Right | 25 (56%) |
| **Histological Subtype** | |
| Well differentiated | 6 (13%) |
| Moderately differentiated | 34 (76%) |
| Poorly differentiated | 5 (11%) |
| **Mucinous component** | |
| No | 30 (67%) |
| Yes | 15 (33%) |
| **Stromal component** | |
| < 50% | 14 (31%) |
| ≥ 50% | 31 (69%) |
| **Inflammatory infiltrate** | |
| Low | 20 (44%) |
| Medium | 16 (36%) |
| High | 11 (25%) |
| **Lymphatic invasion** | |
| No | 23 (51%) |
| Yes | 22 (49%) |
| **Perineural invasion** | |
| No | 26 (58%) |
| Yes | 19 (42%) |
| **Vascular invasion** | |
| No | 28 (62%) |
| Yes | 17 (38%) |

## 2. Processing of clinical tumor samples and establishment of patient derived xenografts (PDXs) models

Tumor samples were obtained just after surgical resection and three adjacent tumor pieces were immediately collected in sterile conditions. One tumor piece was fixed in 4% buffered formalin and then embedded in paraffin (FFPE) for hematoxylin and eosin (H&E) staining and for immunohistochemical (IHC)

studies, another one was snap frozen in liquid nitrogen and stored at -80ºC for gene expression profiling, and the third fresh tumor piece was washed several times in cold sterile phosphate buffered saline (PBS) and used for establishment of PDXs.

The PDXs engraftment was performed in NOD-SCID mice (NOD.CB17-Prkdcscid/Rj mice) (Janvier Laboratory, Paris, France) of 4-6 weeks of age according to Puig and coauthors[118]. In brief, after incubation for 24 h in a disinfection medium (DMEM/F12 medium containing Zell shield antibiotics), the tumor sample was divided into small pieces with a scalpel and a cell suspension was subsequently obtained by enzymatic digestion with collagenase (1.5 mg/ml; Sigma-Aldrich) and DNAse I (20 µg/ml; Sigma-Aldrich) for 1 h at 37ºC and pipetting at 15 min intervals to disperse and separate the cells. This cell suspension was filtered (Cell Strainer 100 µm nylon, Falcon), centrifuged (1800 rpm/10 min) and incubated with an 1X ammonium chloride solution (Invitrogen) for red blood cell lysis for 10 min at room temperature (RT). Finally, cell count was performed in a Neubauer chamber and 200,000 cells resuspended in PBS and mixed with Matrigel (BD Bioscience) in a 1:1 ratio were subcutaneously injected in both flanks of each animal, generating the first PDX passage (P0). Tumor growth was weekly measured using a digital caliper until tumor volume reached 1 $cm^3$. Mice were ethically sacrificed under isoflurane anesthesia followed by cervical dislocation when tumor reached that size or if they appeared to be suffering. Samples were immediately collected, fresh-frozen, formalin-fixed, and reimplanted as described above. Animal care and experimental procedures were approved by the University of Córdoba Bioethics Committee and followed the regulations of the European Union normative (26/04/2016/066).

### 3. Classification into Consensus Molecular Subtypes using IHC

IHC staining was performed on 4-µm FFPE sections mounted on poly-L-lysine coated slides deparaffinized in xylene and rehydrated using graded alcohols. Tissue sections were incubated in 10 mM citrate buffer (pH 6.0) for 5 min at 120ºC for antigen retrieval. Endogenous peroxidase was neutralized by using the EnVision FLEX peroxidase-blocking reagent (Dako, Glostrup, Denmark) for 10 min at RT. Tween Tris-Buffered Saline (TBST) was used as washing solution. Tissue sections were blocked with 3% bovine serum albumin (BSA) or following mouse-on-mouse staining protocol (Abcam, Cambridge, UK) in the case of CRC cell line xenografts and PDXs. Then, sections were incubated with the corresponding primary antibody (**Table 2**) overnight at 4ºC. Then, after incubation with the corresponding EnVision FLEX+ mouse or rabbit linker (Dako, Glostrup, Denmark) for 30 min at RT, sections were incubated for 1h with the secondary antibody EnVision FLEX/HRP (Dako, Glostrup, Denmark). The staining was visualized using 3,3-diaminobenzidine (DAB) chromogen (Dako, Glostrup, Denmark) and counterstained with Harris hematoxylin. Tissue samples were finally dehydrated and mounted on Eukitt mounting medium (Sigma-Aldrich, St. Louis, MO, USA). Negative controls without incubation with primary antibodies were also performed.

The molecular CMS classification by IHC described by Trinh and coauthors[72] was used in both the clinical samples and the corresponding PDXs. This IHC-based patient stratification tool uses five markers: CDX2 as epithelial marker; HTR2B, FRMD6, and ZEB1 as mesenchymal-like and EMT markers, and the pan-cytokeratin used as both normalizer and epithelial-like marker, as well as using four MMR markers (MSH2, MLH1, MSH6, and PMS2) to assess MSI, to classify CRC tumors into three subtypes CMS1, CMS2/3 and CMS4 by using an on line website mini-IHC-classifier[50]. Then, MSI status was first performed using

the antibodies hMSH2, hMSH6, hMLH1, and hPMS2. The absence of expression of any of these MMR proteins defined samples which are MSI and belong to the CMS1 subtype. Otherwise, sample was defined as microsatellite stable (MSS), and were further analyzed for the content and intensity of FRMD6, HRT2B, ZEB1, CDX2 and AE1/AE3 expression. Then, corresponding scores for each marker were analyzed using a random forest classifier in the online classification platform (https://crcclassifier.shinyapps.io/appTesting/) and tumors were classified into "epithelial" (CMS2/3) or "mesenchymal" (CMS4) subtypes. In addition to IHC-based CRC classification, we performed a IHC analysis of eNOS expression in CRC patient samples, using a monoclonal antibody (dilution 1:200, Cell Signaling, #5880S). For that, expression for eNOS in 10% or more of tumor epithelial cells was considered as positive.

**Table 2. List of antibodies used for IHC-Based CMS Classification**

| Antibody | Specie | Dilution | Company |
|---|---|---|---|
| **hMSH2** | mAb[a], mouse | 1:1 | Master Diagnostica S.L., Spain |
| **hMSH6** | mAb, rabbit | 1:1 | Master Diagnostica S.L., Spain |
| **hMLH1** | mAb, mouse | 1:1 | Leica Biosystems, UK |
| **hPMS2** | mAb, mouse | 1:1 | BIOCARE Medical, CA, USA |
| **FRMD6** | pAb, rabbit | 1:500 | SIGMA Aldrich, MO, USA |
| **HTR2B** | pAb, rabbit | 1:75 | SIGMA Aldrich, MO, USA |
| **ZEB1** | pAb, rabbit | 1:500 | SIGMA Aldrich, MO, USA |
| **CDX2** | pAb, rabbit | 1:500 | NOVUS Biologicals, USA |
| **KER (AE1/AE3)** | mAb, mouse | 1:500 | Thermo Scientific, IL, USA |

[a]mAb: monoclonal antibody. pAb: polyclonal antibody

## 4. Assessment of tumor budding

Tumor budding was defined as single tumor cell or cell clusters up to four cells in the stroma of the invasive front[62]. For this determination, tumor buds were assessed in human samples and PDXs analyzing the pan-cytokeratin (clone

AE1/AE3) immunostaining (**Table 2**) in a single hot spot measuring 0.785 $mm^2$ for more accurate identification in cases of obscuring factors like inflammation or reactive stroma. For budding grade stratification, cut-offs defined by ITBCC were used: low (BD1), 0–4 buds; intermediate (BD2), 5–9 buds; and high (BD3) ≥10 buds)[62].

**5. Immune gene expression profiling**

Immune gene expression was analyzed using the nCounter PanCancer immune profiling panel from NanoString (Seattle, WA, USA) both in patient tumors and their corresponding PDXs. In the case of PDXs, P0 passage was used for immune gene expression profiling to minimize the variability between patients and xenografts. For each sample, total RNA was extracted using the commercial RNeasy Mini Kit (Qiagen, Hilden, Germany) according to the manufacturer's instructions. Then, total RNA was quantified using the NanoDrop™ 1000 spectrophotometer (NanoDrop® ND-1000 UV-Vis Spectrophotometer, NanoDrop Technology), and RNA integrity Number (RIN) was measured using the Agilent 2200 TapeStation equipment. Data analysis was performed by using nSolver software (NanoString Technologies, Seattle, WA, USA) to manage the raw expression data generated for each gene and for normalization[117]. For each particular gene the positive or negative expression indicates that the number of RNA molecules is above or below the mean, respectively.

**6. Statistical analysis**

Data were analyzed using GraphPad Prism 7 and R Software (version 3.5.0). Previously, in order to assess normality of the data, D'Agostino and Pearson Normality test was performed. The clinicopathological data were compared using Fisher's exact test or Mann–Whitney's test for qualitative and quantitative variables, respectively. Multivariate regression analysis was carried out with

multinomial regression model for budding grades, including the variables selected by using the Akaike information criterion (AIC) with stepwise model selection. Differences in DFS were expressed as hazard ratios (HR) with 95% confidence intervals, and survival curves were constructed using the Kaplan–Meier method. All $p$ values $\leq 0.05$ were considered statistically significant.

## B. Study 2: Association between GSNOR/ADH5 expression, CMS subtypes and immune tumor microenvironment in CRC

### 1. Patients and inclusion criteria

For this study, a series of fifty-three patients over 18 years of age with resectable colon cancer submitted to Reina Sofia Hospital (Córdoba, Spain) was prospectively included **table 3**. The study was approved by the Reina Sofía Hospital ethical committee (Protocol number PI-0150-2017) in accordance with the Code of Ethics of the World Medical Association (Declaration of Helsinki).

**Table 3. Clinicopathological data of the patients included in the study 2.**

| Patients characteristics (n=53) | All subjects, n (%) |
|---|---|
| **Age (mean ± SD)** | 73.4±10.4 |
| **Gender** | |
| Male | 35 (66%) |
| Female | 18 (34%) |
| **Anatomical Location** | |
| Right | 31 (58%) |
| Left | 22 (42%) |
| **Tumoral grade differentiation** | |
| High grade | 6 (11%) |
| Low grade | 47 (89%) |
| **Tumoral stage** | |
| 0 | 1 (2%) |
| I | 2 (4%) |
| II | 27 (51%) |
| III | 17 (32%) |
| IV | 6 (11%) |
| **Tumor size (cm, mean ± SD)** | 4.2±1.1 |
| <4.2 cm | 28 (53%) |
| >4.2 cm | 25 (47%) |

| | |
|---|---|
| **Histological Subtype** | |
| Well differentiated | 6 (11%) |
| Moderately differentiated | 41 (78%) |
| Poorly differentiated | 6 (11%) |
| **MSI status** | |
| MSS | 44 (83%) |
| MSI | 9 (17%) |
| **Mucinous** | |
| Yes | 17 (32%) |
| No | 36 (68%) |
| **Lymphatic invasion** | |
| Yes | 23 (43%) |
| No | 30 (57%) |
| **Vascular invasion** | |
| Yes | 18 (34%) |
| No | 35 (66%) |
| **Perineural invasion** | |
| Yes | 23 (43%) |
| No | 30 (57%) |
| **Metastases or recurrence** | |
| Yes | 15 (28%) |
| No | 38 (72%) |
| **CMS subtype** | |
| CMS1 | 10 (19%) |
| CMS2/3 | 27 (51%) |
| CMS4 | 16 (30%) |
| **Budding grade** | |
| BD1 | 14 (26%) |
| BD2 | 13 (25%) |
| BD3 | 26 (49%) |
| **Immune infiltrate** | |
| Low | 16 (38%) |
| Medium | 16 (38%) |
| High | 10 (24%) |

## 2. IHC analysis

Tumor tissues and tumorspheres were formalin-fixed paraffin embedded (FFPE) prior to IHC staining, that was performed as described above (Classification into CMS using IHC) using the conditions and primary antibodies described in **Table 4**. ADH5 expression was evaluated as high (more than 10% of positive cells with moderate/high intensity), or low (less than 10% of positive cells) in human tissue samples, and as positive (when 10% of cells or more were positive) or negative expression (less than 10% of positive cells) in tumorsphere samples. For CDX2 analysis in human tissue we used the expression obtained from CMS classification. For CDX2 and PDL1 assessment in tumorospheres, the percentage of positive cells from total cells was calculated using *QPath* software (version 0.2.3).

**Table 4. List of antibodies used for IHC analysis**

| Antibody | Specie | Dilution | Antigen retrieval | Company |
|---|---|---|---|---|
| **ADH5** | mAb, mouse | 1:50 | 10mM citrate buffer (pH 6.0) | SIGMA Aldrich, MO, USA |
| **PDL1** | mAb, rabbit | 1:200 | Tris EDTA buffer (pH 9.0) | Cell Signaling Technology, MA, USA |
| **CDX2** | pAb, rabbit | 1:500 | 10mM citrate buffer (pH 6.0) | NOVUS Biologicals, USA |

mAb: monoclonal antibody. pAb: polyclonal antibody

## 3. Immune gene expression profiling

Immune gene expression was analyzed using the nCounter PanCancer immune profiling panel from NanoString (Seattle, WA, USA), as described above.

## 4. Cell lines and chemicals

HCT116 cell line (DSMZ, Braunschweig, Germany) was cultured in McCoy's 5A medium (Biowest, Nuaillé, France) supplemented with 10% fetal bovine serum (FBS) (PAA Laboratories, Pasching, Austria), 2 mM Glutamine (Biowest, Nuaillé, France) and 1X Zell Shield antibiotics (Minerva Biolabs, Berlin, Germany). DLD1 cell line (kindly provided by Dr. Teresa Roldán Arjona, Universidad de Córdoba, España) was cultured in Dulbecco's modified Eagle medium (DMEM) high glucose (4.5 g/L) (Capricorn Scientific, Ebsdorfergrund, Germany) supplemented with 10% FBS (PAA Laboratories, Pasching, Austria), 2 mM Glutamine (Biowest, Nuaillé, France) and 1X Zell Shield antibiotics (Minerva Biolabs, Berlin, Germany). Cells were maintained in a humidified atmosphere at 37ºC and 5% $CO_2$. Molecular characteristics of each cell lines used are described in the **Table 5**.

**Table 5. CRC cell lines molecular characteristics**

| Cell line | MSI status | CIN | KRAS | BRAF | PIK3CA | PTEN | P53 |
|---|---|---|---|---|---|---|---|
| **HCT116** | MSI | - | G13D | wt | H1047R | wt | wt |
| **DLD1** | MSI | - | G13D | wt | E545K;D549N | wt | S241F |

S-nitrosocysteine (CSNO) was synthesized as previously described by Jourd'heuil and coauthors[119] by incubating one volume of L-cysteine with one volume of equimolar concentration of acidified sodium nitrite and quantifying by absorbance at 334 nm using a molar absorption coefficient of 0.74/mM/cm. 2-Deoxy-glucose (2DG) was purchased from Sigma Aldrich (#D8375) and a stock solution of 100 μM 2DG was prepared in distilled $H_2O$ for the *in vitro* assays.

## 5. Genetic ablation of ADH5 gene using CRISPR-Cas9 technology

### 5.1 sgRNA design and cloning

In order to generate the CRISPR-Cas9 constructs, specific sgRNAs were designed and cloned in a commercial plasmid vector. Each sgRNA comprises a 20-nt guide sequence and a scaffold sequence. Pairs of DNA oligonucleotides encoding the variable 20-nt sgRNA guide sequence were annealed together to generate short double strand DNA fragments with 4-bp overhangs and inserted upstream the sgRNA scaffold in the expression plasmid pSpCas9(BB)-2A-GFP (PX458) (Addgene, plasmid ref #48138).

The 20-nt guide sequence that precedes NGG (PAM, protospacer adjacent motif required for sgRNA targeting) was selected for each sgRNA using the "Feng Zhang lab's Target Finder" software (***http://crispr.mit.edu/***). This software provided a list of all possible guide sequences for the submitted target sequence, scored by inversed likelihood of off-target binding. Those guide sequences with a high score (low off-target binding) and complementary to a sequence located at a desire position in the target gene (*ADH5* gene, NM_000671.4) were selected.

Overhangs for BbsI restriction sites were added to forward and reverse oligonucleotides guides for their cloning into the expression plasmid pSpCas9(BB)-2A-GFP (PX458). When the first base at the 5´end of the guide sequence was not a G, an additional G:C base pair was added at this position for efficient U6-dependent transcription without affecting the targeting efficiency. Oligonucleotides (**Table 6**) were ordered from Metabion (Condalab, Madrid, Spain) and were purified by HPSF (High Purify Salt Free) before use. Then, *E. coli* bacteria were transformed with the constructs generated, and plasmids were purified and checked by DNA sequencing (Research Support Services, University of Córdoba).

**Table 6. Oligonucleotides used for sgRNA design and cloning.**

| sgRNA Name | Sequence (5´-3´) | Target |
|---|---|---|
| **ADH5 RNAg Fw A** | CACCGTCTTGCTAACGCGCGCTGAA | sense |
| **ADH5 RNAg Rv A** | AAACTTCAGCGCGCGTTAGCAAGAC | sense |
| **ADH5 RNAg Fw B** | CACCGCCTTTGAACGTTAATCCGAC | sense |
| **ADH5 RNAg Rv B** | AAACGTCGGATTAACGTTCAAAGGC | sense |

Red: overhangs for BBsI Green: additional G base for U6 promoter

### 5.2 Cell transfection and clone selection

One day before transfection, 6.5 x $10^5$ cells (HCT116 or DLD1) were seeded in 6-well plates. The co-transfection mix included constructs expressing Cas9, GFP and either double strand sgRNA site A or site B (250 ng DNA/well each), diluted in 500 µL Opti-MEM® I Reduced Serum Media (Invitrogen), 5 µL Lipofectamine 3000 and 5 µL P3000 Reagent (Lipofectamine™ 3000 Transfection Reagent, Invitrogen). After 30 min incubation at room temperature, culture media was refreshed, and the co-transfection mix was added drop by drop to cells (1.5 mL/well). Forty-eight hours after co-transfection, cells were trypsinized, harvested by centrifugation at 1800 rpm for 5 min and resuspended in 1mL of filtered (0.2 µm) basic Sorting Buffer (1X phosphate buffer Ca/Mg free, 2 mM EDTA, 25 mM HEPES pH 7.0, 1% FBS, and Zell Shield antibiotics) in flow cytometry tubes and green fluorescent protein-positive cells were sorted by flow cytometry (FACSAria III, BD) with a 100-µm nozzle in a cloning 96-well plate. *ADH5* KO clones were grown in 50% FBS complete media and cells were expanded to obtain enough amount for selection transfected cells. Positive clones were confirmed by conventional Polymerase Chain Reaction (PCR) and by Western blot.

## 6. Genomic DNA extraction and PCR

Cells from generated clones were harvested by centrifugation and genomic DNA was extracted with lysis buffer (TRIS 10 mM pH 8, EDTA 5 mM, and NaCl 100 mM) supplemented with 10% SDS and Proteinase K (20 mg/mL) and followed by an overnight incubation at 37ºC. Next, samples were centrifugated for 40 min at 10,000g, and supernatant was collected and placed in a new microcentrifuge tube. To allow DNA precipitation, a ratio 1:1 (vol/vol) of isopropanol was added to each sample and then centrifugated for 15 min at maximum speed. Then, pellets were incubated at RT to dry DNA and then resuspended in 70% ethanol and centrifuged for 15 min at maximum speed. Finally, pellets were incubated at RT to dry DNA and then resuspended in ultrapure MQ water and quantified in a DS-11 DeNOVIX spectrophotometer (DeNovix Inc, Wilmington, DE, USA). The obtained genomic DNA (100 ng) was used for PCR amplification with the commercial kit MyTaq HS (Bioline) according to the manufacturer's instructions. PCR conditions were as follow: one step for PCR started at 95ºC for one min, followed by 35 amplification cycles at 95ºC for 15 sec, 60ºC for 15 sec, and 72ºC for 2 min for extension. Finally, the samples were kept at 72ºC for 7 min and at 16ºC until completion. The primers used for PCR amplification are indicated in **Table 7**.

**Table 7. Oligonucleotides used PCR confirmation of *ADH5* Knock-out**.

| Primer name | Sequence (5´-3´) | Tm (ºC) | PCR product (pb) |
|---|---|---|---|
| **ADH5 Fw2** | GAAGGTGCTGGAATTGTGGAAA | 58 | 578 |
| **ADH5 Rv2** | GAAACAAATGCAAAGACATCCTGA | 58.3 | |
| **hRPL13 Fw1** | CCTGGAGGAGAAGAGGAAAGAGA | 60 | 357 |
| **hRPL13 Rv1** | TTGAGGACCTCTGTGTATTTGTC | 60 | |

To analyze PCR products, 1% agarose gel was prepared in 1X TAE buffer (40 mM Tris-acetate, 1 mM EDTA), and 8 μL of amplified sample was mixed with 2 μL of Bluxyo Safe 1X (gTPbio) and loaded into the gel. After completion of the electrophoresis, the gel was visualized on a ChemiDoc XRS Imaging equipment (BioRad; Hercules, CA, USA) and analyzed using the Image Lab 5.2.1 program (BioRad; Hercules, CA, USA).

**7. Cell proliferation assay**

The live-cell imaging and analysis IncuCyte ZOOM system (Essen Bioscience, Ann Arbor, MI, USA) was used for dynamic monitoring of tumor cells proliferation over time. Thus, HCT116 and DLD1 cells were seeded at 5,000 cells/well in 96-well plates. To analyze cell proliferation, each plate was scanned and phase-contrast images of cell confluence per well at each time point were acquired every 6 h. Quantified time-lapse curves were analyzed using Incucyte ZOOM software. Cell proliferation was also determined using the CellTiter-Glo® Luminescent Cell Viability Assay kit (Promega, Madison, WI) according to the manufacturer's instructions. For this assay, HCT116 and DLD1 cells were seeded at 5,000 cells/well in 96-well plates and grown for 48-72 h. Then, culture media was removed and 90 μL of fresh culture media was added in each well and plates were incubated for 30 min at RT. Each sample was mixed with 90 μL of CellTiter-Glo® Reagent, gently shaken for 2 min and then incubated for 10 min at RT. Luminescent signal was recorded on an Infinite F200 Pro (TECAN) equipment, and the Relative Light Unit (RLU) value was obtained for each sample. This luminescent signal is proportional to the amount of ATP present in the cell culture.

**8. Detection of S-nitrosylated proteins**

S-nitrosylated proteins were detected using the Pierce™ S-Nitrosylation Western Blot assay (Pierce; Thermo Fisher Scientific, Inc.) according to the

manufacturer's instructions. In brief, thiol groups (-SH) of unmodified cysteines were first blocked using a sulfhydryl-reactive compound, the methyl methanethiosulfonate (MMTS). Then, S-nitrosylated cysteines were selectively reduced with ascorbate in HENS Buffer for specific labeling with iodoTMTzero reagent, which irreversibly binds to the cysteine thiol that was previously S-nitrosylated. Proteins labelled with iodoTMTzero were detected by western blot using an anti-TMT antibody. This procedure was carried out under dark conditions until proteins were covalently labelled with iodoTMTzero reagent, since the S-NO bonds are sensitive to light. Cell pellets were previously washed twice in wash buffer for 5 min and centrifuged at 500 x *g*, discarding the supernatant. For positive control, one sample was heavily S-nitrosylated by incubating with 10 mM of GSNO for 30 min. Each sample was lysed in 500 µL HENS buffer and then protein concentration was quantified using a BCA assay (Pierce; Thermo Fisher Scientific, Inc.) according to the manufacturer`s instructions. Then, 100 µg protein was resuspended in 100 µL of HENS buffer and free cysteine thiol groups were blocked by incubating with MMTs for 30 min at RT. Next, protein was precipitated with six volumes of pre chilled acetone (-20ºC) and an incubation at -20ºC for 1 h, following by a 4ºC centrifugation for 10 min at 10,000*g*. Protein pellets were resuspended in 100 µL of HENS buffer and divided into two 50 µL aliquots for protein reduction with ascorbate and labelling with iodoTMTzero reagent for 1 h at RT. Next, protein precipitation with acetone was performed and protein pellets were resuspended in 100 µL HENS buffer and stored at -80ºC until use. Detection of iodoTMT labelled-nitrosylated proteins was performed by electrophoresis of 20-25 µg of protein, followed by western blot and immunodetection with primary anti-TMT antibody and secondary anti-mouse HRP antibody.

**9. Western Blot Analysis**

Cells were harvested by centrifugation and then incubated for 15 min on ice with lysis buffer (50 mM Tris-HCl (pH 7.4), 150 mM NaCl, 5 mM ethylenediamine tetraacetic acid (EDTA), 1 mM ethylene glycol tetraacetic acid (EGTA), 1.5 mM MgCl2, 10% glycerol, 1% NP40, 0.1 M dithiothreitol (DTT), 0.1 phenylmethylsulfonyl fluoride (PMSF), 1% v/v protease inhibitor cocktail (SERVA, Heidelberg, Germany) and 1% v/v phosphatase inhibitor cocktails 2 and 3 (Sigma- Aldrich) and centrifuged at 10,000g for 15 min at 4°C. Total protein quantification was performed using Bradford technique (BioRad; Hercules, CA, USA). Protein lysate (20 μg) was mixed with loading buffer (1 M Tris-HCl pH 6.8, 30% Glycerol, 10% SDS, 2% Bromophenol blue, and 8% β-mercaptoethanol) and boiled at 95ºC for 5 min. Samples were then separated in a 4-20% polyacrylamide gradient gel (MiniProtean TGX Stain-free o Criterion TGX Stain-free, BioRad; Hercules, CA, USA) using a BioRad Criterion electrophoresis System for 40 min at 200V. After electrophoresis, stain-free polyacrylamide gels were activated using the ChemiDoc XRS+ transilluminator (BioRad; Hercules, CA, USA) which makes proteins fluorescent directly on the gel with a short photoactivation, allowing immediate protein visualization.

Proteins were transferred to PVDF membranes using the Transfer Turbo buffer (Buffer Transfer Turbo, BioRad; Hercules, CA, USA). Membranes were blocked for 1 h at RT in gentle shaking in Tween Tris-Buffered Saline, pH 7.5 (TTBS) with 5% non-fat dried milk (Panreac) or BSA, depending on the specifications of the corresponding primary antibody. Blots were then incubated overnight at 4ºC in gentle shaking with primary antibodies Anti-ADH5 Rabbit pAb (Ref: TA321174; Origene; Rockville, MA, USA, 1:1000) or Anti-TMT™ Antibody (Ref: 90075; Pierce; Thermo Fisher Scientific, Inc. Waltham, MA, USA, dilution 1:1000). Blots were incubated for 1 h at RT in gentle shaking with

the appropriate secondary HRP-conjugated antibody (goat anti-rabbit; Santa Cruz Biotechnology, Heidelberg, Germany, Inc; 1:10000). Protein bands were detected by enhanced chemiluminescence with the ECL Plus Western Blotting Detection System (BioRad; Hercules, CA, USA) and images were obtained using the ChemiDoc XRS Imaging equipment (BioRad; Hercules, CA, USA) and analyzed using the Image Lab 5.2.1 software (BioRad).

**10. Tumorspheres formation assay**

Parental and *ADH5* KO HCT116 and DLD1 cells growing in adherence were trypsinized, harvested by centrifugation at 1800 rpm for 5 min and seeded at 2 cell/ μL density in ultra-low attachment surface 24-well plates (Costar, Corning, NY, USA) with serum free Dulbecco's Modified Eagle Medium/Nutrient Mixture F-12 HAM (DMEM/F12; Gibco; Thermo Fisher Scientific, Inc., Waltham, MA, USA) supplemented with 1x B27 (Gibco, Waltham, MA, USA), 20 ng/ml EGF (Santa Cruz Biotechnology, Heidelberg, Germany), 10 ng/ml bFGF (Prepro Tech, London, UK) and 1:3 dilution (v/v) methylcellulose (R&D systems) to prevent cell aggregation. Freshly supplements were added every 3-4 days, and tumorspheres number and size were analyzed 12-14 days after seeding by optical microscopy. For immunohistochemistry analysis, tumorspheres were embedded in 1% Agarose (Agarose D1 Low EEO, CondaLab, Madrid, Spain) 12-14 days after seeding. Then tumorospheres were formalin fixed and embedded in paraffin for IHC analysis.

**11. Tumor spheroids formation assay**

Parental and *ADH5* KO HCT116 and DLD1 cells growing in adherence were trypsinized and embedded in 30 μL of Matrigel GFR (Corning® Matrigel® Growth Factor Reduced (GFR) Basement Membrane Matrix, Phenol Red-free; Corning, NY, USA) on ice and seeded in 24-well cell culture plates at 10-15

cells/µL matrigel per well. After matrigel polymerization at 37ºC for 15 min, 500 µL of advanced DMEM/F12 (Dulbecco's Modified Eagle Medium/Ham's F12; Gibco, Waltham, MA, USA) supplemented with 1x Zell Shield antibiotics, 1x B27 and 1x N-2 supplement (Gibco; Thermo Fisher, Waltham, MA, USA) were added to each well. Freshly supplemented media were added every 3-4 days, and tumor spheroids number and size were analyzed by optical microscopy 12-14 days after seeding.

**12. Tumorigenicity assay in immunocompromised mice**

To compare the *in vivo* capacity of parental and *ADH5* KO HCT116 cells to generate tumors, a Limiting Dilution Assay (LDA) was performed. For this, 8 experimental groups of 3 male 5-weeks old NSG mice (NOD.CB17/AlhnRj-Prkdcscid, Janvier Labs) were used to perform the assay. To establish the tumor xenografts increasing number of cells (10, 50, and 100) embedded in 100 µL matrigel (Matrigel® Basement Membrane Matrix; Corning, NY, USA) were subcutaneously implanted into both flanks of mice. Animals were daily monitored, and tumor growth was monitored by weekly measurement of apparent tumor volume using a digital caliper. The experiment was terminated when tumors reached 1 $cm^3$ volume. The apparent tumor volume was calculated as lw2/2 and final tumor volume as $(\pi/6) \times lw \times h$ (l: length; w: width; h: height).

**13. Lactate assay**

Lactate concentration in the cell culture medium was determined using the Lactate-Glo™ Assay kit (Promega, Madison, WI) according to the manufacturer's instructions. Cell culture media were collected and centrifuged for 5 min at 1500 rpm to eliminate cell debris. Each sample was diluted 1:20 in PBS and 50 µL were added per well (each sample per duplicate) plus 50 µL of Lactate Detection Reagent in a 96-well White Polystyrene Luminometer Microplate. Samples were

gently shaken for 1 min and then incubated for 1 h at RT. Luminescent signal was recorded on an Infinite F200 Pro (TECAN) equipment, the RLU value was obtained for each sample and normalized dividing by the number of cells.

**14. Mitochondrial network analysis**

To evaluate the mitochondrial network in tumor cells, immunofluorescence confocal microscopy was performed by staining mitochondria with mitotracker red. Prior to cell culture, glass slides were placed in a 24-well plate and treated with 1 mL of poly-L-lysine hydrobromide (Sigma, #1274) at a final concentration of 0.1 mg/mL for 1 h at 37ºC, followed by 1X PBS washes and 1-2 h of incubation at RT for glass drying. For live cell imaging, cells were trypsinized, harvested by centrifugation at 1800 rpm for 5 min and plated in the poly-L-lysine coated slides ($10^5$ cell/well in 500 µL of growth medium) and allowed to attach overnight. The following day, cells were incubated for 30 min at 37ºC with Mitotracker red (MitoTracker® Red CM-H2XRos, Invitrogen) and fixed with 4% paraformaldehyde for 10 min at RT. Nuclear DNA was stained by incubating cells with 1/15000 µL DAPI (Sigma-Aldrich, Spain) in culture medium for 5 min at RT. Finally, samples were mounted with 25-30 µL Fluorescent Mounting Medium (DAKO, Carpinteria, CA, USA).

Serial images were taken by using a LSM 710 Spectral Confocal Microscope (carl Zeiss) equipped with ZEN imaging software. For adherent cell culture, confocal digital single-plane (1 µm) images from z-stacks were generated. Counting of mitochondrial particles was performed on at least 30 cells per experimental point using FIJI software (https://imagej.net/Fiji) and mitochondrial fragmentation (MF) was calculated. For this procedure, mitotracker red fluorescence was scored summing the signal of z-stacks (seven to 11 planes, 0.35 µm). The same number of z-stacks for each image was merged, and an automatic

threshold level was set to create the binary image to isolate mitochondrial signal from background. To analyze mitochondrial particles, the plugin *Analise Particles* was used to obtain the area fraction and Feret´s diameter. Mitochondrial particles larger than 0.02 μm were analyzed. The total area of mitochondria, the area of the single particles, and Feret´s diameter were obtained from each field. MF was calculated by dividing the number of particles by the total number of cells.

**15. Statistical Analysis**

All data are expressed as mean ± standard deviation (SD). Statistical analysis of the data was performed using paired Student's t-test and the $\chi 2$ test using the statistical software GraphPad Prism 7 and R Software (version 3.5.0), considering those values with $p \leq 0.05$ as significant. Previously, to determine the normal distribution of the data, an analysis with the D'Agostino & Pearson test was carried out. The Kaplan-Meier curves for the association analysis of the expression levels of the *ADH5* gene and progression-free survival in CRC patients were performed using the R2 Genomics Analysis and Visualization Platform database (***https://hgserver1.amc.nl/***). The immune gene signature analysis from clinical CRC samples was performed using the normalized data from nCounter nanoString as described in the Study 1, and the online software Metaboalayst 5.0 (https://www.metaboanalyst.ca/).

# *VI. RESULTS*

# 1. Association between tumor budding, CMS subtypes and immune tumor microenvironment in CRC

Tumor budding is an important contributor of the tumor invasion prognosis and has been recently associated with the poor prognosis CMS4 subtype of CRC[72]. However, the potential relationship between the immunosuppressive microenvironment of this poor prognosis subtype and tumor buds still remain unknown. Therefore, we first examined early passages of CRC PDXs as potential models to analyze tumor budding and, secondly, we elucidated a link between high-grade budding and CMS4 subtype and specific signatures of immune evasion.

## 1.1Tumor Budding is robustly recapitulated in PDX models and is closely associated with the CMS4 Molecular Subtype of CRC

Overall, the tumor engraftment rate in mice was 84% (38 out of 45 transplanted tumors) and the mean latency period (time in days from inoculation to palpable tumor) was 30.7 ± 26.9 days for P0. This latency period was shortened in subsequent passages (15.1 ± 9.8 for P1, 10.7 ± 5.0 for P2, and 8.1 ± 3.0 for P3). Histopathological analysis of patient tumors and their corresponding PDXs revealed that the general tumor architecture, as well as the histological subtype, was preserved over several passages (**Figure 8**).

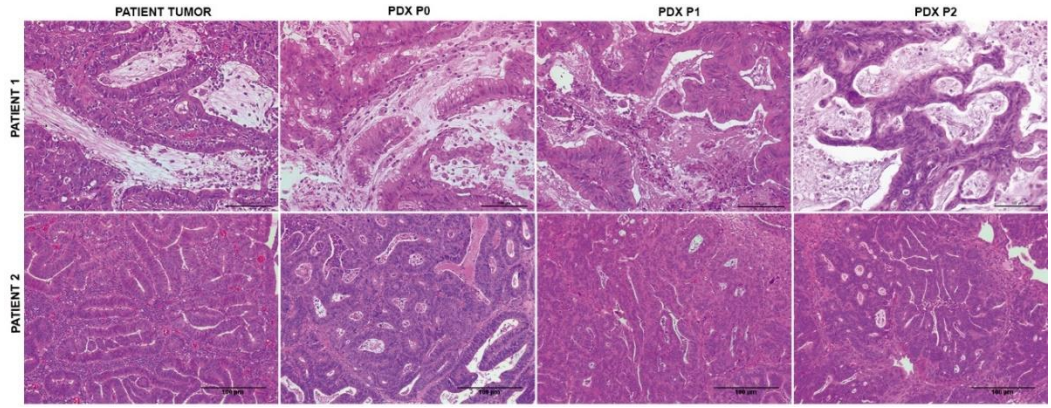


**Figure 8. Histomorphological comparison of patient tumors and their corresponding patient-derived xenografts (PDX) from passage 0 (P0), passage 1 (P1) and passage 2 (P2).** Figure shows hematoxylin-eosin staining of two representative clinical tumors and their corresponding PDXs. Scale bars correspond to 100 µm.

Next, patient tumors and xenografts were classified into CMS subtypes following the IHC-based method implemented by Trinh et al[49], in order to explore the relationship between tumor budding and molecular subtypes of CRC. Notably, each PDX model faithfully recapitulated the CMS subtype of the corresponding patient´s tumor, with a high concordance and a Cohen´s kappa coefficient of 0.96 (**Figure 9A**). Just in one case (patient 57), clinical sample and PDX model differed from each other in the CMS subtype (**Figure 9B).**

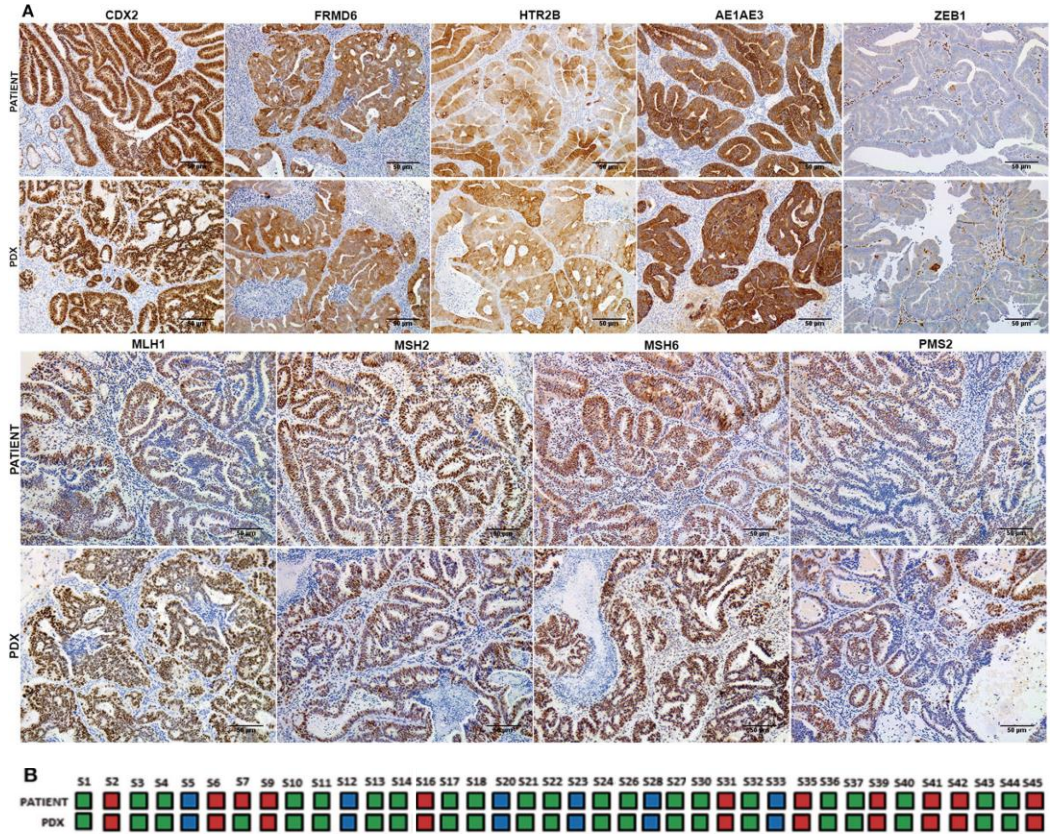


**Figure 9. IHC classification into CMS subtypes of patient tumor samples and their corresponding PDX models. (A)** Representative IHC staining for CDX2, FRMD6, HTR2B, AE1AE3, ZEB1, MLH1, MSH2, MSH6, and PMS2 of a clinical tumor and its corresponding PDX model. **(B)** CMS classification concordance between patient tumors and their corresponding PDX models. Blue color corresponds to CMS1 subtype, green color corresponds to CMS2/3 subtype, and red color corresponds to CMS4 subtype. Scale bars: 100 μm.

Notably, the determination of tumor budding status revealed a strong correlation between the number of tumor buds in patient tumor and PDX models (r=0.72, $p$<0.001) (**Figure 10A**). Moreover, most of the BD1 tumors (80% in tumor patients and 63% in PDXs) were CMS2/3, while BD3 tumors were mostly classified as poor prognosis CMS4, both in patient tumors and xenografts (**Figure**

**10B and 10C**). In addition, only 13% of human CMS4 subtypes were low budding grade (BD1) tumors.

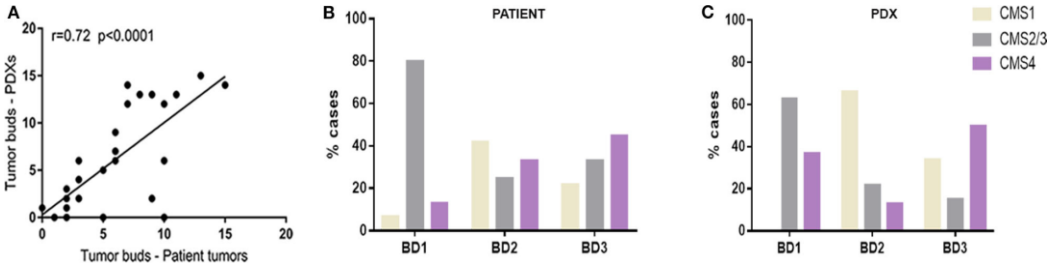


**Figure 10. Tumor budding in clinical tumors and PDX models. A)** Correlation between the number of tumor buds in clinical tumors and in their corresponding PDX models. **(B)** Distribution of CMS molecular subtypes according to tumor budding grade in patient tumors. **(C)** Distribution of CMS molecular subtypes according to tumor budding grade in xenograft models (PDX).

### 1.2. High-Grade Budding (BD3) is associated with adverse clinicopathological factors

The association of tumor budding grade with clinicopathological data was next analyzed to further deepen its relevance in the prognosis CRC. As shown in **table 8** high-grade tumor budding (BD3) was identified in 18 (40%) patient samples, followed by 12 (27%) BD2 tumors and 15 (33%) BD1 tumors. Significantly, univariate analysis revealed that high-grade tumor budding was associated with poorly differentiated carcinomas ($p$=0.02), higher stromal component ($p$=0.02), tumor vascular invasion ($p$=0.005), and presence of distant metastases ($p$=0.02) **(Table 8)**. The histological subtype, tumor size, and stromal component were entered as covariates into the final multivariate model, based on the variable selection with the Akaike information criterion (AIC) using stepwise selection **(Table 9)**. This multivariate analysis confirmed that poor histological grade was an independent factor associated with high-grade budding. Regarding the progression free survival (PFS) rate, no event data (disease progression) were

observed in low-grade budding. However, BD2 and BD3 tumors were significantly associated with poor PFS ($p$=0.03) when compared with low-grade budding **(Figure 11)**. Additionally, survival probability between BD2 and BD3 tumors were compared but no significant difference was found [HR: 95% CI De-long BD3 vs. BD2: 1.38 (0.31–6.21)] **(Figure 11)**.

**Table 8. Association between clinicopathological data of tumors and budding grade on univariate analysis.**

| Parameters | BD1 | BD2 | BD3 | *p-value* |
|---|---|---|---|---|
| **Patient characteristic (n=45)** | | | | |
| Age (years, mean ± SD) | 74.07 ± 10.33 | 75.50 ± 10.34 | 72.50 ± 10.19 | 0.7 |
| **Tumor's characteristic (n=45)** | | | | |
| **Tumor grade** | | | | |
| Low | 14 | 11 | 14 | 0.35 |
| High | 1 | 1 | 4 | |
| **TNM staging** | | | | |
| 0–I–II | 11 | 6 | 7 | 0.13 |
| III–IV | 4 | 6 | 11 | |
| **Anatomical location** | | | | |
| Left | 8 | 4 | 8 | 0.58 |
| Right | 7 | 8 | 10 | |
| **Histological subtype** | | | | |
| Well differentiated | 5 | 0 | 1 | |
| Moderately differentiated | 10 | 11 | 13 | **0.02** |
| Poorly differentiated | 0 | 1 | 4 | |
| **Mucinous component** | | | | |
| No | 10 | 10 | 10 | 0.28 |
| Yes | 5 | 2 | 8 | |
| **Inflammatory infiltrate** | | | | |
| Low | 7 | 7 | 4 | |
| Medium | 5 | 2 | 9 | 0.28 |
| High | 3 | 3 | 5 | |

| | | | | |
|---|---|---|---|---|
| **Lymphatic invasion** | | | | |
| No | 11 | 7 | 7 | 0.13 |
| Yes | 4 | 5 | 11 | |
| **Perineural invasion** | | | | |
| No | 10 | 5 | 10 | 0.43 |
| Yes | 5 | 7 | 8 | |
| **Vascular invasion** | | | | |
| Yes | 1 | 5 | 11 | **0.005** |
| No | 14 | 7 | 7 | |
| **Distant metastases** | | | | |
| No | 14 | 10 | 12 | **0.05** |
| Yes | 0 | 3 | 6 | |
| Tumor size **(cm, mean ± SD)** | 4.50 ± 1.26 | 3.75 ± 0.91 | 4.25 ± 1.10 | 0.07 |
| Stromal component **(%, mean ± SD)** | 23.33 ± 19.88 | 26.67 ± 18.74 | 41.67 ± 19.47 | 0.02 |
| **PDX model's approach** | | | | |
| Engraftment rate **(%, cases)** | 80 (12/15) | 92 (11/12) | 83 (15/18) | 0.69 |
| Latency period **(days, mean ± SD)** | 32.08 ± 35.50 | 35.40 ± 25.52 | 28.20 ± 22.53 | 0.16 |

**Table 9. Multivariate analysis of clinicopathological data of the tumors.**

| **Variables** | **BD2 vs BD1** | | | **BD3 vs BD1** | | |
|---|---|---|---|---|---|---|
| | Coef (SD) | *p*-value | OR 95% CI | Coef (SD) | *p*-value | OR 95% CI |
| **Tumor size** | −0.91 (0.46) | 0.046 | 0.40 [0.16-0.98] | −0.73 (0.44) | 0.097 | 0.48 [0.20–1.14] |
| **Moderate vs. well diff.** | 12.33 (0.92) | <0.001 | $2.27 \times 10^5$ [$3.73 \times 10^4$-$1.38 \times 10^6$] | 1.90 (1.43) | 0.184 | 6.72 [0.4–112.30] |
| **Poorly vs. well diff.** | 23.12 (0.80) | <0.001 | $1.10 \times 10^{10}$ [$2.28 \times 10^9$-$5.38 \times 10^{10}$] | 13.66 (0.80) | <0.001 | $8.57 \times 10^5$ [$2.28 \times 10^9$-$5.38 \times 10^{10}$] |
| **Stromal component** | 0.007 (0.02) | 0.772 | 1.007 [0.95–1.05] | 0.04 (0.02) | 0.055 | 1.04 [0.99–1.08] |

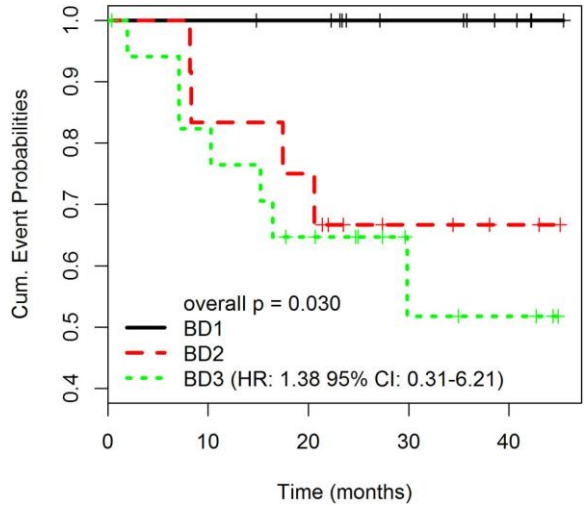


**Figure 11. Progression-free survival (PFS) rates according to different grades of tumor budding.** Overall *p* is 0.030 (BD3, HR: 1.38 95% CI: 0.31–6.21). The *p-values* for pairwise comparisons are BD1 vs. BD2 = 0.034; BD1 vs. BD3 = 0.022; BD2 vs. BD3 = 0.595.

### 1.3. Gene expression of immune checkpoints, Toll-like receptors (TLRs), and chemokines profiles reveals distinct patterns according to tumor budding grade in patients and xenografts

Next, we sought to investigate the association between tumor budding and immune-related genes expression profiles. Hence, those immune-related genes overexpressed in high-grade tumor budding compared with low-grade budding were identified using the PanCancer immune profiling panel from NanoString. In addition, the immune gene expression profiles of patient tumors were compared with those of their corresponding xenograft models (P0).

The comparative analysis revealed a general upregulation of immune checkpoint-related genes in BD3 tumors in comparison with BD1 tumors **(Figure 12)**. Interestingly, these immune signatures were remarkably preserved in their corresponding PDX models. Particularly, a higher expression of *PDL1*, *TIM-3*, *NOX2* and *IDO1* genes was observed in BD3 tumors. However, *PD1* and *CTLA4*

genes were less expressed in higher tumor budding grade tumors, both in patients and xenografts **(Figure 12)**.

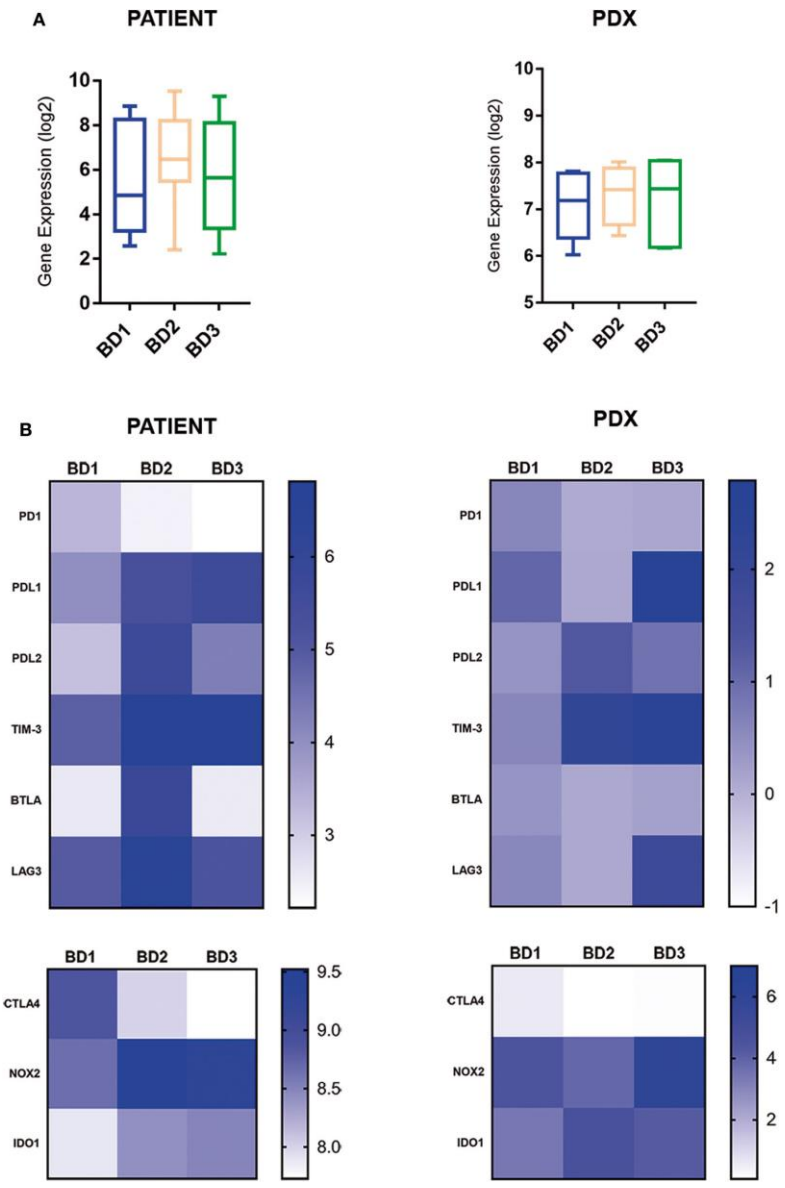


**Figure 12. Expression of immune checkpoint-related genes in clinical tumors and PDX models.** Global (**A**) and single (**B**) gene expression levels of immune inhibitor checkpoints in patient tumors and their corresponding PDX models, according to different grades of tumor budding (BD1, BD2, BD3).

The expression of the *TLR* superfamily also displayed a high correspondence between patients and PDXs and a higher expression in high-grade budding tumors **(Figure 13)**. Specially, *TLR1*, *TLR3*, *TLR4*, and *TLR6* were notably overexpressed in BD3 compared to BD1 tumors **(Figure 13)**.

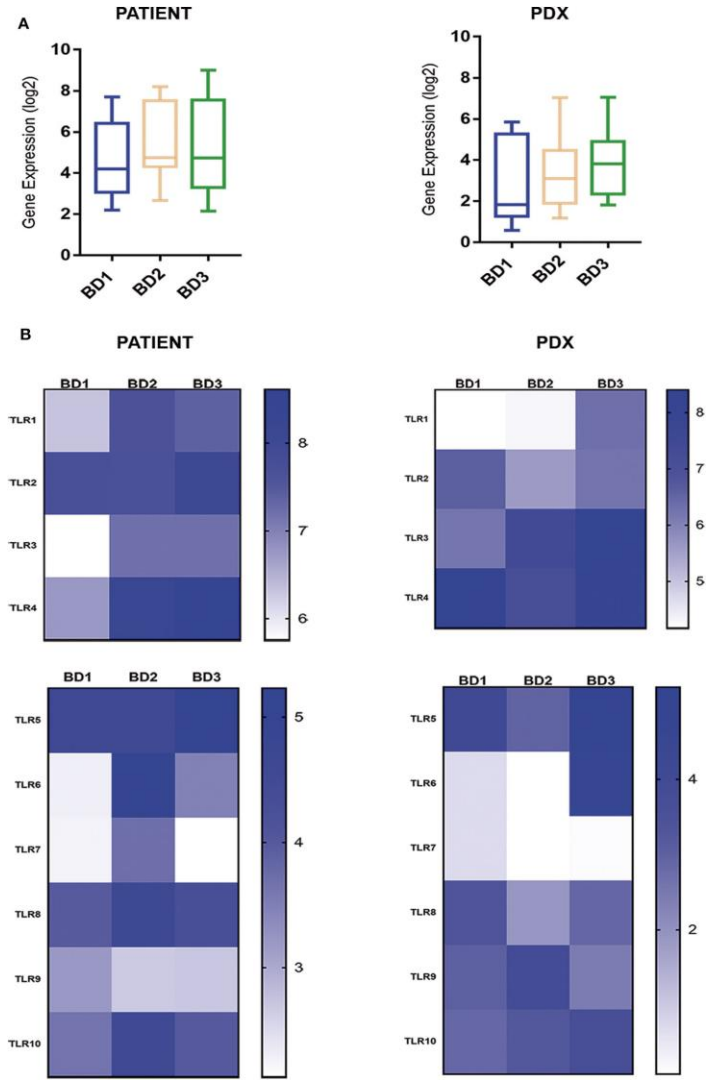


**Figure 13. Expression of TLR gene family in clinical tumors and PDX models.** Global (**A**) and single (**B**) gene expression levels of the TLR gene family in patient tumors and their corresponding PDX models according to different grades of tumor budding (BD1, BD2, BD3).

Regarding the CX chemokine receptor gene family, the results showed that BD3 tumors were associated with a higher expression of *CXCR2* and *CXCR4* **(Figure 14)** than BD1 tumors. Among the chemokine ligands, *CXCL1*, *CXCL2*, *CXCL6*, and *CXCL9* genes also displayed a higher expression in BD3 tumors compared to low-grade tumor budding **(Figure 15)**. Notably, these distinct gene expression profiles of chemokine receptors and ligands according to different budding grades were in general well preserved in the PDX models.

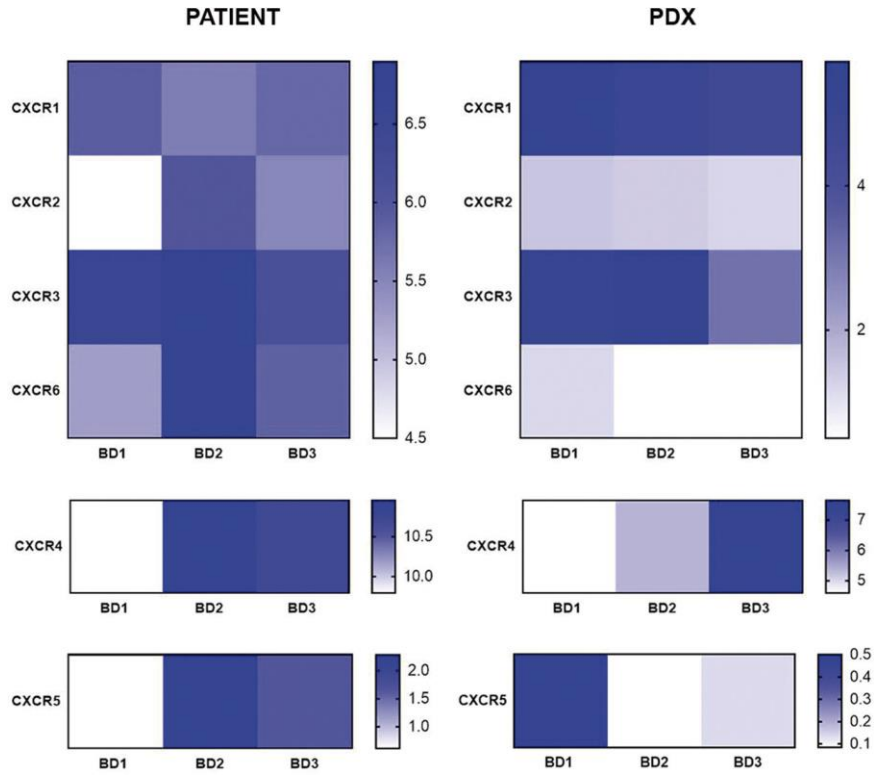


**Figure 14. Expression of CX chemokine receptor gene family in clinical tumors and PDX models.** Gene expression of CX chemokine receptors in patient tumors and their corresponding PDX models, according to different grades of tumor budding (BD1, BD2, BD3).

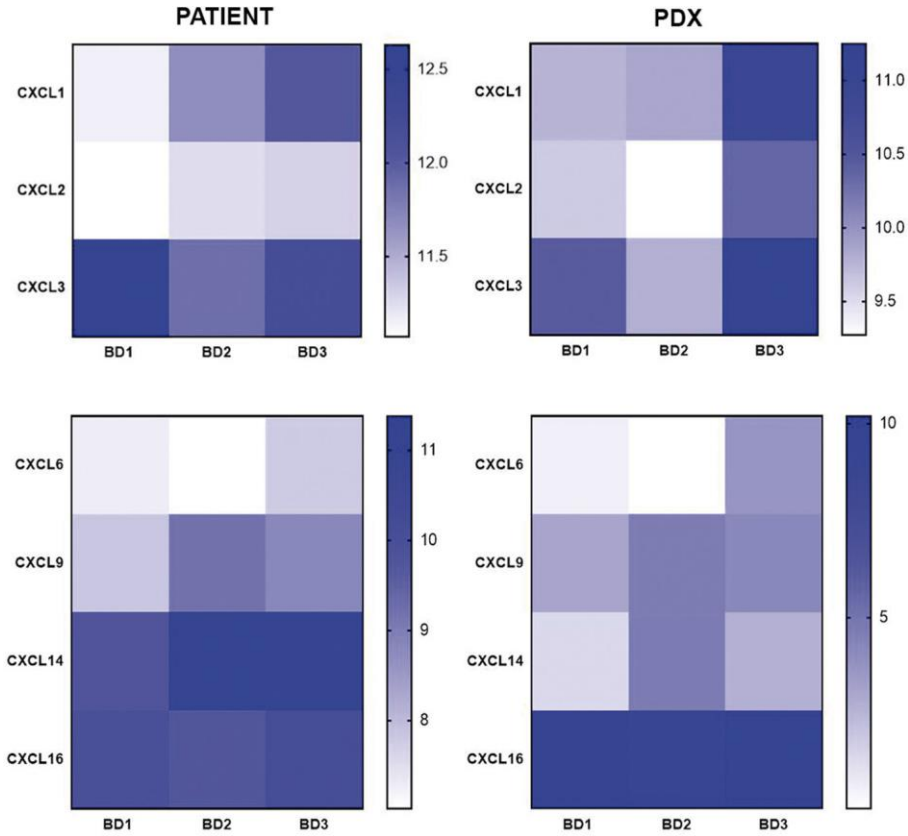


**Figure 15. Expression of CX chemokine ligand gene family in clinical tumors and PDX models.** Gene expression of CX chemokine ligands in patient tumors and their corresponding PDX models, according to different grades of tumor budding (BD1, BD2, BD3).

## 1.4. Expression of eNOS in tumor cells is associated with poor prognosis CMS4 tumors

We have previously reported that eNOS is upregulated in human mesenchymal/stem-like tumors, and poorly differentiated aggressive adenocarcinomas[117]. Therefore, we next investigated the potential association between the expression of this NO synthase isoform, CMS subtype and tumor budding grade in CRC tumors. Notably, a significant higher epithelial expression

of eNOS was found in CMS4 tumors ($p$=0.0213, **Figure 16)**. Thus, 91% of the CMS4 cases displayed eNOS expression in the tumor epithelial compartment, while for CMS1 and CMS2/3 tumors the eNOS epithelial expression was 62% and 44% respectively **(Figure 16A)**. Moreover, more epithelial eNOS positive tumors were found in high-grade budding (BD3) tumors than in low budding grade tumors **(Figure 16B)**.

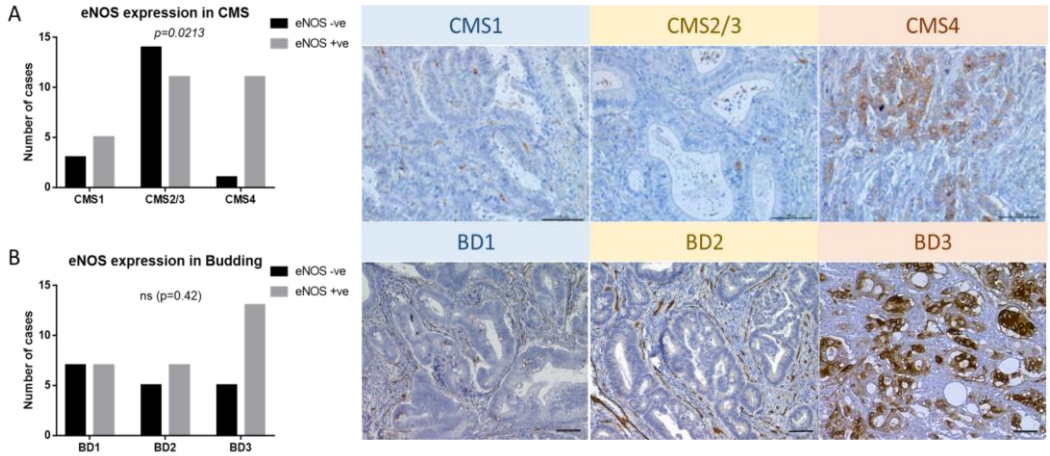


**Figure 16. Endothelial nitric oxide (eNOS) expression according to CMS molecular subtypes and budding grades in CRC.** (**A**) eNOS expression in the epithelial compartment according to CMS subtype (left) and representative images from IHC detection of eNOS in CMS1, CMS2/3 and CMS4 tumors (right). (**B**) eNOS expression in the epithelial compartment according to budding grade (left) and representative images from IHC detection of eNOS in BD1, BD2 and BD3 tumors (right).

## 2. Association between GSNOR/ADH5 expression, CMS subtypes and immune tumor microenvironment in CRC

It is plausible that eNOS upregulation in CMS4 and BD3 tumors may be also associated with an altered SNO homeostasis in these particularly aggressive CRC tumors. On the other hand, we have previously reported that impaired expression of GSNOR/*ADH5*, which is a key enzyme for SNO homeostasis, is associated with poor response to treatment and survival in HER-2 aggressive type of breast cancer[115]. Therefore, we next investigated the significance of GSNOR/*ADH5* in CRC.

### 2.1 Low GSNOR/ADH5 expression is associated with poor prognostic histopathological features and the CMS4 subtype

We first performed an inmunohistochemical analysis to evaluate GSNOR/*ADH5* expression in primary tumors from 53 CRC patients. IHC expression of GSNOR/*ADH5* was detected in the cytoplasm of epithelial cells. Notably, GSNOR/*ADH5* expression was higher in peritumoral tissue compared to tumor tissue **(Figure 17A)** and, accordingly those tumors with low expression of GSNOR/*ADH5* were characterized by poor prognostic histopathological features (**Table 10**). Hence, a low expression of GSNOR/*ADH5* was significantly associated with higher tumor TNM stage ($p$=0.045) and higher tumor size ($p$=0.0006). Besides, a statistical trend was observed towards low expression of this denitrosylase enzyme in poor differentiated tumors ($p$=0.057). Regarding budding grade, a comparatively higher number of BD3 tumors was observed in the group of tumors with low expression of GSNOR/*ADH5*.

**Table 10**. **Association of GSNOR/ADH5 expression with clinicopathological characteristics of CRC patients.**

| Clinicopathological characteristics | GSNOR/ADH5 high expression n (%) | GSNOR/ADH5 low expression n (%) | *p-value* |
|---|---|---|---|
| **Gender** | | | |
| Male | 22 (62.9%) | 13 (37.1%) | *p=0.380* |
| Female | 9 (50.0%) | 9 (50.0%) | |
| **Anatomical location** | | | |
| Right | 19 (61.3%) | 12 (38.7%) | *p=0.413* |
| Left | 11 (50.0%) | 11 (50.0%) | |
| **Tumoral grade differentiation** | | | |
| High grade | 2 (33.3%) | 4 (66.7%) | *p=0.222* |
| Low grade | 28 (59.6%) | 19 (40.4%) | |
| **Tumor stage** | | | |
| Stage 0-I-II | 20 (69.0%) | 9 (31.0%) | ***p=0.045*** |
| Stage III-IV | 10 (43.5%) | 13 (56.5%) | |
| **Tumor size** | | | |
| < 4.2 cm | 22 (78.6%) | 6 (21.4%) | ***p<0.001*** |
| > 4.2 cm | 8 (32.0%) | 17 (68.0%) | |
| **Histopathological diagnosis** | | | |
| Well differentiated | 5 (83.3%) | 1 (16.7%) | |
| Moderately diff. | 24 (58.5%) | 17 (41.5%) | ***p=0.057*** |
| Poor differentiated | 1 (16.7%) | 5 (83.3%) | |
| **MSI status** | | | |
| MSS | 23 (52.3%) | 21 (47.7%) | *p=0.159* |
| MSI | 7 (77.8%) | 2 (22.2%) | |
| **Mucinous** | | | |
| Yes | 10 (58.8%) | 7 (41.2%) | *p=0.822* |
| No | 20 (55.6%) | 16 (44.4%) | |
| **Lymphatic invasion** | | | |
| Yes | 11 (47.8%) | 12 (52.2%) | *p=0.258* |
| No | 19 (63.3%) | 11 (36.7%) | |
| **Vascular invasion** | | | |
| Yes | 9 (50.0%) | 9 (50.0%) | *p=0.486* |
| No | 21 (60.0%) | 14 (40.0%) | |

| | | | |
|---|---|---|---|
| **Perineural invasion** | | | |
| Yes | 13 (56.5%) | 10 (43.5%) | *p=0.991* |
| No | 17 (56.7%) | 13 (43.3%) | |
| **Metastasis or recurrence** | | | |
| Yes | 6 (40.0%) | 9 (60.0%) | *p=0.125* |
| No | 24 (63.2%) | 14 (36.8%) | |
| **Immune infiltrate** | | | |
| Low | 9 (56.3%) | 7 (43.7%) | |
| Medium | 10 (62.5%) | 6 (37.5%) | *p=0.818* |
| High | 5 (50.0%) | 5 (50.0%) | |
| **Immune infiltrate** | | | |
| BD1 | 10 (71.4%) | 4 (28.6%) | |
| BD2 | 8 (61.5%) | 5 (38.5%) | *p=0.179* |
| BD3 | 11 (42.3%) | 15 (57.7%) | |
| **Molecular subtype** | | | |
| CMS1 | 8 (80.0%) | 2 (20.0%) | |
| CMS2/3 | 18 (66.7%) | 9 (33.3%) | ***p=0.007*** |
| CMS4 | 4 (25.0%) | 12 (75.0%) | |

Next, the CRC tumors were classified into the different consensus molecular subtypes (CMS1, CMS2/3 and CMS4). Remarkably, the poor prognosis CMS4 molecular subtype was characterized by a significantly lower expression of the denitrosylase enzyme compared to the rest of CRC subtypes ($p$=0.007, **Table 10, Figure 17B-C**). Hence, 75% (12/16) of CMS4 tumors displayed low GSNOR/*ADH5* expression in comparison with 33% (9/27) or 20% (2/10) of CMS2/3 or CMS1 subtypes, respectively. The poorer differentiation of low GSNOR/*ADH5* tumors was also confirmed by their comparatively low expression of the intestinal differentiation marker CDX2 ($p$=0.0276) and AE1AE3 cytokeratin ($p$=0.0391) **(Figure 17D-E)**.

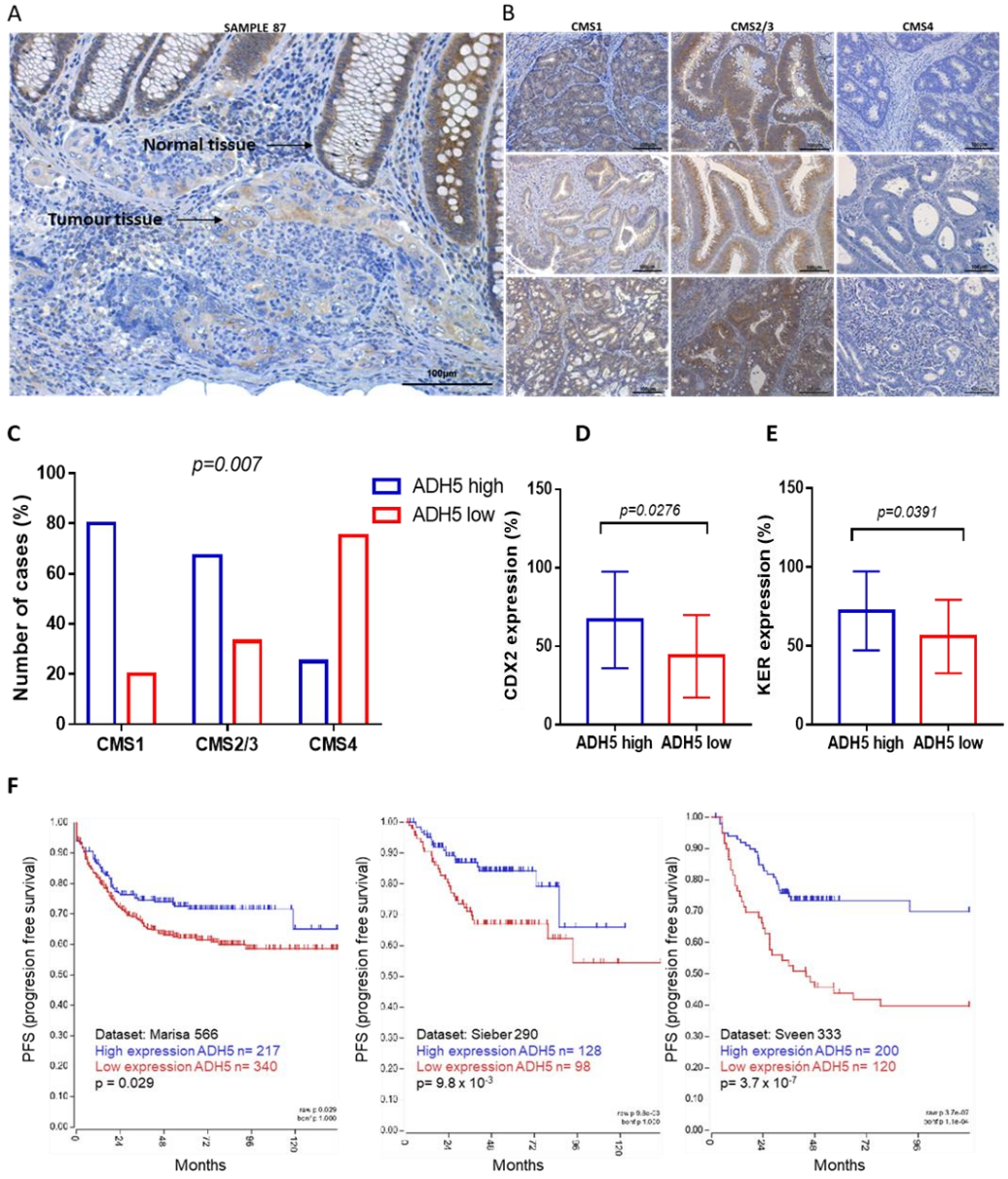


**Figure 17. GSNOR/ADH5 expression in CRC is associated with the poor prognosis CMS4 subtype**. (**A**) IHC analysis of GSNOR/*ADH5* in peritumoral and tumor tissue and (**B**) in the consensus molecular subtypes of CRC. Scale bars: 100 µm. (**C**) Association between GSNOR/*ADH5* positivity by IHC and CMS subtypes. (**D**) IHC quantification of the intestinal differentiation marker CDX2 and (**E**) cytokeratin (KER) in high and low ADH5 tumors. (**F**) Progression-free survival rates according to *ADH5* gene expression in different CRC patient datasets.

To further confirm the association between a lower expression of GSNOR/*ADH5* and a worse prognosis, the relationship between *ADH5* gene expression and PFS was analyzed in different datasets of gene expression and CRC survival. To do this, the R2 Genomics Analysis and Visualization Platform database (***https://hgserver1.amc.nl/***) was used. As shown in **Figure 17F**, corresponding Kaplan-Meier curves confirmed that a low *ADH5* expression in tumors was significantly associated with a poor PFS rate in CRC patients.

### 2.2. Low GSNOR/ADH5 expression is associated with an immunosuppressive microenvironment and cytotoxic T cell exclusion in clinical CRC tumors

As shown above, our analysis of GSNOR/*ADH5* expression in clinical CRC tumors, indicated that the low expression of this denitrosylase enzyme was associated with the CMS4 subtype. Importantly, this poor prognosis CMS subtype has been related with an inflamed, angiogenic and immunosupressive tumor microenvironment[56,120]. Therefore, we next used the nCounter PanCancer immune profiling panel in 20 CRC tumors to explore the relationships between GSNOR/*ADH5* expression and the tumor immune microenvironment. As shown in **Figure 18A**, ADH5-low tumors were characterized by a significant reduction in gene signatures of cytotoxic cell populations compared to ADH5-high tumors. Specifically, ADH5-low tumors displayed a significant downregulation of genes related to CD8+ T cells and exhausted CD8+ T cells. Moreover, ADH5-low tumors were characterized by the downregulation of genes associated with cytotoxic cell function, including T cell function, chemokines, cytokines, cytotoxicity, NK function and antigen processing (**Figure 18B**). Importantly, a specific immune gene signature was found in ADH5-low tumors, with 12 and 11 genes found to be upregulated and downregulated, respectively, compared to ADH5-high tumors (**Figure 18C**). A sub-set of downregulated genes were

cytotoxicity-related, and they were also found to be downregulated in ADH5-high non-MSI tumors (*GNLY*, *GZMA*, *CXCR6*, *CD3D* and *TARP*). On the contrary, the other sub-set of downregulated genes and all the upregulated genes were restricted to ADH-low tumors. Hence, a number of genes known to inhibit (*ITGA2*, *LGALS3* and *CD46*) and promote (*CASP3*, *CD40*, *CKLF*) anti-tumor immunity were upregulated and downregulated, respectively, in ADH5-low tumors (**Figure 18C**).

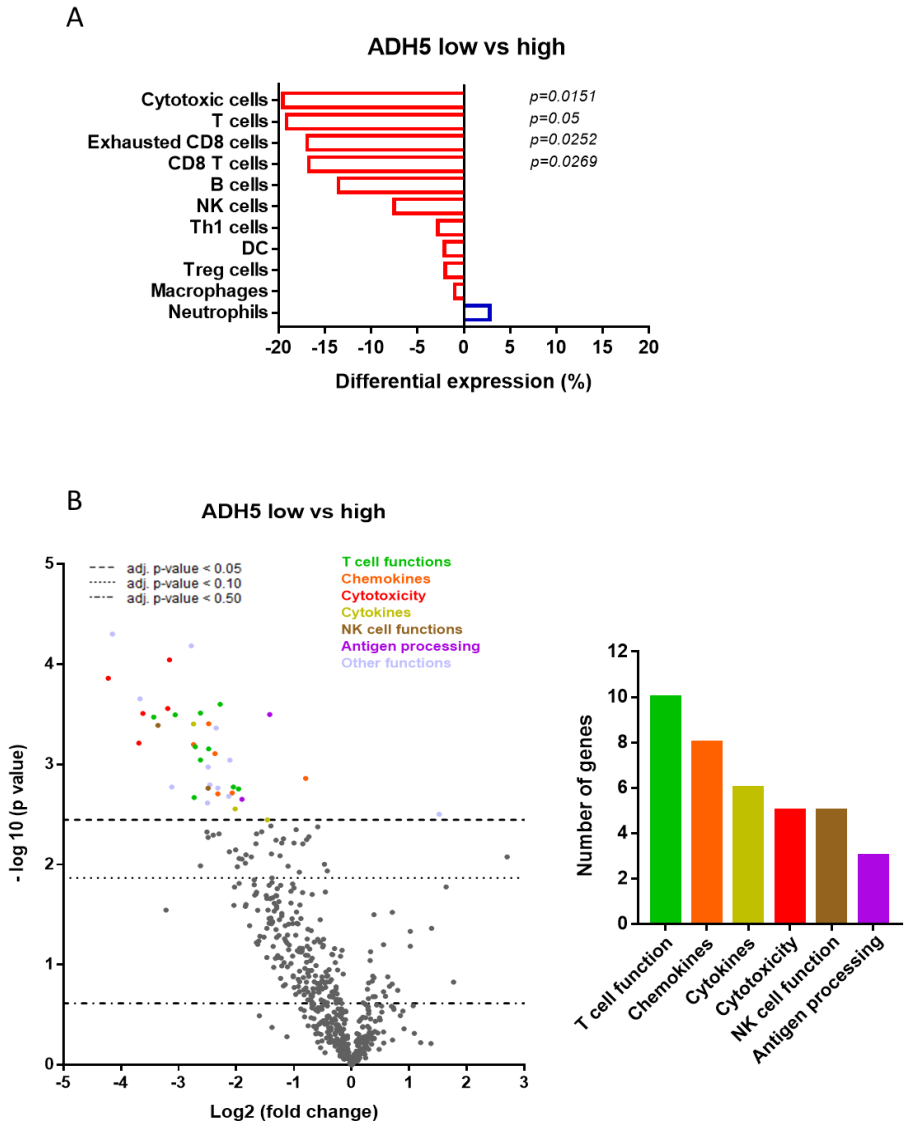

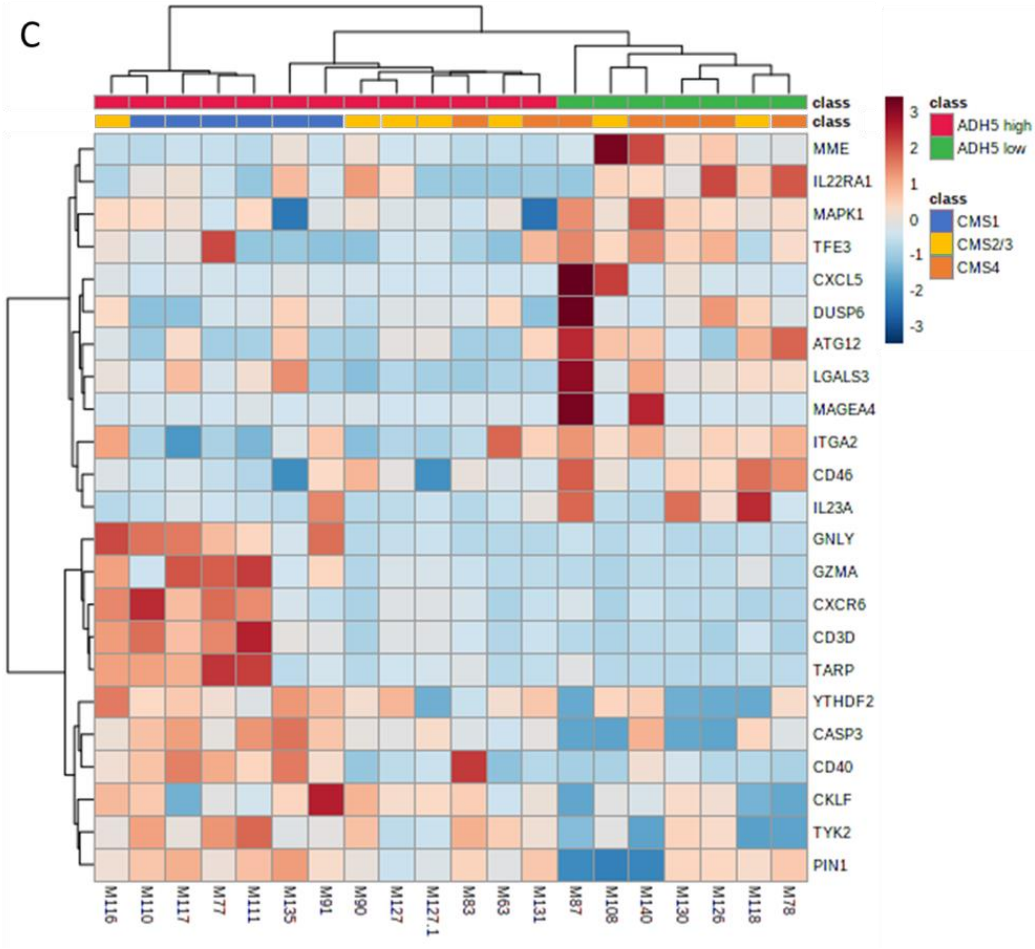


**Figure 18. Immune profiling gene expression panel in CRC patient samples.** (**A**) Immune cell populations in ADH5-high and low tumor samples. (**B**) Differential expression analysis showing the overexpressed genes in ADH5-high tumors in colors according to different categories and functions, and the number of genes differentially expressed between ADH5-high and low tumors according to different categories and functions. (**C**) Top 23 genes showing a distinct expression profile between ADH5-low and ADH5-high tumors.

### 2.3. GSNOR-deficient (ADH5-KO) CRC cells show higher basal levels of S-nitrosylated proteins

In order to deepen the role of GSNOR/*ADH5* in CRC, we next generated CRC cells deficient in this denitrosylase enzyme. To achieve this, we used the CRISPR-Cas9 methodology in HCT116 and DLD1 cells to generate a genomic deletion encompassing exons 3 and 4 of *ADH5* gene, which also includes the sequence coding for the active site of GSNOR enzyme **(Figure 19A and 19B)**. As shown in **Figure 19C**, CRC cells completely deficient in GSNOR (*ADH5*-KO) were characterized by significant higher basal levels of S-nitrosylated proteins, compared to parental cells (*ADH5*-WT) **(Figure 19C)**. Accordingly, *ADH5*-KO cells also displayed a higher sensitivity to high nitrosative levels of CSNO (**Figure 19D**).

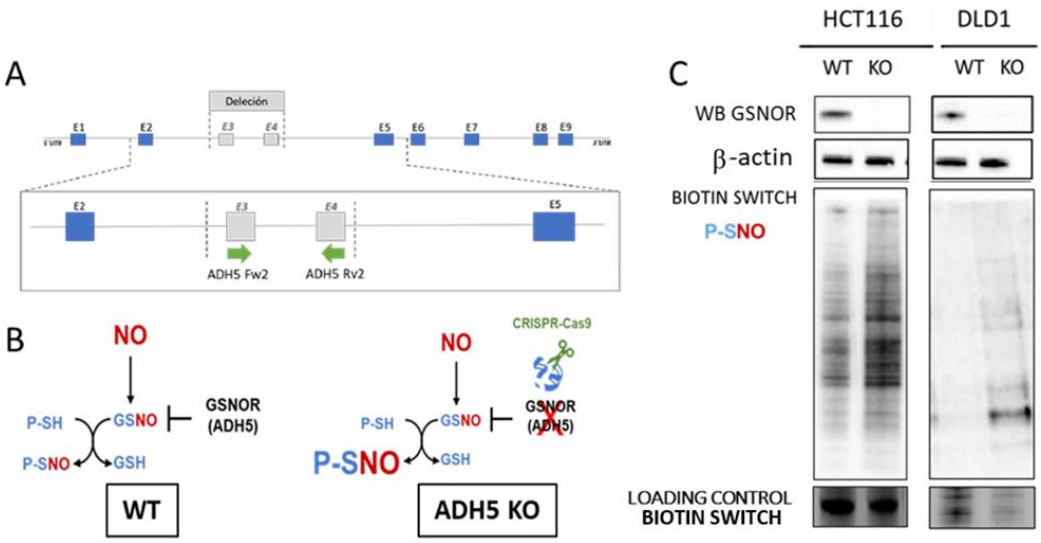

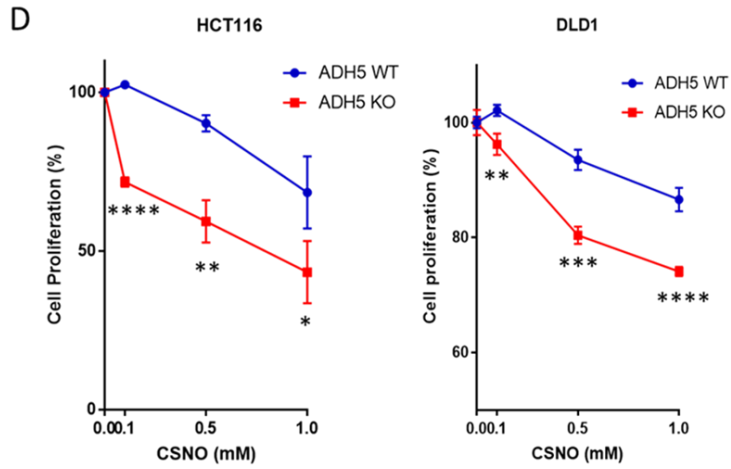


**Figure 19**. **Genetic deletion of GSNOR/*ADH5* increases the basal levels of S-nitrosylated proteins in CRC cells.** (**A**) Detail of the genomic region in the *ADH5* gene deleted by CRISPR-Cas9. The *ADH5* Fw2 and *ADH5* Rv2 primer pair was used for PCR verification of the deletion. (**B**) Balance between GSNO and S-nitrosylated proteins (P-SNO) in *ADH5*-WT and *ADH5*-KO cells. (**C**) Immunodetection of GSNOR/*ADH5* protein expression and basal levels of S-nitrosylated proteins (biotin-switch) in *ADH5*-WT and *ADH5*-KO cells. (**D**) Proliferation of *ADH5*-WT and *ADH5*-KO cells treated with high nitrosative levels of CSNO.

## 2.4. GSNOR deficiency increases the tumorigenic and tumor-initiating capacity of CRC cells

Since our analyzes in clinical samples indicated that low GSNOR/*ADH5* expression in tumors was associated with a worse prognosis, we next analyzed the tumorigenic capacity of GSNOR-deficient CRC cells. The analyses of tumorospheres or tumor spheroids generated from the proliferation of a tumor stem or progenitor cell constitute *in vitro* functional tests of these cell subpopulations[121]. Therefore, the ability of *ADH5*-WT and *ADH5*-KO cells to generate tumorospheres and tumor spheroids *in vitro* were compared. As shown in **Figure 20**, both HCT116 and DLD1 *ADH5*-KO cells possessed significantly greater capacity to generate tumorospheres (**Figure 20A**) and tumor spheroids (**Figure 20B**), compared to their corresponding parental counterparts.

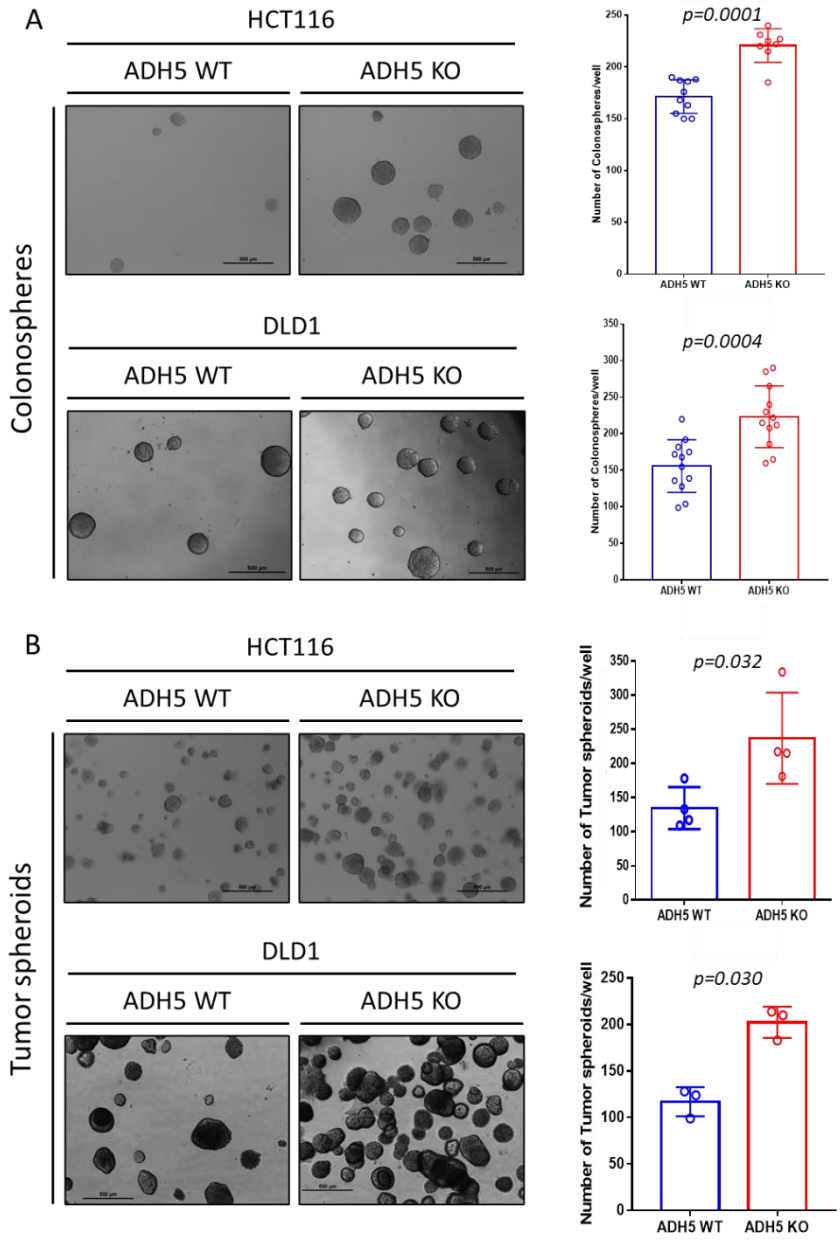


**Figure 20. GSNOR/*ADH5* deficiency increases the capacity of CRC cells to form tumorospheres and tumor spheroids *in vitro***. (**A**) Representative images (left) and number (right) of tumorospheres formed *in vitro* by *ADH5*-WT and *ADH5*-KO CRC cells. (**B**) Representative images (left) and number (right) of tumor spheroids formed *in vitro* by *ADH5*-WT and *ADH5*-KO CRC cells. Data are mean ± SD of at least three independent assays. Scale bars: 500 μm.

As shown above, those primary CRC tumors with low GSNOR/*ADH5* expression were also characterized by a lower expression of CDX2 by IHC. Of note, decreased expression of CDX2 has been related with a cellular stem cell state in human CRC[122]. Accordingly, IHC analysis of paraffin-embedded tumorospheres demonstrated significantly lower expression of CDX2 in both HCT116 and DLD1 *ADH5*-KO cells compared to their parental counterparts (**Figure 21**). Interestingly, the decrease of CDX2 expression in *ADH5*-KO tumorospheres was accompanied by an upregulation of IHC PDL1 expression (**Figure 21**), which also has been reported to promote cancer stem cell (CSC) expansion in CRC[123]. Therefore, these results also suggest that GSNOR/*ADH5* deficiency promoted the stemness of CRC cells increasing their tumorosphere formation capacity.

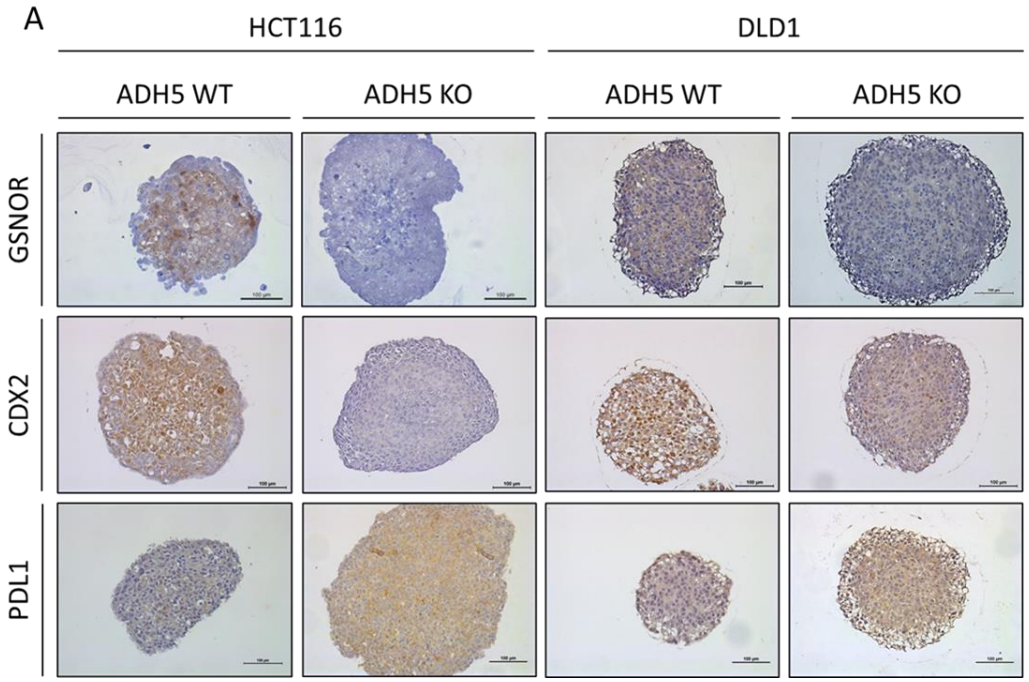

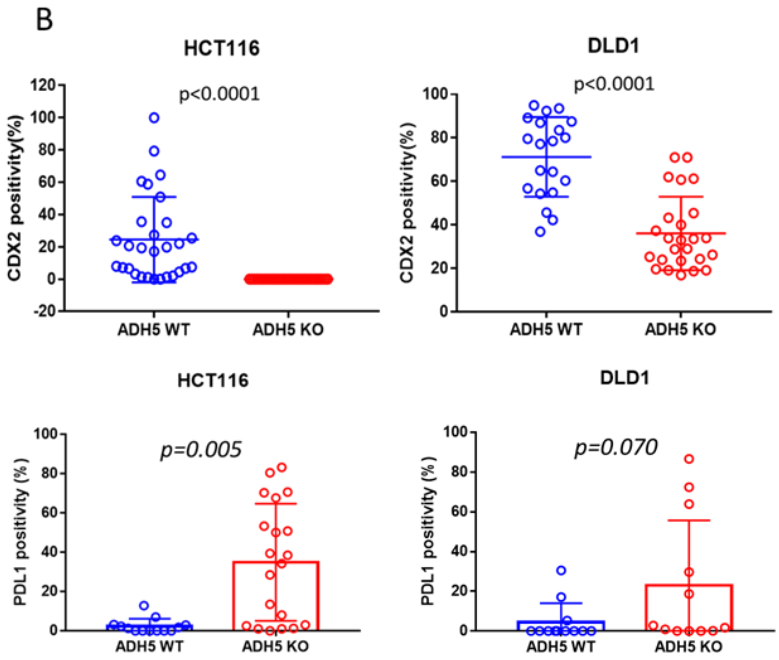


**Figure 21. GSNOR/*ADH5* deficiency promotes dedifferentiation in CRC cells.** (**A**) Representative images of IHC detection of GSNOR, CDX2 and PDL1 in tumorospheres from *ADH5*-WT and *ADH5*-KO CRC cells. (**B**) Quantitative analysis of CDX2 and PDL1 expression in tumorospheres from *ADH5*-WT and *ADH5*-KO CRC cells.

Because CSCs are thought to be responsible for tumor propagation and re-initiation, they are also identified by analyzing their tumor-initiating capacity using the *in vivo* LDA. Therefore, an *in vivo* tumor formation assay was performed by implanting a limited number of *ADH5*-WT or *ADH5*-KO HCT116 cells in immunodeficient mice **(Figure 22A)**. As shown in **figure 22B**, GSNOR/*ADH5* deficiency in CRC cells increased by 5-fold their tumor-initiating competence. Hence, tumor-initiating cell frequency by limiting dilution analysis was 1 in 33 for *ADH5*-KO and 1 in 175 for *ADH5*-WT cells ($p$=0.001, $X^2$ test)**.** Besides, when a non-limiting number of cells were implanted, *ADH5*-KO cells generated tumors with a significant higher final volume ($p$=0.0463) than those obtained by implanting *ADH5*-WT cells (**Figure 22C-D**).

Taken as a whole, the above results indicate that deficiency of GSNOR/*ADH5* CRC cells increases their tumorigenic and tumor-initiating capacities.

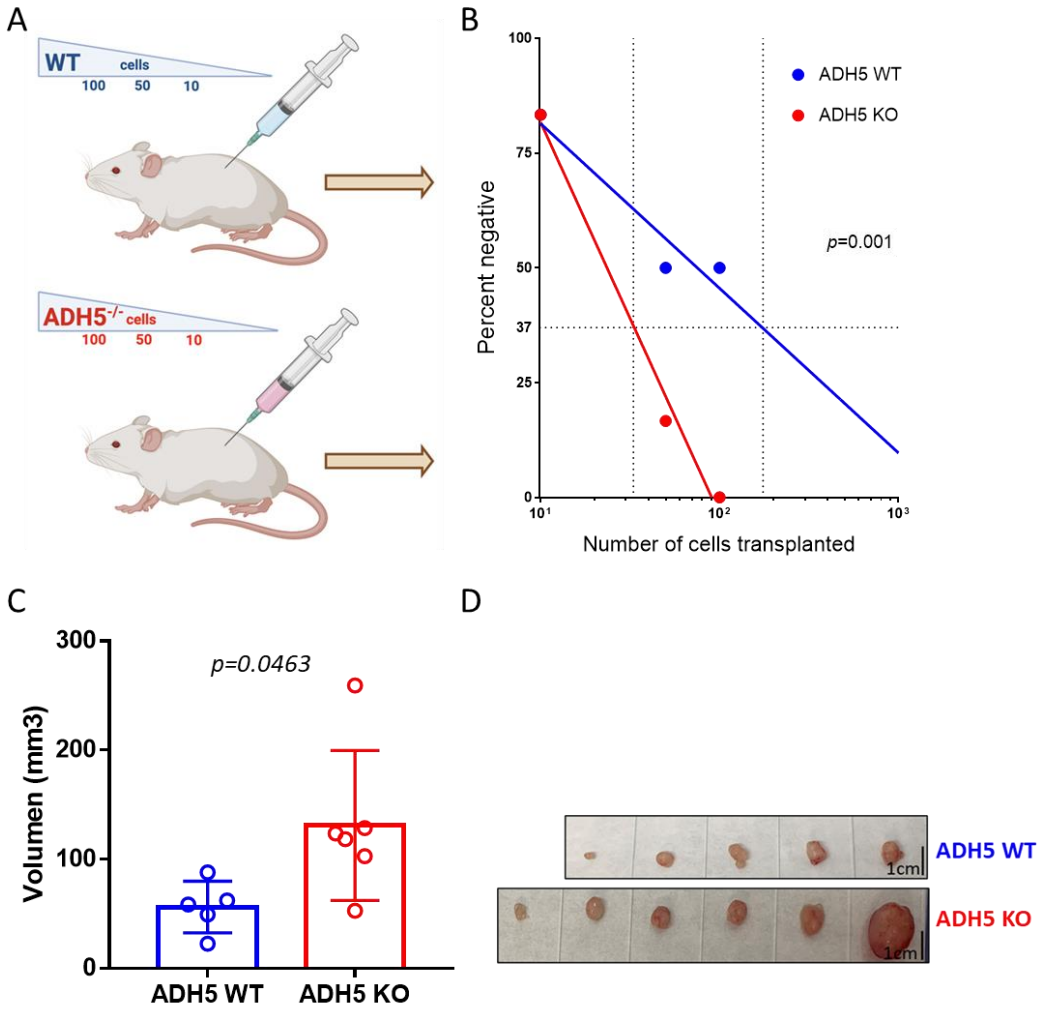


**Figure 22. *In vivo* limiting dilution assay.** (**A**) For the *in vivo* limiting dilution assay the indicated number of *ADH5*-WT or *ADH5*-KO HCT116 cells were subcutaneously injected in the flanks of immunodeficient mice and tumor formation was assayed 30 days following injection**. (B)** Final volume of tumors formed after 30 days from injection of a non-limiting number (500 cells) of *ADH5*-WT or *ADH5*-KO HCT116 cells. Data are mean ± SD.

### 2.5 Higher tumorigenic capacity of GSNOR-deficient cells is not associated with a greater proliferative capacity but with metabolic disturbances

Higher cell proliferation would explain the greater aggressiveness of GSNOR/*ADH5* deficient cells. However, cell proliferation experiments showed that there were no significant differences in their proliferative capacity, compared to parental cells (**Figure 23A)**. On the other hand, it is known that cancer cells adopt various strategies that allow them to be more aggressive, such as reprogramming their cellular metabolism[124]. Thus, it is known that stem cells and tumor cells share a distinct metabolic profile from other cell types. Both cell types obtain energy preferentially through high glycolytic activity, converting glucose to lactate, even in aerobic conditions. This process is known as aerobic glycolysis or the "*Warburg effect*", and it is one of the metabolic alterations in cancer cells most directly related to tumor aggressiveness[125]. For this reason, the levels of lactate secreted to the culture medium were determined in GSNOR deficient and parental cells. As shown in **Figure 23B**, although their proliferation capacity was comparable to that of parental cells, *ADH5*-KO cells showed significantly higher levels of lactate production. Moreover, *ADH5*-KO cells were also characterized by a lower basal ATP content and a higher sensibility to the glycolysis inhibitor 2DG compared to *ADH5*-WT cells **(Figure 23B).** These data suggest that GSNOR/*ADH5* deficiency in CRC cells is accompanied by metabolic disturbances involving an increased aerobic glycolytic activity.

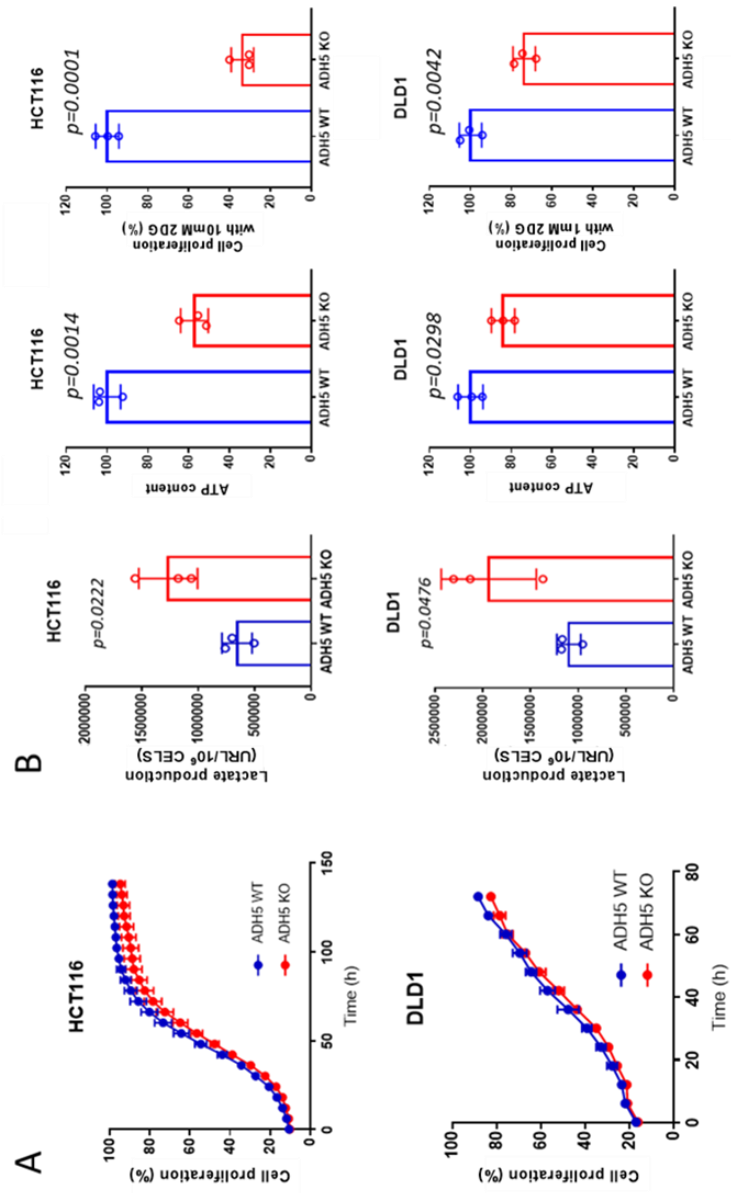


**Figure 23. GSNOR/*ADH5* deficiency in CRC cells is associated with an increased aerobic glycolytic activity**. (**A**) Cell proliferation rates of *ADH5*-WT and *ADH5*-KO cells. (**B**) Lactate production (relative light unit per million cells), basal ATP content and cell proliferation under treatment with the glycolysis inhibitor 2-deoxy-D-glucose (2DG) in *ADH5*-WT and *ADH5*-KO cells. Data are mean ± SD.

## 2.6. The metabolic alteration in GSNOR/ADH5 deficient CRC cells is related to changes in the mitochondrial network

Mitochondrial dynamics has been proposed to play an important role in regulating the cellular dedifferentiation mechanisms that accompany the acquisition of stem characteristics and may also play a role in the generation and maintenance of tumor stem cell populations. Thus, when cell dedifferentiation is induced or during malignant transformation of normal cells, fragmentation of the mitochondrial network occurs, accompanied by increased aerobic glycolytic activity, and increased lactate production[126,127]. Therefore, we next analyzed the mitochondrial network morphology in *ADH5*-WT and *ADH5*-KO cells. For this, cells were stained with MitoTracker Red CMXRos, a red fluorescent compound that stains mitochondria in living cells allowing visualization of the mitochondrial network. As seen in the confocal microscopy images **(Figure 24A)**, parental cells showed a continuous mitochondrial network, with numerous ramifications and fusions, whereas in *ADH5*-KO cells the mitochondria appeared with a much more punctuated morphology. Quantitative analysis confirmed a significantly higher number of mitochondria per cell in *ADH5*-KO cells compared to parental cells **(Figure 24B)**. Furthermore, when the size of the mitochondria was analyzed through Feret diameter, which is a common parameter in the analysis of irregularly shaped particles, a significantly smaller mitochondrial diameter was observed in *ADH5*-KO cells compared to their parental counterparts **(Figure 24C)**, Altogether, these data confirm that GSNOR/*ADH5* deficiency in CRC cells is accompanied by an alteration of the cellular mitochondrial network, which is compatible with a higher rate of mitochondrial fission, increased aerobic glycolytic activity, and increased lactate production.

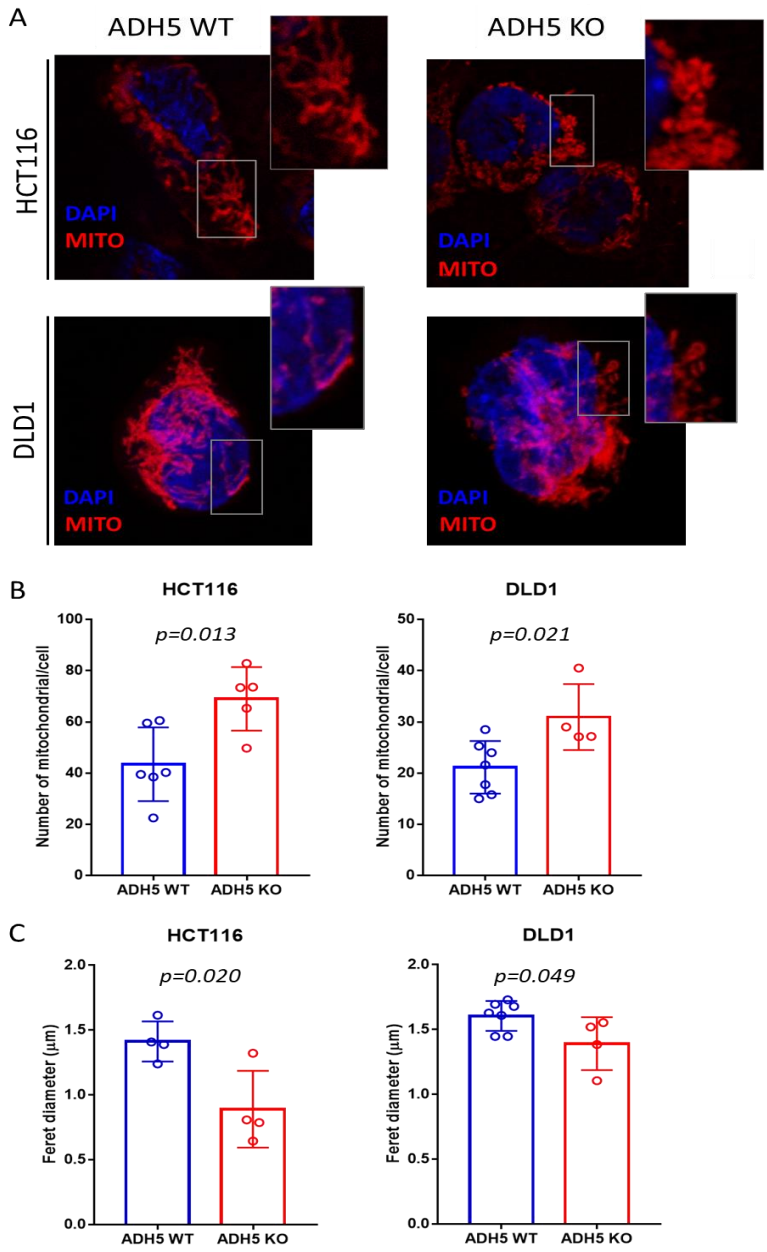


**Figure 24. GSNOR deficiency is associated with a more fissioned mitochondrial network.** (**A**) Representative images obtained through confocal microscopy, mitochondria appear marked in red after staining with MitoTracker Red and nuclear staining with DAPI in blue. (**B**) Graphs representing the number of mitochondria per cell (mean ± SD). (**C**) Graphs representing the mean mitochondrial diameter (Feret) in both HCT116 and DLD1 cell lines (mean ± SD).

# *VII. DISCUSSION*

## 1. Association of Tumor Budding with Immune Evasion Pathways in Primary CRC and PDXs

Taking into account that tumor heterogeneity is one of the major obstacles in the success of the new personalized therapies for CRC, preclinical platforms which faithfully represent the complex tumor biology are urgently needed. Furthermore, the significance of tumor budding as an independent prognostic factor has now been well established, reinforcing the notion that may constitute a promising target for cancer therapy. However, the interaction between tumor budding and the immune tumor microenvironment still remains unclear. The present study demonstrates that tumor budding is reliably reproduced in early passages of PDXs of CRC. Moreover, our data support that high-grade tumor budding is intimately connected with poor prognosis CMS4 subtype and with specific gene signatures related to tumor immune evasion.

Our data confirmed that tumor budding is associated with adverse clinicopathological characteristics, such as tumor size, poor histological differentiation, vascular invasion, and poor outcome, as previously reported in several types of cancer[63,69,72,128]. An interesting finding derived from our study was the high level of correspondence between the budding score in clinical tumors and their corresponding PDX models. Intriguingly, the immune deficiency in host mice did not promote an increase in tumor budding. Pu et al.[129] demonstrated that patient-derived immune cells coexist in the first and second passages with a survival rate of 290 days in the mouse. Recently, tumor budding has also been demonstrated in both the core and the invasion front in CRC cell line-derived xenografts[130]. All these findings strongly suggest that early passages of PDXs preserve the distinctive cross talk between cancer cells and the immune microenvironment and determine the suitability of this preclinical platform as a model of tumor budding in CRC.

Recently, Trihn et al.[72] reported the potential association of high-grade budding with the CMS4 subtype of CRC in a series of CMS2/3 and CMS4 patient tumors. In our study, we found similar results with the CMS4 subtype enriched by high-grade tumor budding compared with CMS1 and CMS2/3 subtypes. The fact that tumor buds are well-established independent adverse prognostic factors in CRC[62,63] as well as the correspondence of CMS subtypes and tumor budding grade between PDXs and their human counterparts observed in our study, supports the use of PDX models as powerful tools for the development of targeted therapies against mechanisms involved in tumor budding.

We also found that high-grade budding was also significantly associated with stroma-rich tumors. Earlier reports in CRC and breast cancer have suggested an association between tumor budding and the presence of a high density of stromal myofibroblasts[131,132]. Tumor-associated stroma has been shown to facilitate EMT by inducing growth factors, which has been linked with higher capacity of migration and invasion of bud cells[132,133]. Thus, these findings highlight the potential role of the stroma in establishing a microenvironment supportive of the formation of tumor buds. Taken together, the budding phenotype seems to be associated with the high stromal component, which is also accentuated in the mesenchymal CMS4 subtype of CRC.

It is important to note the remarkable overexpression of inhibitory immune checkpoint-related genes (*PDL1*, *TIM-3*, *NOX2*, and *IDO1*) in BD3 tumors in comparison to BD1 observed in this study. All these upregulated genes have been previously related with tumor invasion and metastasis. However, limited studies have analyzed the expression of immune checkpoint genes in relation with tumor budding[134,135]. In agreement with our data, an upregulation of *PDL1* expression has been reported in high-grade tumor budding of CRC suggesting that *PDL1*

might be specifically overexpressed during EMT to allow invasion and immune escape[135,136,137]. On the other hand, *TIM-3*, which has been shown to inhibit antitumor immunity by mediating CD8 T-cell exhaustion and pathways involved in metastasis, is an emerging immune checkpoint in several cancers including CRC[138,139,140]. *IDO1* and *NOX2* are known to exert a potent immunosuppressive effect in a variety of human solid tumors by reducing both tumor-infiltrating T cells as well as B cells[141,142]. Recent studies suggest that *NOX2* knockdown reduces metastasis via mechanisms involving amelioration of immune-mediated clearance of metastatic tumor cells[141,143]. The overexpression of these inhibitory immune checkpoints in BD3 tumors observed in our study could explain the immune-permissive microenvironment that facilitates tumor bud formation, invasion, and progression even in early passages of PDXs. Nevertheless, *PD1* and *CTLA4* genes were more expressed in low tumor budding grade in both patients and xenografts. The distinct expression of *PD1* and *CTLA4* in immune cells and *PDL1* in tumor cells, respectively, would explain these apparent contradictory findings. Hence, the high expression of *PDL1* in BD3 tumors would be associated with the immune evasion mechanisms deployed by cancer cells at the invasive front in these tumors, while the overexpression of *PD1* and *CTLA4* genes in BD1 tumors would reflect their comparative higher immunogenicity. In this regard, the overexpression of these immune checkpoints has been observed in highly immunogenic tumors and with good clinical response to anti-PD1 and anti-CTLA4 therapy[144,145]. Moreover, high *PD1* expression has been recently reported to be associated with a favorable outcome in CRC patients while high-level *PDL1* expression, either alone or in combination with *PD1*, was associated with a worse recurrence-free survival[146]. The prognostic value of *PD1* expression in lymphocytes and tumor cells and its interaction with *PDL1* expression for the prognosis impact in CRC remain to be more deeply investigated. In this context,

it may be plausible that CRC patients with low grade budding will most likely benefit from anti-PD1 and anti-CTLA4 therapies.

TLRs are a diverse family of receptors that regulate gut inflammation but also found to be aberrantly expressed and associated with poor survival and with invasive and metastatic phenotypes in tumors[147,148]. In our study, *TLR* family expression, specifically *TLR1, TLR3*, *TLR4*, and *TLR6*, was upregulated in BD3 tumors in comparison with low-grade budding tumors (both in patient and PDX tumors) suggesting the presence of *TLR*-mediated alterations in the tumor invasive front. Overexpression of these TLRs has been previously detected in CRC[147,148,149,150,151]. Although the specific mechanisms of *TLR*-mediated immune escape are still unknown, current evidence indicates that the high expression of *TLRs* in tumors can contribute to tumor-cell resistance to apoptosis, malignant transformation of epithelial cells, and tumor progression[148]. Results from our study support that *TLRs* upregulation is closely related to BD3 of CRC, and these receptors may constitute promising targets for tumor immunotherapy. In addition, it has been previously reported that the activation of *TLRs* is also accompanied by the expression of *PDL1* and other inhibitory molecules in tumor cells, as we have observed in this study[149].

Many cancer types show altered chemokine secretion profiles, favoring the recruitment of pro-tumorigenic immune cells such as MDSCs, tumor-associated neutrophils (TAN), tumor-associated macrophages (TAM), and regulatory T cells. Particularly, *CXCR2* and *CXCR4* are chemokine receptors for T-cells implicated in cancer invasion and metastasis[152,153]. Interestingly, these chemokines were overexpressed in BD3 tumors in patients and xenografts in our study. These two chemokine receptors play a crucial role in establishing the “pre-metastatic niche” for tumor cells and are now emerging as key players in the

regulation of antitumor immunity[149,154,155,156,157]. In addition to these chemokine receptors, chemokine ligands such as *CXCL1*, *CXCL2*, *CXCL5*, *CXCL6*, *CXCL8*, and *CXCL9* have been also significantly correlated with poor survival and metastasis in several cancers by recruiting MDSCs and suppressing the antitumoral activity of CD8+ T effectors cells. In agreement with these reports, our study reinforces the notion that many different chemokines contribute to antitumoral T cell recruitment and likely some of them may be related to the establishment of a pro-metastatic niche for the tumor buds.

Finally, we have previously reported that eNOS is upregulated in human mesenchymal/stem-like CRC tumors, and poorly differentiated aggressive adenocarcinomas[117]. In this regard, it is important to note the remarkable overexpression of epithelial eNOS in both the poor prognosis CMS4 subtype as well as in the high-grade tumor budding in our study. This result suggests that eNOS is the most relevant enzymatic source of NO in this subtype of CRC. Although the NO-mediated effects in the tumor microenvironment are diverse and context-dependent, this pleiotropic molecule can be considered as an immunosuppressive mediator. Hence, it has been described the critical role of NO in the different immune evasion strategies of tumors cells, including the acquisition of stem cell like capacities and the metabolic reprogramming of tumor infiltrating immune cells[96]. Notably, NO induces suppression of the immune system by inhibiting T lymphocyte activation and proliferation[158,159] and also by interfering with migration of T cells into the tumor[160]. Therefore, NO signaling and metabolism may also facilitate tumor bud formation by promoting immune evasion.

In summary, our findings support that tumor budding is strongly associated with the mesenchymal poor prognosis subtype of CRC and the presence of

immunosuppressive mechanisms to evade antitumor immunity. Besides, our study suggests that PDXs constitute robust preclinical platforms for reproducing CMS subtypes and tumor budding, hence allowing the development of novel challenging therapies directed against tumor budding in CRC, with special focus in the most aggressive CMS4 subtype.

## 2. Low GSNOR/ADH5 expression is associated with worse prognosis, poor survival and an immunosuppressive microenvironment in CRC.

GSNOR/*ADH5* is an evolutionarily highly conserved denitrosylase enzyme that regulates the S-nitrosylation of proteins by influencing the cellular balance between S-nitrosylated proteins and GSNO. The deficiency or inhibition of this enzyme in various animal models has revealed the important role of NO bioactivity in different pathological contexts such as cellular senescence and the development of liver tumors[161]. Moreover, this denitrosylase enzyme seems to play an essential role in the correct development of the immune system, since its deficiency results in severe lymphopenia, due to an increase of apoptosis of immature B and T lymphocytes in the thymus[161].

We have previously reported that GSNOR inhibition increases protein S-nitrosylation and reduces the efficacy of the anti-HER2 monoclonal antibody trastuzumab in HER2+ breast cancer[115]. Furthermore, HER2+ tumors, which are more aggressive than HER2-negative tumors, were characterized by a lower expression of GSNOR protein, while low expression of the *ADH5* gene was associated with poor survival rates in patients with HER2 tumors[115]. Accordingly, in the present study, we now show that the low expression of GSNOR/*ADH5* in CRC is also intimately linked to more aggressive clinicopathological characteristics of the tumor such as tumor size, advanced clinical stage and poor

differentiated tumors. Moreover, our results support that GSNOR/*ADH5* low tumors are strongly associated with the poor prognosis mesenchymal-like CMS4 subtype, and with the loss of intestinal epithelial markers such as cytokeratin and CDX2. Interestingly, loss of CDX2 expression has been described as a factor of poor prognosis in CMS4 patients for both relapse free and overall survival[162]. In this regard, we also show that low GSNOR/*ADH5* expression in tumors is associated with a significant lower PFS rate in CRC patients, additionally supporting a likely tumor suppressor role for this enzyme in CRC.

Recent evidence correlates the poor prognosis CMS4 subtype with an inflamed, angiogenic and immunosupressive tumor microenvironment[47,56]. In contrast, CMS1 (MSI) tumors are highly infiltrated by memory T cells, particularly cytotoxic $CD8^+$ T lymphocytes, and are associated with good prognosis[47,56]. In our study GSNOR/*ADH5*-low tumors displayed a marked reduction in the expression of genes related to cytotoxic cell function, including CD8+ T cell function, chemokines, cytokines, cytotoxicity, NK function and antigen processing. Additionally, a sub-set of cytotoxicity-related genes were also downregulated in ADH5-high non-MSI tumors (*GNLY*, *GZMA*, *CXCR6*, *CD3D* and *TARP*). Recent studies have shown that high T-and B-cell infiltration and high expression T cell-attracting chemokines, as well as genes involved in cytotoxicity (*GNLY* and *GZMA*)[55,163,164] , are associated with favorable prognosis[55,165,166]. We also provide other data that further reinforce the idea of an immune evasive microenvironment and poor prognosis in GSNOR/*ADH5*-low tumors. Hence, a number of genes known to inhibit (*ITGA2, LGALS3* and *CD46*) and promote (*CASP3*, *CD40*, *CKLF*) anti-tumor immunity were upregulated and downregulated, respectively, in GSNOR/*ADH5*-low tumors. Galectin-3, a protein encoded by *LGALS3* gene, is known to suppresses immune surveillance by killing T cells and interfering with NK cell function[167]. On the other hand, the

overexpression of the complement receptor CD46 has been reported in several human cancers, including CRC, and constitutes an immune evasion mechanism by which tumor cells protect themselves from complement dependent cytotoxity[168]. Interestingly, the downregulation of CD40-CD40L axis has been recently related with a reduction in CD8+ cytotoxic T lymphocyte effectiveness leading to an impaired immune response in cancer[169]. Therefore, taken as a whole, our results support that GSNOR/*ADH5* deficiency in CRC tumors appears to be closely associated with mechanisms of immune evasion by which cancer cells escape from immune system surveillance thereby promoting tumor progression.

## 3. Metabolic reprogramming induced by impaired denitrosylation contributes to tumor progression and immune evasion in CRC

CMS4 subtype of CRC has been associated with a stem-like phenotype, in which tumor cells possess a cellular phenotype similar to that of stem cells[46,117]. These tumor stem cells possess the capacity for self-renewal, differentiation potential and are responsible for initiating and maintaining tumor growth, which ultimately results in the dissemination and development of metastases[170]. Our results show that GSNOR/*ADH5* deficiency in CRC cells led to the acquisition of a higher capacity for self-renewal, as indicated by an increased capacity to generate tumorospheres and tumor spheroids *in vitro*, and a higher proportion of tumor initiating cells, as indicated by the LDA assay. In addition, tumorospheres generated by *ADH5*-KO cells displayed a lower expression of CDX2 and a higher expression of PDL1 in comparison with those tumorospheres formed by their WT counterparts. As mentioned above, it has been reported that CMS4 subtype and CDX2-negative tumors identify high-risk patients with very poor prognosis[162]. On the other hand, aside from its known effect on the immunological response, PDL1 expression plays an inherent role in tumor cells themselves. Notably, PDL1

has been recently reported to play a critical role in CRC CSC expansion that is independent of its immune checkpoint role[123]. Therefore, GSNOR/*ADH5* deficiency appears to be closely connected with the acquisition of a more aggressive CSC phenotype in CRC.

Although higher cell proliferation would explain the greater aggressiveness of GSNOR/*ADH5* deficient cells, there were no significant differences in their proliferative capacity, compared to parental cells. However, GSNOR deficiency and the consequent alteration of SNOs homeostasis in CRC cells was accompanied by an alteration in their metabolism of glucose which was compatible with a higher rate of aerobic glycolysis, a metabolic alteration related to greater tumor aggressiveness[124]. Significantly, it has been shown in several types of cancer that CSCs display an altered metabolic state compared to the rest of the tumor cells. This metabolic reprogramming enables CSCs to maintain their self-renewal capacity and is associated with lower rates of oxidative phosphorylation and higher aerobic glycolytic activity[171,172,173]. Importantly, the high glycolytic activity of tumor cells plays important roles in the establishment of immunosuppression. Hence, T-cell function is suppressed by restricted glucose availability and enhanced accumulation of lactate in tumor microenvironment due to increased aerobic glycolysis by cancer cells[174]. Moreover, lactate also contributes to tumor cell protection from cytotoxic T cells by inducing up-regulation of PDL1 in tumor cells[175].

Advances in living cell imaging have revealed that mitochondria are not static and isolated entities, but rather dynamic organelles that can modulate their morphology to form tubular networks or fragmented granules through coordinated cycles of fusion and fission[176]. Mitochondrial dynamics alter the number, shape, and cytoplasmic distribution of mitochondria, allowing the cell to

survive under changing environmental conditions of stress, nutrient availability, and energy requirements. Consequently, the alteration of mitochondrial morphology is probably one of the main mechanisms by which tumor cells reprogram their metabolism. Tubular mitochondria appear to provide an ideal arrangement of components of the electronic transport chain that facilitates efficient oxidative phosphorylation[177,178], while fragmentation of the mitochondrial network is generally associated with less active oxidative metabolism[179]. Reduced oxidative phosphorylation helps channel glycolytic intermediates into anabolic pathways, and mitochondrial fission has been associated with highly activated glycolysis in many types of cancer[180]. In our study, *ADH5*-KO cells showed an alteration of the cellular mitochondrial network, compatible with a higher rate of mitochondrial fission, and which would explain the enhanced aerobic glycolytic activity of these cells.

The processes of mitochondrial fusion and fission are regulated by a small number of highly conserved guanosine triphosphatases (GTPases), including OPA1 (optic atrophy 1) and Drp1 (dynamin-related protein 1). It is important to note that OPA1[181] and Drp1[182,183] are post-translationally modified by S-nitrosylation, although the functional effects of these modifications are not very clear. Thus, it has been described that NO produced in response to the β-amyloid protein increases dimerization and GTPase activity of neuronal Drp1 through its S-nitrosylation at Cys644, which triggers mitochondrial fission and damage to neurons[182]. However, another study has shown that S-nitrosylation of Drp1 does not alter its dimerization or its GTPase activity[181]. More recently, the S-nitrosylation of Drp1, but also of the PINK1 protein (PTEN-induced putative kinase 1), has been described in mice deficient in GSNOR, inhibiting the elimination of damaged mitochondria through the mitophagy process, as well as the decrease of OPA1 expression[183], which suggests the concurrence of different

mechanisms through which S-nitrosylation impacts on mitochondrial dynamics. Therefore, future studies are needed to clarify whether GSNOR/*ADH5* deficiency in CRC cells can lead to modifications and alterations in the levels and activity of the proteins that regulate mitochondrial dynamics.

# *VIII. CONCLUSIONS*

1. Tumor budding in CRC is strongly associated with the mesenchymal poor prognosis CMS4 subtype and the presence of a combination of immunosuppressive mechanisms to evade antitumor immunity.
2. The close association between TLRs, chemokines, and tumor budding, raises the hypothesis that the activation of these immune targets may have a determinant role in tumor budding, especially in the case of the CMS4 subtype.
3. PDXs constitute robust preclinical platforms for reproducing CMS subtypes and tumor budding, hence allowing the development of novel challenging therapies directed against tumor budding in CRC, with special focus in the most aggressive CMS4 subtype.
4. The low expression of GSNOR/*ADH5* denitrosylase in CRC tumors appears to be closely associated with the poor prognosis mesenchymal-like CMS4 subtype and with mechanisms of immune evasion, suggesting a likely tumor suppressor role for this enzyme in CRC.
5. The impaired protein S-nitrosylation induced by GSNOR/*ADH5* deficiency in CRC cells is accompanied by higher rates of mitochondrial fission and aerobic glycolytic activity, and this metabolic rewiring constitutes an important novel mechanism for the acquisition of aggressive and immune evasive phenotypes in CRC.
6. This new role of nitric oxide in tumor metabolic reprogramming may help explain some of the puzzling aspects of this signaling molecule in cancer, suggesting new therapeutic approaches in this disease.

## *IX. REFERENCES*

1. Clarke, C. N. & Kopetz, E. S. BRAF mutant colorectal cancer as a distinct subset of colorectal cancer: Clinical characteristics, clinical behavior, and response to targeted therapies. *J. Gastrointest. Oncol.* **6**, 660–667 (2015).

2. Sung, H. *et al.* Global cancer statistics 2020: GLOBOCAN estimates of incidence and mortality worldwide for 36 cancers in 185 countries. *CA. Cancer J. Clin.* (2021) doi:10.3322/caac.21660.

3. Sociedad Española de Oncología Médica. Las cifras del cáncer en España 2020 Hombres. *Soc. Española Oncol. Médica* 36 (2020).

4. Keum, N. N. & Giovannucci, E. Global burden of colorectal cancer: emerging trends, risk factors and prevention strategies. *Nat Rev Gastroenterol Hepatol.* **16**, 713–732 (2019).

5. Biancone, L. *et al.* Cancer Risk in Inflammatory Bowel Disease: A 6-Year Prospective Multicenter Nested Case-Control IG-IBD Study. *Inflamm. Bowel Dis.* **26**, 450–459 (2020).

6. Chong, D. Q. *et al.* Association of family history and survival in patients with colorectal cancer: a pooled analysis of eight epidemiologic studies. *Cancer Med.* **7**, 2192–2199 (2018).

7. Van Cutsem, E., Cervantes, A., Nordlinger, B., Arnold, D. & The ESMO Guidelines Working Group. Metastatic colorectal cancer: ESMO clinical practice guidelines for diagnosis, treatment and follow-up. *Ann. Oncol.* **25**, iii1–iii9 (2014).

8. Jasperson, K. W., Tuohy, T. M., Neklason, D. W. & Burt, R. W. Hereditary and Familial Colon Cancer. *Gastroenterology* **138**, 2044–2058 (2010).

9. De La Chapelle, A. Genetic predisposition to colorectal cancer. *Nat. Rev. Cancer* **4**, 769–780 (2004).

10. Armaghany, T., Wilson, J. D., Chu, Q. & Mills, G. Genetic alterations in colorectal cancer in older patients. *Genet. Alterations Color. Cancer* **5**, 19–27 (2012).

11. Pancione, M., Remo, A. & Colantuoni, V. Genetic and epigenetic events generate multiple pathways in colorectal cancer progression. *Patholog. Res. Int.* **2012**, (2012).

12. Dickinson, B. T., Kisiel, J., Ahlquist, D. A. & Grady, W. M. Molecular markers for colorectal cancer screening. *Gut* **64**, 1485–1494 (2015).

13. Fearon, E. R. & Vogelstein, B. A genetic model for colorectal tumorigenesis. *Cell* **61**, 759–67 (1990).

14. Müller, M. F., Ibrahim, A. E. K. & Arends, M. J. Molecular pathological classification of colorectal cancer. *Virchows Arch.* **469**, 125–134 (2016).

15. Boland, C. R. & Goel, A. Microsatellite Instability in Colorectal Cancer. *Gastroenterology* **138**, 2073–2087.e3 (2010).

16. Jeong, M. B., Kim, J. H. & Kang, G. H. Epigenetic alterations in colorectal cancer: The CpG island methylator phenotype. *Histol Histopathol*. **28**, 585–595 (2013).

17. Network, T. C. G. A. *et al.* Comprehensive molecular characterization of human colon and rectal cancer. *Nature* **487**, 330–337 (2012).

18. Yu, M. & Grady, W. M. Therapeutic targeting of the phosphatidylinositol 3-kinase signaling pathway: Novel targeted therapies and advances in the treatment of colorectal cancer. *Therap. Adv. Gastroenterol.* **5**, 319–337 (2012).

19. Steinhart, Z. & Angers, S. Wnt signaling in development and tissue homeostasis. *Development* **145**, 1–8 (2018).

20. Dickinson, M. E. & McMahon, A. P. The role of Wnt genes in vertebrate development. *Curr. Opin. Genet. Dev.* **2**, 562–566 (1992).

21. Wu, W. K. K. *et al.* Dysregulation and crosstalk of cellular signaling pathways in colon carcinogenesis. *Crit Rev Oncol Hematol*. **86**, 251–277 (2013).

22. Powell, S. M. *et al. APC mutations occur early during colorectal tumorigenesis*. *Nature* **359**, 235–237 (1992).

23. Groden, J. *et al.* Identification and characterization of the familial adenomatous polyposis coli gene. *Cell* **66**, 589–600 (1991).

24. Scartozzi, M. *et al.* Epidermal growth factor receptor (EGFR) downstream signalling pathway in primary colorectal tumours and related metastatic sites: Optimising EGFR-targeted treatment options. *Br. J. Cancer* **97**, 92–97 (2007).

25. Luo, H. Y. & Xu, R. H. Predictive and prognostic biomarkers with therapeutic targets in advanced colorectal cancer. *World J. Gastroenterol.* **20**, 3858–3874 (2014).

26. You, B. & Chen, E. X. Anti-EGFR monoclonal antibodies for treatment of colorectal cancers: Development of cetuximab and panitumumab. *J Clin Pharmacol*. **52**, 128–155 (2012).

27. Serebriiskii, I. G. *et al.* Comprehensive characterization of RAS mutations in colon and rectal cancers in old and young patients. *Nat. Commun.* **10**, 3722 (2019).

28. Sorich, M. J. *et al.* Extended RAS mutations and anti-EGFR monoclonal antibody survival benefit in metastatic colorectal cancer: A meta-analysis of randomized, controlled trials. *Ann Oncol*. **26**, 13–21 (2015).

29. Jung, B., Staudacher, J. J. & Beauchamp, D. Transforming Growth Factor β Superfamily Signaling in Development of Colorectal Cancer. *Gastroenterology*. **152**, 36–52 (2017).

30. Massagué, J. TGFβ signalling in context. *Nat Rev Mol Cell Biol*. **13**, 616–630 (2012).

31. Principe, D. R. *et al.* TGF-β: Duality of function between tumor prevention and carcinogenesis. *J Natl Cancer Inst*. **106**, (2014). doi: 10.1093/jnci/djt369.

32. Ihara, S., Hirata, Y. & Koike, K. TGF-β in inflammatory bowel disease: a key regulator of immune cells, epithelium, and the intestinal microbiota. *J Gastroenterol*. **52**, 777–787 (2017).

33. Batlle, R. *et al.* Regulation of tumor angiogenesis and mesenchymal–endothelial transition by p38α through TGF-β and JNK signaling. *Nat. Commun.* **10**, (2019). doi: 10.1038/s41467-019-10946-y.

34. Itatani, Y., Kawada, K. & Sakai, Y. Transforming growth factor-β signaling pathway in colorectal cancer and its tumor microenvironment. *Int. J. Mol. Sci.* **20**, 5822 (2019). doi: 10.3390/ijms20235822.

35. Harris, S. L. & Levine, A. J. The p53 pathway: Positive and negative feedback loops. *Oncogene*. **24**, 2899–2908 (2005).

36. Jin, S. & Levine, A. J. The p53 functional circuit. *J Cell Sci*. **114**, 4139–4140 (2001).

37. Russo, A. *et al.* The TP53 colorectal cancer international collaborative study on the prognostic and predictive significance of p53 mutation: influence of tumor site, type of mutation, and adjuvant treatment. *J. Clin. Oncol.* **23**, 7518–28 (2005).

38. Kimberly H. Allison, MD, George W. Sledge, Jr, M. Heterogeneity and Cancer. *Oncology* **28**, 772–778 (2014).

39. Blank, A., Roberts, D. E., Dawson, H., Zlobec, I. & Lugli, A. Tumor heterogeneity in primary colorectal cancer and corresponding metastases. Does the apple fall far from the tree? *Front. Med.* **5**, 1–8 (2018).

40. Greaves, M. Evolutionary determinants of cancer. *Cancer Discov.* **5**, 806–821 (2015).

41. Fakhri, B. & Lim, K.-H. Molecular landscape and sub-classification of gastrointestinal cancers: a review of literature. *J. Gastrointest. Oncol.* **8**, 379–386 (2017).

42. Shia, J., Klimstra, D. S., Bagci, P., Basturk, O. & Adsay, N. V. TNM staging of colorectal carcinoma: Issues and caveats. *Semin. Diagn. Pathol.* **29**, 142–153 (2012).

43. Edge, S. B. & Compton, C. C. The american joint committee on cancer: The 7th edition of the AJCC cancer staging manual and the future of TNM. *Ann Surg Oncol*. **17**, 1471–1474 (2010).

44. Gress, D. M. *et al.* Principles of Cancer Staging. *AJCC Cancer Staging Man.* 3–33 (2017) doi:10.1007/978-3-319-40618-3_1.

45. Souglakos, J. *et al.* Prognostic and predictive value of common mutations for treatment response and survival in patients with metastatic colorectal cancer. *Br. J. Cancer* **101**, 465–472 (2009).

46. Guinney, J. *et al.* The consensus molecular subtypes of colorectal cancer. *Nat. Med.* **21**, 1350–1356 (2015).

47. Dienstmann, R. *et al.* Consensus molecular subtypes and the evolution of precision medicine in colorectal cancer. *Nat Rev Cancer*. **17**, 79–92 (2017).

48. Fontana, E., Eason, K., Cervantes, A., Salazar, R. & Sadanandam, A. Context matters - Consensus molecular subtypes of colorectal cancer as biomarkers for clinical trials. *Ann Oncol*. **30**, 520–527 (2019).

49. Trinh, A. *et al.* Practical and robust identification of molecular subtypes in colorectal cancer by immunohistochemistry. *Clin. Cancer Res.* **23**, 387–398 (2017).

50. Ten Hoorn, S., Trinh, A., de Jong, J., Koens, L. & Vermeulen, L. Classification of colorectal cancer in molecular subtypes by immunohistochemistry. *Methods Mol Biol*. **1765**, 179–191 (2018).

51. Vinay, D. S. *et al.* Immune evasion in cancer: Mechanistic basis and therapeutic strategies. *Semin Cancer Biol*. **35**, S185–S198 (2015).

52. Dyck, L. & Mills, K. H. G. Immune checkpoints and their inhibition in cancer and infectious diseases. *Eur J Immunol*. **47**, 765–779 (2017).

53. Cohen, R. *et al.* Immune Checkpoint Inhibition in Colorectal Cancer: Microsatellite Instability and Beyond. *Target Oncol*. **15**, 11–24 (2020).

54. Tosolini, M. *et al.* Clinical impact of different classes of infiltrating T cytotoxic and helper cells (Th1, Th2, Treg, Th17) in patients with colorectal cancer. *Cancer Res.* **71**, 1263–1271 (2011).

55. Galon, J. *et al.* Type, density, and location of immune cells within human colorectal tumors predict clinical outcome. *Science.* **313**, 1960–1964 (2006).

56. Becht, E. *et al.* Immune and stromal classification of Colorectal cancer is associated with molecular subtypes and relevant for precision immunotherapy. *Clin. Cancer Res.* **22**, 4057–4066 (2016).

57. Soldevilla, B. *et al.* The correlation between immune subtypes and consensus molecular subtypes in colorectal cancer identifies novel tumour microenvironment profiles, with prognostic and therapeutic implications. *Eur. J. Cancer* **123**, 118–129 (2019).

58. Llosa, N. J. *et al.* The vigorous immune microenvironment of microsatellite instable colon cancer is balanced by multiple counter-inhibitory checkpoints. *Cancer Discov.* **5**, 43–51 (2015).

59. Angelova, M. *et al.* Characterization of the immunophenotypes and antigenomes of colorectal cancers reveals distinct tumor escape mechanisms and novel targets for immunotherapy. *Genome Biol.* **16**, (2015).

60. Lugli, A., Karamitopoulou, E. & Zlobec, I. Tumour budding: A promising parameter in colorectal cancer. *Br J Cancer*. **106**, 1713–1717 (2012).

61. Cho, S. J. & Kakar, S. Tumor budding in colorectal carcinoma: Translating a morphologic score into clinically meaningful results. *Arch Pathol Lab Med*. **142**, 952–957 (2018).

62. Lugli, A. *et al.* Recommendations for reporting tumor budding in colorectal cancer based on the International Tumor Budding Consensus Conference (ITBCC) 2016. *Mod. Pathol.* **30**, 1299–1311 (2017).

63. Dawson, H. *et al.* Validation of the International Tumor Budding Consensus Conference 2016 recommendations on tumor budding in stage I-IV colorectal cancer. *Hum. Pathol.* **85**, 145–151 (2019).

64. Dawson, H. *et al.* Tumor budding is a strong predictor of disease-free survival in stage II colorectal cancer: Validation study based on the International Tumor Budding Consensus Conference (ITBCC) recommendations. *J. Clin. Oncol.* **35**, 594–594 (2017).

65. Graham, R. P. *et al.* Tumor budding in colorectal carcinoma: Confirmation of prognostic significance and histologic cutoff in a population-based cohort. *Am. J. Surg. Pathol.* **39**, 1340–1346 (2015).

66. Lugli, A. *et al.* CD8+ lymphocytes/ tumour-budding index: An independent prognostic factor representing a pro-/anti-tumour approach to tumour host interaction in colorectal cancer. *Br. J. Cancer* **101**, 1382–1392 (2009).

67. Dawson, H. *et al.* Tumour budding/T cell infiltrates in colorectal cancer: proposal of a novel combined score. *Histopathology* **76**, 572–580 (2020).

68. van Wyk, H. C. *et al.* The Relationship Between Tumor Budding, Tumor Microenvironment, and Survival in Patients with Primary Operable Colorectal Cancer. *Ann. Surg. Oncol.* **26**, 4397–4404 (2019).

69. De Smedt, L. *et al.* Expression profiling of budding cells in colorectal cancer reveals an EMT-like phenotype and molecular subtype switching. *Br. J. Cancer* **116**, 58–65 (2017).

70. Galván, J. A. *et al.* Expression of E-cadherin repressors SNAIL, ZEB1 and ZEB2 by tumour and stromal cells influences tumour-budding phenotype and suggests heterogeneity of stromal cells in pancreatic cancer. *Br. J. Cancer* **112**, 1944–1950 (2015).

71. Jensen, D. H. *et al.* Molecular profiling of tumour budding implicates TGFβ-mediated epithelial-mesenchymal transition as a therapeutic target in oral squamous cell carcinoma. *J. Pathol.* **236**, 505–16 (2015).

72. Trinh, A. *et al.* Tumour budding is associated with the mesenchymal colon cancer subtype and RAS/RAF mutations: a study of 1320 colorectal cancers with Consensus Molecular Subgroup (CMS) data. *Br. J. Cancer* **119**, 1244–1251 (2018).

73. Saltz, L. B. Value in colorectal cancer treatment: Where it is lacking, and why. *Cancer J.* **22**, 232–235 (2016).

74. Carethers, J. M. Systemic treatment of advanced colorectal cancer: tailoring therapy to the tumor. *Therap. Adv. Gastroenterol.* **1**, 33–42 (2008).

75. Heidelberger, C. *et al.* Fluorinated pyrimidines, a new class of tumour-inhibitory compounds. *Nature* **179**, 663–666 (1957).

76. Petrelli, N. *et al.* The modulation of fluorouracil with leucovorin in metastatic colorectal carcinoma: A prospective randomized phase III trial. *J. Clin. Oncol.* **7**, 1419–1426 (1989).

77. Goldberg, R. M. *et al.* A randomized controlled trial of fluorouracil plus leucovorin, irinotecan, and oxaliplatin combinations in patients with previously untreated metastatic colorectal cancer. *J. Clin. Oncol.* **22**, 23–30 (2004).

78. de Gramont, A. *et al.* Leucovorin and fluorouracil with or without oxaliplatin as first-line treatment in advanced colorectal cancer. *J. Clin. Oncol.* **18**, 2938–2947 (2000).

79. Douillard, J. Y. *et al.* Irinotecan combined with fluorouracil compared with fluorouracil alone. as first-line treatment for metastatic colorectal cancer: a multicentre randomised trial. *Lancet* **355**, 1041–1047 (2000).

80. Bignucolo, A., De Mattia, E., Cecchin, E., Roncato, R. & Toffoli, G. Pharmacogenomics of targeted agents for personalization of colorectal cancer treatment. *Int. J. Mol. Sci.* **18**, 1522 (2017). doi: 10.3390/ijms18071522.

81. Moriarity, A., O'Sullivan, J., Kennedy, J., Mehigan, B. & McCormick, P. Current targeted therapies in the treatment of advanced colorectal cancer: A review. *Ther. Adv. Med. Oncol.* **8**, 276–293 (2016).

82. Hagan, S., M Orr, M. C. & Doyle, B. Targeted therapies in colorectal cancer-an integrative view by pppm. *EPMA J.* **4**, 3 (2013). doi: 10.1186/1878-5085-4-3.

83. Hurwitz, H. *et al.* Bevacizumab plus irinotecan, fluorouracil, and leucovorin for metastatic colorectal cancer. *N. Engl. J. Med.* **350**, 2335–2342 (2004).

84. Kaklamanis, L., Gatter, K. C., Mortensen, N. & Harris, A. L. Interleukin-4 receptor and epidermal growth factor receptor expression in colorectal cancer. *Br. J. Cancer* **66**, 712–716 (1992).

85. Yasui, W. *et al.* Expression of Epidermal Growth Factor Receptor in Human Gastric and Colonic Carcinomas. *Cancer Res.* **48**, 137–141 (1988).

86. Khan, K. *et al.* Targeting EGFR pathway in metastatic colorectal cancer-tumour heterogeniety and convergent evolution. *Crit. Rev. Oncol. Hematol.* **143**, 153–163 (2019).

87. Bardelli, A. & Siena, S. Molecular mechanisms of resistance to cetuximab and panitumumab in colorectal cancer. *J. Clin. Oncol.* **28**, 1254–1261 (2010).

88. Hodi, F. S. *et al.* Improved Survival with Ipilimumab in Patients with Metastatic Melanoma. *N. Engl. J. Med.* **363**, 711–723 (2010).

89. Passardi, A., Canale, M., Valgiusti, M. & Ulivi, P. Immune checkpoints as a target for colorectal cancer treatment. *Int. J. Mol. Sci.* **18**, 1324 (2017). doi: 10.3390/ijms18061324.

90. Sarshekeh, A. M., Overman, M. J. & Kopetz, S. Nivolumab in the treatment of microsatellite instability high metastatic colorectal cancer. *Futur. Oncol.* **14**, 1869–1874 (2018).

91. Smith, K. M. & Desai, J. Nivolumab for the treatment of colorectal cancer. *Expert Rev. Anticancer Ther.* **18**, 611–618 (2018).

92. Ganesh, K. *et al.* Immunotherapy in colorectal cancer: rationale, challenges and potential. *Nat. Rev. Gastroenterol. Hepatol.* **16**, 361–375 (2019).

93. Moncada, S. Nitric oxide: discovery and impact on clinical medicine. *J. R. Soc. Med.* **92**, 164–169 (1999).

94. Maher, A., Abdel Rahman, M. F. & Gad, M. Z. The Role of Nitric Oxide from Neurological Disease to Cancer. *Adv. Exp. Med. Biol.* **1007**, 71–88 (2017).

95. Aranda, E., Lopez-Pedrera, C., R. De La Haba-Rodriguez, J. & Rodriguez-Ariza, A. Nitric Oxide and Cancer: The Emerging Role of S-Nitrosylation. *Curr. Mol. Med.* **12**, 50–67 (2012).

96. PeÑarando, J., Aranda, E. & RodrÍguez-Ariza, A. Immunomodulatory roles of nitric oxide in cancer: tumor microenvironment says “NO” to antitumor immune response. *Transl Res.* **210**, 99–108 (2019).

97. López-Sánchez, L. M., Aranda, E. & Rodríguez-Ariza, A. Nitric oxide and tumor metabolic reprogramming. *Biochem Pharmacol.* **176**, 113769 (2020). https://doi.org/10.1016/j.bcp.2019.113769

98. Ridnour, L. A. *et al.* The biphasic nature of nitric oxide responses in tumor biology. *Antioxid Redox Signal.* **8**, 1329–1337 (2006).

99. Förstermann, U. & Sessa, W. C. Nitric oxide synthases: Regulation and function. *Eur. Heart J.* **33**, 829–837 (2012).

100. Knowles, R. G. & Moncada, S. Nitric oxide synthases in mammals. *Biochem J.* **298**, 249–258 (1994).

101. López-Sánchez, L. M., López-Pedrera, C. & Rodríguez-Ariza, A. Proteomics insights into deregulated protein S-nitrosylation and disease. *Expert Rev. Proteomics* **9**, 59–69 (2012).

102. Stomberski, C. T., Hess, D. T. & Stamler, J. S. Protein S-Nitrosylation: Determinants of Specificity and Enzymatic Regulation of S-Nitrosothiol-Based Signaling. *Antioxid Redox Signal.* **30**, 1331–1351 (2019).

103. Thomas, D. D. & Wink, D. A. NOS2 as an Emergent Player in Progression of Cancer. *Antioxid Redox Signal.* **26**, 963–965 (2017).

104. Korde Choudhari, S., Chaudhary, M., Bagde, S., Gadbail, A. R. & Joshi, V. Nitric oxide and cancer: A review. *World J. Surg. Oncol.* **11**, 118 (2013). doi: 10.1186/1477-7819-11-118.

105. Yu, S. *et al.* Increased expression of activated endothelial nitric oxide synthase contributes to antiandrogen resistance in prostate cancer cells by suppressing androgen receptor transactivation. *Cancer Lett.* **328**, 83–94 (2013).

106. Wang, H. *et al.* Nitric oxide (NO) and NO synthases (NOS)-based targeted therapy for colon cancer. *Cancers* **12**, 1–25 (2020).

107. Jang, M. J. *et al.* Association of eNOS polymorphisms (-786T>C, 4a4b, 894G>T) with colorectal cancer susceptibility in the Korean population. *Gene* **512**, 275–281 (2013).

108. De Oliveira, G. A. *et al.* Inducible Nitric Oxide Synthase in the Carcinogenesis of Gastrointestinal Cancers. *Antioxid Redox Signaling*. **26**, 1059–1077 (2017).

109. López-Sánchez, L. M., López-Pedrera, C. & Rodríguez-Ariza, A. Proteomic approaches to evaluate protein *s* -nitrosylation in disease. *Mass Spectrom. Rev.* **33**, 7–20 (2014).

110. Hess, D. T. & Stamler, J. S. Regulation by S-nitrosylation of protein post-translational modification. *J. Biol. Chem.* **287**, 4411–4418 (2012).

111. Stomberski, C. T., Zhou, H. L., Wang, L., Van Den Akker, F. & Stamler, J. S. Molecular recognition of S-nitrosothiol substrate by its cognate protein denitrosylase. *J. Biol. Chem.* **294**, 1568–1578 (2019).

112. Liu, L. *et al.* A metabolic enzyme for S-nitrosothiol conserved from bacteria to humans. *Nature* **410**, 490–494 (2001).

113. Wei, W. *et al.* S-nitrosylation from GSNOR deficiency impairs DNA repair and promotes hepatocarcinogenesis. *Sci. Transl. Med.* **2**, 19ra13 (2010).

114. López-Sánchez, L. M., Corrales, F. J., López-Pedrera, C., Aranda, E. & Rodríguez-Ariza, A. Pharmacological impairment of 5-nitrosoglutathione or thioredoxin reductases augments protein S-nitrosation in human hepatocarcinoma cells. *Anticancer Res.* **30**, 415–421 (2010).

115. Cañas, A. *et al.* Altered S-nitrosothiol homeostasis provides a survival advantage to breast cancer cells in HER2 tumors and reduces their sensitivity to trastuzumab. *Biochim. Biophys. Acta - Mol. Basis Dis.* **1862**, 601–610 (2016).

116. Doulias, P. T., Tenopoulou, M., Greene, J. L., Raju, K. & Ischiropoulos, H. Nitric oxide regulates mitochondrial fatty acid metabolism through reversible protein S-nitrosylation. *Sci. Signal.* **6**, 1–17 (2013).

117. Peñarando, J. *et al.* A role for endothelial nitric oxide synthase in intestinal stem cell proliferation and mesenchymal colorectal cancer. *BMC Biol.* **16**, 1–14 (2018).

118. Puig, I. *et al.* A personalized preclinical model to evaluate the metastatic potential of patient-derived colon cancer initiating cells. *Clin. Cancer Res.* **19**, 6787–6801 (2013).

119. Jourd'Heuil, D., Gray, L. & Grisham, M. B. S-Nitrosothiol foundation in blood of lipopolysaccharide-treated rats. *Biochem. Biophys. Res. Commun.* **273**, 22–26 (2000).

120. Dienstmann, R. *et al.* Consensus molecular subtypes and the evolution of precision medicine in colorectal cancer. *Nat Rev Cancer*. **17**, 79–92 (2017).

121. Ishiguro, T. *et al.* Tumor-derived spheroids: Relevance to cancer stem cells and clinical applications. *Cancer Sci*. **108**, 283–289 (2017).

122. Lundberg, I. V. *et al.* SOX2 expression is associated with a cancer stem cell state and down-regulation of CDX2 in colorectal cancer. *BMC Cancer* **16**, (2016).

123. Wei, F. *et al.* PD-L1 promotes colorectal cancer stem cell expansion by activating HMGA1-dependent signaling pathways. *Cancer Lett.* **450**, 1–13 (2019).

124. Pavlova, N. N. & Thompson, C. B. The Emerging Hallmarks of Cancer Metabolism. *Cell Metab*. **23**, 27–47 (2016).

125. Intlekofer, A. M. & Finley, L. W. S. Metabolic signatures of cancer cells and stem cells. *Nat Metab*. **1**, 177–188 (2019).

126. Vyas, S., Zaganjor, E. & Haigis, M. C. Mitochondria and Cancer. *Cell*. **166**, 555–566 (2016).

127. Chen, H. & Chan, D. C. Mitochondrial Dynamics in Regulating the Unique Phenotypes of Cancer and Stem Cells. *Cell Metab*. **26**, 39–48 (2017).

128. Giger, O. T., Comtesse, S. C. M., Lugli, A., Zlobec, I. & Kurrer, M. O. Intra-tumoral budding in preoperative biopsy specimens predicts lymph node and distant metastasis in patients with colorectal cancer. *Mod. Pathol.* **25**, 1048–1053 (2012).

129. Pu, X. *et al.* Patient-derived tumor immune microenvironments in patient-derived xenografts of lung cancer. *J. Transl. Med.* **16**, 328 (2018). doi: 10.1186/s12967-018-1704-3.

130. Georges, L. M. C. *et al.* Cell Line Derived Xenograft Mouse Models Are a Suitable in vivo Model for Studying Tumor Budding in Colorectal Cancer. *Front. Med.* **6**, (2019).

131. Gujam, F. J. A., McMillan, D. C., Mohammed, Z. M. A., Edwards, J. & Going, J. J. The relationship between tumour budding, the tumour microenvironment and survival in patients with invasive ductal breast cancer. *Br. J. Cancer* **113**, 1066–1074 (2015).

132. Van Wyk, H. C. *et al.* The relationship between tumour budding, the tumour microenvironment and survival in patients with primary operable colorectal cancer. *Br. J. Cancer* **115**, 156–163 (2016).

133. Masugi, Y. *et al.* Solitary cell infiltration is a novel indicator of poor prognosis and epithelial-mesenchymal transition in pancreatic cancer. *Hum. Pathol.* **41**, 1061–1068 (2010).

134. Prall, F., Maletzki, C., Hühns, M., Krohn, M. & Linnebacher, M. Colorectal carcinoma tumour budding and podia formation in the xenograft microenvironment. *PLoS One* **12**, (2017). doi: 10.1371/journal.pone.0186271.

135. Martinez-Ciarpaglini, C. *et al.* Low miR200c expression in tumor budding of invasive front predicts worse survival in patients with localized colon cancer and is related to PD-L1 overexpression. *Mod. Pathol.* **32**, 306–313 (2019).

136. Prall, F. & Hühns, M. PD-L1 expression in tumour buds of colorectal carcinoma. *Histopathology*. **69**, 158–160 (2016).

137. Korehisa, S. *et al.* Clinical significance of programmed cell death-ligand 1 expression and the immune microenvironment at the invasive front of colorectal cancers with high microsatellite instability. *Int. J. Cancer* **142**, 822–832 (2018).

138. Zhou, E. *et al.* Up-regulation of Tim-3 is associated with poor prognosis of patients with colon cancer. *Int. J. Clin. Exp. Pathol.* **8**, 8018–8027 (2015).

139. Nair, V. S. *et al.* Transcriptomic profiling of tumor-infiltrating CD4+ TIM-3+ T cells reveals their suppressive, exhausted, and metastatic characteristics in colorectal cancer patients. *Vaccines* **8**, 71 (2020). doi: 10.3390/vaccines8010071.

140. Yu, H. *et al.* A novel humanized mouse model with significant improvement of class-switched, antigen-specific antibody production. *Blood* **129**, 959–969 (2017).

141. van der Weyden, L. *et al.* Pulmonary metastatic colonisation and granulomas in NOX2-deficient mice. *J. Pathol.* **246**, 300–310 (2018).

142. Zhang, W. *et al.* Overexpression of Indoleamine 2,3-Dioxygenase 1 Promotes Epithelial-Mesenchymal Transition by Activation of the IL-6/STAT3/PD-L1 Pathway in Bladder Cancer. *Transl. Oncol.* **12**, 485–492 (2019).

143. Aydin, E., Johansson, J., Nazir, F. H., Hellstrand, K. & Martner, A. Role of NOX2-derived reactive oxygen species in NK cell–mediated control of murine melanoma metastasis. *Cancer Immunol. Res.* **5**, 804–811 (2017).

144. Seidel, J. A., Otsuka, A. & Kabashima, K. Anti-PD-1 and anti-CTLA-4 therapies in cancer: Mechanisms of action, efficacy, and limitations. *Front Oncol*. **8**, 86 (2018). doi: 10.3389/fonc.2018.00086.

145. Rotte, A. Combination of CTLA-4 and PD-1 blockers for treatment of cancer. *J Exp Clin Cancer Res*. **38**, 255 (2019). doi: 10.1186/s13046-019-1259-z.

146. Lee, L. H. *et al.* Patterns and prognostic relevance of PD-1 and PD-L1 expression in colorectal carcinoma. *Mod. Pathol.* **29**, 1433–1442 (2016).

147. Ridnour, L. A. *et al.* Molecular pathways: Toll-like receptors in the tumor microenvironment-poor prognosis or new therapeutic opportunity. *Clin Cancer Res*. **19**, 1340–1346 (2013).

148. Sato, Y., Goto, Y., Narita, N. & Hoon, D. S. B. Cancer cells expressing toll-like receptors and the tumor microenvironment. *Cancer Microenviron*. **2**, 205–214 (2009).

149. Wang, K. *et al.* Expression of TLR4 in non-small cell lung cancer is associated with PD-L1 and poor prognosis in patients receiving pulmonectomy. *Front. Immunol.* **8**, (2017).

150. Lu, C. C. *et al.* Upregulation of TLRs and IL-6 as a marker in human colorectal cancer. *Int. J. Mol. Sci.* **16**, 159–177 (2014).

151. Yu, L. & Chen, S. Toll-like receptors expressed in tumor cells: Targets for therapy. *Cancer Immunology, Immunotherapy* vol. 57 1271–1278 (2008).

152. Verbeke, H., Struyf, S., Laureys, G. & Van Damme, J. The expression and role of CXC chemokines in colorectal cancer. *Cytokine and Growth Factor Reviews* vol. 22 345–358 (2011).

153. Susek, K. H., Karvouni, M., Alici, E. & Lundqvist, A. The role of CXC chemokine receptors 1–4 on immune cells in the tumor microenvironment. *Frontiers in Immunology* vol. 9 (2018).

154. Kumar, V. *et al.* Cancer-Associated Fibroblasts Neutralize the Anti-tumor Effect of CSF1 Receptor Blockade by Inducing PMN-MDSC Infiltration of Tumors. *Cancer Cell* **32**, 654-668.e5 (2017).

155. Yang, J. *et al.* Loss of CXCR4 in myeloid cells enhances antitumor immunity and reduces melanoma growth through NK Cell and FASL mechanisms. *Cancer Immunol. Res.* **6**, 1186–1198 (2018).

156. Yang, L. *et al.* Abrogation of TGFβ Signaling in Mammary Carcinomas Recruits Gr-1+CD11b+ Myeloid Cells that Promote Metastasis. *Cancer Cell* **13**, 23–35 (2008).

157. Yu, M. *et al.* Tim-3 is upregulated in human colorectal carcinoma and associated with tumor progression. *Mol. Med. Rep.* **15**, 689–695 (2017).

158. Brito, C. *et al.* Peroxynitrite inhibits T lymphocyte activation and proliferation by promoting impairment of tyrosine phosphorylation and peroxynitrite-driven apoptotic death. *J. Immunol.* **162**, 3356–66 (1999).

159. Bronte, V. *et al.* Boosting antitumor responses of T lymphocytes infiltrating human prostate cancers. *J. Exp. Med.* **201**, 1257–1268 (2005).

160. Molon, B. *et al.* Chemokine nitration prevents intratumoral infiltration of antigen-specific T cells. *J. Exp. Med.* **208**, 1949–1962 (2011).

161. Rizza, S. & Filomeni, G. Chronicles of a reductase: Biochemistry, genetics and physio-pathological role of GSNOR. *Free Radical Biology and Medicine* vol. 110 19–30 (2017).

162. Pilati, C. *et al.* CDX2 prognostic value in stage II/III resected colon cancer is related to CMS classification. *Ann. Oncol. Off. J. Eur. Soc. Med. Oncol.* **28**, 1032–1035 (2017).

163. Narayanan, S. *et al.* Cytolytic Activity Score to Assess Anticancer Immunity in Colorectal Cancer. *Ann. Surg. Oncol.* **25**, 2323–2331 (2018).

164. Santiago, L. *et al.* Extracellular Granzyme A Promotes Colorectal Cancer Development by Enhancing Gut Inflammation. *Cell Rep.* **32**, (2020).

165. Mlecnik, B. *et al.* Functional network pipeline reveals genetic determinants associated with in situ lymphocyte proliferation and survival of cancer patients. *Sci. Transl. Med.* **6**, (2014).

166. Bindea, G. *et al.* Spatiotemporal dynamics of intratumoral immune cells reveal the immune landscape in human cancer. *Immunity* **39**, 782–795 (2013).

167. Ruvolo, P. P. Galectin 3 as a guardian of the tumor microenvironment. *Biochimica et Biophysica Acta - Molecular Cell Research* vol. 1863 427–437 (2016).

168. Cho, Y. S. *et al.* Efficacy of CD46-targeting chimeric Ad5/35 adenoviral gene therapy for colorectal cancers. *Oncotarget* **7**, 38210–38223 (2016).

169. Ara, A., Ahmed, K. A. & Xiang, J. Multiple effects of CD40–CD40L axis in immunity against infection and cancer. *ImmunoTargets Ther.* **Volume 7**, 55–61 (2018).

170. Batlle, E. & Clevers, H. Cancer stem cells revisited. *Nature Medicine* vol. 23 1124–1134 (2017).

171. Wong, T. L., Che, N. & Ma, S. Reprogramming of central carbon metabolism in cancer stem cells. *Biochimica et Biophysica Acta - Molecular Basis of Disease* vol. 1863 1728–1738 (2017).

172. Ahmed, N., Escalona, R., Leung, D., Chan, E. & Kannourakis, G. Tumour microenvironment and metabolic plasticity in cancer and cancer stem cells: Perspectives on metabolic and immune regulatory signatures in chemoresistant ovarian cancer stem cells. *Seminars in Cancer Biology* vol. 53 265–281 (2018).

173. Yadav, U. P. *et al.* Metabolic Adaptations in Cancer Stem Cells. *Frontiers in Oncology* vol. 10 (2020).

174. Chang, C. H. *et al.* Metabolic Competition in the Tumor Microenvironment Is a Driver of Cancer Progression. *Cell* **162**, 1229–1241 (2015).

175. Feng, J. *et al.* Tumor cell-derived lactate induces TAZ-dependent upregulation of PD-L1 through GPR81 in human lung cancer cells. *Oncogene* **36**, 5829–5839 (2017).

176. Archer, S. L. Mitochondrial Dynamics — Mitochondrial Fission and Fusion in Human Diseases. *N. Engl. J. Med.* **369**, 2236–2251 (2013).

177. Galloway, C. A., Lee, H. & Yoon, Y. Mitochondrial morphology-emerging role in bioenergetics. *Free Radical Biology and Medicine* vol. 53 2218–2228 (2012).

178. Galloway, C. A. & Yoon, Y. Mitochondrial morphology in metabolic diseases. *Antioxidants and Redox Signaling* vol. 19 415–430 (2013).

179. Ježek, J., Cooper, K. F. & Strich, R. Reactive oxygen species and mitochondrial dynamics: The yin and yang of mitochondrial dysfunction and cancer progression. *Antioxidants* vol. 7 (2018).

180. Dai, W. & Jiang, L. Dysregulated Mitochondrial Dynamics and Metabolism in Obesity, Diabetes, and Cancer. *Frontiers in Endocrinology* vol. 10 (2019).

181. Bossy, B. *et al.* S-nitrosylation of DRP1 does not affect enzymatic activity and is not specific to Alzheimer's disease. *J. Alzheimer's Dis.* **20**, (2010).

182. Cho, D. H. *et al.* S-Nitrosylation of Drp1 Mediates β-Amyloid-related mitochondrial fission and neuronal injury. *Science (80-. ).* **324**, 102–105 (2009).

183. Rizza, S. *et al.* S-nitrosylation drives cell senescence and aging in mammals by controlling mitochondrial dynamics and mitophagy. *Proc. Natl. Acad. Sci. U. S. A.* **115**, E3388–E3397 (2018).

# *X. ANNEX*

frontiers in Medicine

ORIGINAL RESEARCH
published: 03 July 2020
doi: 10.3389/fmed.2020.00264

# Association of Tumor Budding With Immune Evasion Pathways in Primary Colorectal Cancer and Patient-Derived Xenografts

*Silvia Guil-Luna[1,2*†], Rafael Mena[1†], Carmen Navarrete-Sirvent[1], Laura María López-Sánchez[1,2], Karima Khouadri[1], Marta Toledano-Fonseca[1,2], Ana Mantrana[1], Ipek Guler[1], Carlos Villar[3], Cesar Díaz[4], Francisco Javier Medina-Fernández[4], Juan Rafael De la Haba-Rodríguez[1,2,5], Enrique Aranda[1,2,5,6‡] and Antonio Rodríguez-Ariza[1,2,5‡]*

[1] Instituto Maimónides de Investigación Biomédica de Córdoba, Córdoba, Spain, [2] Centro de Investigación Biomédica en Red de Cáncer (CIBERONC), Madrid, Spain, [3] Unidad de Gestión Clínica de Anatomía Patológica, Hospital Universitario Reina Sofía, Córdoba, Spain, [4] Unidad de Gestión Clínica de Cirugía General y del Aparato Digestivo, Hospital Universitario Reina Sofía, Córdoba, Spain, [5] Unidad de Gestión Clínica de Oncología Médica, Hospital Universitario Reina Sofía, Córdoba, Spain, [6] Departamento de Medicina, Facultad de Medicina de Córdoba, Universidad de Córdoba, Córdoba, Spain

Tumor budding has been found to be of prognostic significance for several cancers, including colorectal cancer (CRC). Additionally, the molecular classification of CRC has led to the identification of different immune microenvironments linked to distinct prognosis and therapeutic response. However, the association between tumor budding and the different molecular subtypes of CRC and distinct immune profiles have not been fully elucidated. This study focused, firstly, on the validation of derived xenograft models (PDXs) for the evaluation of tumor budding and their human counterparts and, secondly, on the association between tumor budding and the immune tumor microenvironment by the analysis of gene expression signatures of immune checkpoints, Toll-like receptors (TLRs), and chemokine families. Clinical CRC samples with different grades of tumor budding and their corresponding PDXs were included in this study. Tumor budding grade was reliably reproduced in early passages of PDXs, and high-grade tumor budding was intimately related with a poor-prognosis CMS4 mesenchymal subtype. In addition, an upregulation of negative regulatory immune checkpoints (PDL1, TIM-3, NOX2, and IDO1), TLRs (TLR1, TLR3, TLR4, and TLR6), and chemokine receptors and ligands (CXCR2, CXCR4, CXCL1, CXCL2, CXCL6, and CXCL9) was detected in high-grade tumor budding in both human samples and their corresponding xenografts. Our data support a close link between high-grade tumor budding in CRC and a distinctive immune-suppressive microenvironment promoting tumor invasion, which may have a determinant role in the poor prognosis of the CMS4 mesenchymal subtype. In addition, our study demonstrates that PDX models may constitute a robust preclinical platform for the development of novel therapies directed against tumor budding in CRC.

**Keywords: patient-derived xenografts, tumor budding, colorectal cancer, immune evasion, toll-like receptors, chemokines**

OPEN ACCESS

***Edited by:***
*Luigi Tornillo, University of Basel, Switzerland*

***Reviewed by:***
*Lucia Bongiovanni, San Raffaele Hospital (IRCCS), Italy*
*Thomas Menter, University Hospital of Basel, Switzerland*

***Correspondence:**
*Silvia Guil-Luna*
*v22gulus@uco.es*

†*These authors have contributed equally to this work*

‡*These authors share senior authorship*

***Specialty section:***
*This article was submitted to Pathology, a section of the journal Frontiers in Medicine*

***Received:*** *01 April 2020*
***Accepted:*** *14 May 2020*
***Published:*** *03 July 2020*

***Citation:***
*Guil-Luna S, Mena R, Navarrete-Sirvent C, López-Sánchez LM, Khouadri K, Toledano-Fonseca M, Mantrana A, Guler I, Villar C, Díaz C, Medina-Fernández FJ, De la Haba-Rodríguez JR, Aranda E and Rodríguez-Ariza A (2020) Association of Tumor Budding With Immune Evasion Pathways in Primary Colorectal Cancer and Patient-Derived Xenografts. Front. Med. 7:264. doi: 10.3389/fmed.2020.00264*

## INTRODUCTION

Tumor budding has recently received much attention in the setting of progression and invasion in several malignancies including colorectal cancer (CRC). Tumor budding is defined as a single tumor cell or cluster of up to 4 cells at the invasive front (1, 2). High-grade tumor budding is now established as an independent prognostic factor since it has been associated with shorter disease-free survival (DFS) and overall survival (OS) in several types of cancer (2–4). Currently, it is widely believed that tumor buds provide the histological basis for invasion and metastasis, but it is still a matter of controversy if it is directly related with the epithelial–mesenchymal transition (EMT) (5, 6).

High-grade tumor budding has been inversely correlated with the presence of immune infiltrate at the invasive front. In addition, an overexpression of stem-cell related genes as ZEB1, ZEB2, DES, and VIM, and the activation of both WNT and TGF-β signaling, has been demonstrated to be expressed in tumor buds (7–9).

In this context, tumor budding has been recently associated with the poor-prognosis CMS4 subtype of CRC (10). This mesenchymal-like subtype is characterized by overexpression of stem cell markers, neoangiogenesis, and activation of TGF-β and WNT/β-catenin pathways which modulate immune evasion and the metastasis process (11–13). CMS4 tumors display low content of immune cells and exhibited the worst DFS and OS, demonstrating an urgent need to develop therapies for this subtype (11, 12). These findings are in line with the described profiles of tumor buds. However, the potential relationship between the immunosuppressive microenvironment of this poor-prognosis subtype and tumor buds still remains unknown (7).

Recognizing that tumor budding is an important contributor of the tumor invasion prognosis and the close relation with the CMS4 subtype, the translation of tumor budding to preclinical models has major challenges. Patient-derived xenografts (PDXs) generated by direct engraftment of human tumor tissue into immunodeficient mice have emerged as powerful preclinical platforms for analysis of predictive biomarkers, therapeutic targets, and drug discovery in cancer (14).

In this study, firstly, we examined early passages of CRC PDXs as potential models to analyze tumor budding and, secondly, we elucidated a link between high-grade budding and CMS4 subtype and specific signatures of immune evasion. PDXs may greatly help in the understanding of tumor budding and the involved mechanisms in the tumor microenvironment, which will provide new strategies and prospects for more effective treatments. In addition, treatments which simultaneously tackle the interactions between tumor buds and surrounding stroma could more effectively kill tumor cells or at least limit tumor progression and metastatic dissemination.

## MATERIALS AND METHODS

### Patient and Inclusion Criteria

A consecutive, population-based series of forty-five patients over 18 years of age with resectable colon cancer submitted to Reina Sofía Hospital (Córdoba, Spain) was prospectively included. To avoid the bias of neoadjuvant treated patients, all rectal cancer patients were excluded. The study was approved by the Reina Sofía Hospital ethical committee (Protocol number PI-0150-2017) in accordance with the Code of Ethics of the World Medical Association (Declaration of Helsinki). Informed consent was obtained from each patient, and clinical and pathological information was prospectively collected. The clinicopathological characteristics of patients are summarized in **Table 1**.

### Processing of Tumor Samples and Establishment of PDX Models

A total of 45 tumor samples were obtained just after surgical resection. Three adjacent tumor pieces were immediately collected in sterile conditions. One tumor piece was snap frozen and stored in liquid nitrogen for gene expression profiling, another one was fixed in 4% buffered formalin and then embedded in paraffin (FFPE) for hematoxylin and eosin staining and IHC studies, and the third fresh tumor piece was included in sterile PBS and used for establishment of PDXs.

The PDX engraftment was performed according to Puig and coauthors in NOD-SCID mice (NOD.CB17-Prkdcscid/Rj) (Janvier Laboratory, Paris, France) of 4–6 weeks of age (15). The animals were fed with a standard diet (D03-SAFE, Augy, France) and provided with drinking water *ad libitum*. Mice were daily monitored, and tumor growth was weekly measured until tumor volume was 1 $cm^3$. Mice were ethically sacrificed under isoflurane anesthesia followed by cervical dislocation when tumor reached that size, if they appeared to be suffering, or after 6 months without tumor growth. Samples were immediately collected, fresh-frozen, formalin-fixed, and reimplanted (P1) as described above. This process was repeated to produce subsequent passages (until P3). Animal care and experimental procedures were approved by the University of Córdoba Bioethics Committee and followed the regulations of the European Union normative (26/04/2016/066).

### Histological and Immunohistochemical Analysis of Patient Tumor Samples and PDX Models

Hematoxylin and eosin-stained tissue sections were evaluated by 2 trained pathologists (CVP and SGL) for the following criteria: histological subtype, invasion (lymphatic, vascular, or perineural), and stromal and inflammatory component. The degree of inflammatory cell infiltration was assessed in the center of the tumor and invasive margin of the tumor as reported previously (16). For the analysis of stroma, a representative 10× magnification area of the invasive margin was selected and the percentage of the stroma for each sample was calculated as described by Gujam et al. (17).

On the other hand, IHC staining was performed on 4-μm FFPE sections using the antibodies detailed in **Supplementary Table 1** for molecular classification of patient tumors and PDXs. Tissue sections were incubated in 10 mM citrate buffer (pH 6.0) for 5 min at 120°C for antigen retrieval. Endogenous peroxidase was neutralized by using the EnVision FLEX peroxidase-blocking reagent (Dako, Glostrup, Denmark)

**TABLE 1 |** Clinicopathological data of the patients included in the study.

| | **All subjects, *n* (%)** |
|---|---|
| **Patients characteristics (*n* = 45)** | |
| Gender | |
| Female | 15 (33%) |
| Male | 30 (67%) |
| Age (mean ± SD) | 73.8 ± 10.1 |
| Distant metastasis at the diagnosis | |
| No | 40 (89%) |
| Yes | 5 (11%) |
| **Tumor characteristics (*n* = 45)** | |
| Tumor size (cm, mean ± SD) | 4.2 ± 1.1 |
| Tumor histological grade | |
| Low | 39 (87%) |
| High | 6 (13%) |
| TNM staging | |
| 0 | 2 (4%) |
| I | 1 (2%) |
| II | 21 (47%) |
| III | 16 (36%) |
| IV | 5 (11%) |
| Anatomical location | |
| Left | 20 (44%) |
| Right | 25 (56%) |
| Histological subtype | |
| Well differentiated | 6 (13%) |
| Moderately differentiated | 34 (76%) |
| Poorly differentiated | 5 (11%) |
| Mucinous component | |
| No | 30 (67%) |
| Yes | 15 (33%) |
| Stromal component | |
| < 50% | 14 (31%) |
| ≥ 50% | 31 (69%) |
| Inflammatory infiltrate | |
| Low | 20 (44%) |
| Medium | 16 (36%) |
| High | 11 (25%) |
| Lymphatic invasion | |
| No | 23 (51%) |
| Yes | 22 (49%) |
| Perineural invasion | |
| No | 26 (58%) |
| Yes | 19 (42%) |
| Vascular invasion | |
| No | 28 (62%) |
| Yes | 17 (38%) |
| Molecular subtype | |
| CMS1 | 8 (18%) |
| CMS2/3 | 25 (58%) |
| CMS4 | 12 (24%) |

for 10 min. After blocking with 3% bovine serum albumin or following mouse-on-mouse staining protocol (Abcam, Cambridge, UK) in the case of PDXs, sections were incubated with the primary antibodies overnight at 4°C. Then, after incubation with the corresponding EnVision FLEX+ mouse or rabbit linker (Dako, Glostrup, Denmark) (30 min at room temperature), sections were incubated for 1 h with the secondary antibody EnVision FLEX/HRP (Dako, Glostrup, Denmark). The staining was visualized using 3,3-diaminobenzidine chromogen (Dako, Glostrup, Denmark) and counterstained with Harris hematoxylin. Negative controls without incubation with primary antibodies were also performed.

## Immunohistochemistry-Based Molecular CMS Classification

Molecular classification by IHC was performed as described elsewhere (18). Individual cores were scored by trained pathologists (CVP and SGL) for FRMD6, ZEB1, HTR2B, AE1AE3, and CDX2 intensity and content. For MSI status, an analysis was performed with specific antibodies against hMLH1, hMSH2, hMSH6, and hPMS2, as described above. Immunohistochemical scores for each antibody were entered in the online classification tool (crclassifier.shinyapps.io/appTesting/) as described elsewhere (18). Using this classification, tumors were classified as CMS1, CMS2/3, or CMS4 subtypes.

## Tumor Budding Determination

Tumor budding was defined as single tumor cells or tumor cell clusters of up to four cells in the stroma of the invasive front as previously reported (1). Tumor buds were assessed on pan-cytokeratin (clone AE1/AE3) immunostaining in a single hot spot measuring 0.785 $mm^2$ for more accurate identification in cases of obscuring factors like inflammation or reactive stroma. Cutoffs as defined by International Tumor Budding Consensus Conference (ITBCC) were used: low (BD1), 0–4 buds; intermediate (BD2), 5–9 buds; and high (BD3) ≥10 buds (18).

## Immune Gene Expression Profiling of Patient Tumors and PDX Models

The expression of genes encoding molecules involved in immune checkpoints, Toll-like receptors (TLRs), and chemokine receptors and their ligands was analyzed using the nCounter PanCancer immune-profiling panel from NanoString (Seattle, WA, USA) both in patient tumors and their corresponding PDXs. In order to minimize the variability between patients and xenografts, P0 passage was used for immune gene expression profiling. For this purpose, total RNA extraction was performed using RNeasy Mini Kit (Qiagen, Hilden, Germany) following the manufacturer's recommendations. Quantification and determination of the RNA purity were performed using a NanoDrop™ 1000 spectrophotometer (NanoDrop® ND-1000 UV-Vis Spectrophotometer, NanoDrop Technology), and RNA integrity Number (RIN) was measured using an Agilent 2200 TapeStation equipment. Data analysis was performed using nSolver software (NanoString Technologies, Seattle, WA, USA)

to manage the raw data generated from the expression of each gene (19). The positive or negative expression of one particular gene indicates that the number of RNA molecules is higher or lower than the mean, respectively.

## Statistical Analysis

Data were analyzed using GraphPad Prism 7 and R Software (version 3.5.0). Previously, in order to assess normality of the data, D'Agostino and Pearson Normality test was performed. The clinicopathological data were compared using Fisher's exact test or Mann–Whitney's test for qualitative and quantitative variables, respectively. Multivariate regression analysis was carried out with multinomial regression model for budding grades, including the variables selected by using the Akaike information criterion (AIC) with step-wise model selection. Differences in disease-free survival (DFS) were expressed as hazard ratios (HR) with 95% confidence intervals, and survival curves were constructed using the Kaplan–Meier method. All $p$ values $\leq 0.05$ were considered statistically significant.

# RESULTS

## Tumor Budding Is Robustly Recapitulated in PDX Models and Is Closely Associated With the CMS4 Molecular Subtype of CRC

Overall, 82% (37/45) tumors were successfully engrafted with a mean latency period (time from day of inoculation to palpable tumor) of 30.7 ± 26.9 days for P0, which was shortened in subsequent passages (15.1 ± 9.8 for P1, 10.7 ± 5.0 for P2, and 8.1 ± 3.0 for P3).

Histopathological analysis of clinical tumors and their corresponding PDXs showed the preservation of the general tumor architecture and the histological subtype over several passages (**Supplementary Figure 1**). Remarkably, the determination of tumor budding status revealed a strong correlation between patient tumors and xenograft models ($r = 0.72, p < 0.001$) (**Figure 1A**).

In order to analyze the relationship between tumor budding and molecular subtypes of CRC, a molecular classification of patient tumors and xenografts was performed following the IHC-based method implemented by Trinh et al. (18). A strong concordance in the IHC expression patterns and consequently with the molecular CMS subtypes was observed between patient tumors and their corresponding PDXs with a Cohen's kappa coefficient of 0.96 (**Figure 2A**). Just in one case did the molecular subtype in the patient tumor (CMS4) shift to a different subtype (CMS2/3) in its PDX model (**Figure 2B**).

In particular, while most of the BD1 tumors (80% in tumor patients and 63% in PDXs) were classified as CMS2/3 subtype, BD3 tumors were more abundantly present in the poor-prognosis CMS4 subtype in both patient tumors and xenografts (**Figures 1B,C**). In addition, only 13% of human CMS4 subtypes were classified with low grade of tumor budding (BD1).

## High-Grade Budding (BD3) Is Associated With Adverse Clinicopathological Factors

**Table 1** summarizes clinicopathological characteristics of patients included in this study. A high-grade tumor budding (BD3) was identified in 18 (40%) patients, followed by 12 (27%) patients with BD2 tumor budding and 15 (33%) patients with low-grade budding (BD1). The relationship between tumor budding and clinicopathological characteristics of patients is presented in **Table 2**. On univariate analysis, high-grade tumor budding was associated with poorly differentiated carcinomas ($p = 0.02$), higher stromal component ($p = 0.02$), tumor vascular invasion ($p = 0.005$), and presence of distant metastasis ($p = 0.02$). The histological subtype, tumor size, and stromal component were entered as covariates into the final multivariate model, based on the variable selection with the Akaike information criterion (AIC) using stepwise selection (**Table 3**). Regarding survival analysis, no event data (disease progression) were observed in low-grade budding. The intermediate- and high-grade tumor budding (BD2 and BD3) was significantly associated with poor DFS ($p = 0.03$) when compared with low-grade budding (**Figure 3**). Additionally, survival probability of intermediate- and high-grade tumor budding was compared but no significant difference was found [HR: 95% CI De-long BD3 vs. BD2: 1.38 (0.31–6.21)] (**Figure 3**).

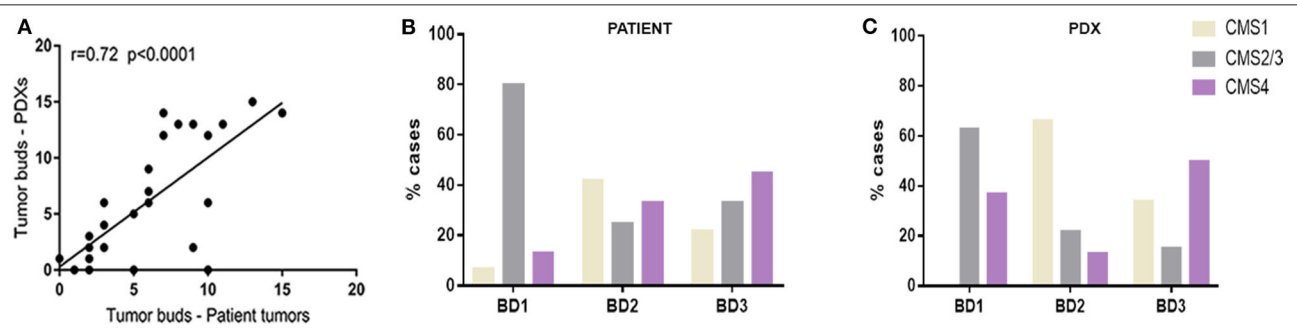


**FIGURE 1 | (A)** Correlation between number of tumor buds in clinical tumors and in their corresponding PDX models. **(B)** Distribution of CMS molecular subtypes according to tumor budding grade in patient tumors. **(C)** Distribution of CMS molecular subtypes according to tumor budding grade in xenograft models (PDX).

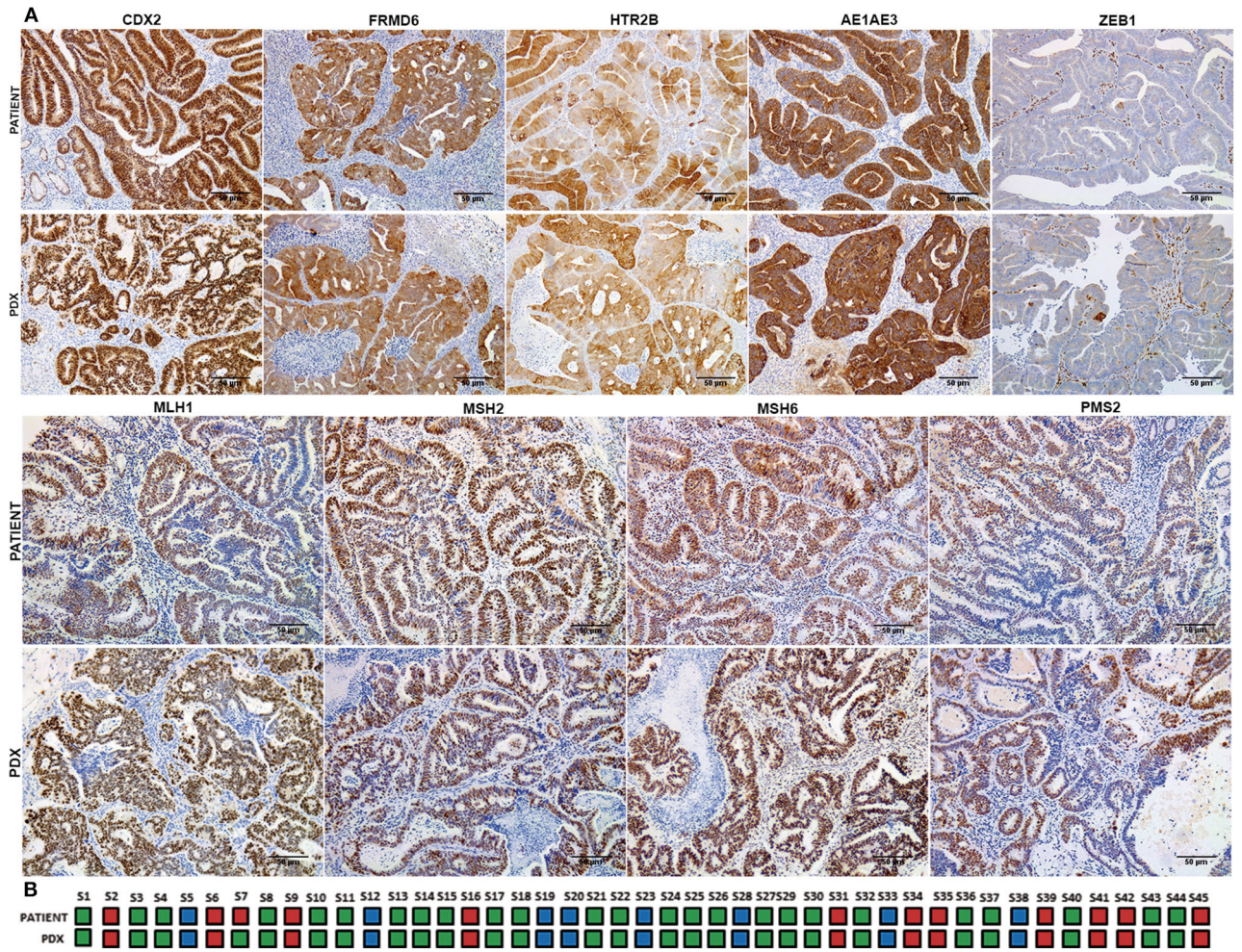


**FIGURE 2 |** Immunohistochemical classification into CMS subtypes of patient tumor samples and their corresponding PDX models. **(A)** Representative immunohistochemical staining for CDX2, FRMD6, HTR2B, AE1AE3, ZEB1, MLH1, MSH2, MSH6, and PMS2 of a clinical tumor and its corresponding PDX model. **(B)** CMS classification concordance between patient tumors and their corresponding PDX models. Blue color corresponds to CMS1 subtype, green color corresponds to CMS2/3 subtype, and red color corresponds to CMS4 subtype. Scale bars: 100 μm.

## Gene Expression of Immune Checkpoint, TLRs, and Chemokine Profiles Reveals Similar Distinct Patterns According to Tumor Budding Grade in Patients and Xenografts

By using a PanCancer immune-profiling panel from the NanoString platform, we identified those immune-related genes overexpressed in high-grade tumor budding compared with low-grade budding. In addition, the immune gene expression profiles of patient tumors were compared with the gene expression profiles of their corresponding xenograft models (P0).

The expression of inhibitory immune checkpoints according to tumor budding grade is displayed in **Figure 4**. The comparative analysis revealed a general upregulation of immune checkpoint-related genes in tumors with BD3 tumors in comparison with BD1 tumors (**Figure 4**). Interestingly, these immune signatures were remarkably preserved in their corresponding PDX models. Particularly, a higher expression of PDL1, TIM-3, NOX2, and IDO1 genes was observed in BD3 tumors. However, PD1 and CTLA4 genes were less expressed in the higher tumor budding grades in both patients and xenografts (**Figure 4**).

The expression of the TLR superfamily also displayed a high correspondence between patients and PDXs with the highest values for high-grade tumor budding (**Figure 5**). Of note, TLR1, TLR3, TLR4, and TLR6 were overexpressed in tumors with BD3 compared to BD1 tumors (**Figure 5**).

Regarding the CX chemokine receptor family, the results showed that BD3 tumors were associated with a higher expression of CXCR2 and CXCR4 (**Figure 6**) than BD1 tumors were. Among the chemokine ligands, CXCL1, CXCL2, CXCL6, and CXCL9 genes also displayed a higher expression in tumors

**TABLE 2 |** Association between clinicopathological data of tumors and budding grade on univariate analysis.

| Parameters | BD1 | BD2 | BD3 | *P*-value |
|---|---|---|---|---|
| **Patients' characteristic (*n* = 45)** | | | | |
| Age (years, mean ± SD) | 74.07 ± 10.33 | 75.50 ± 10.34 | 72.50 ± 10.19 | 0.7 |
| **Tumor's characteristic (*n* = 45)** | | | | |
| Tumor grade | | | | |
| Low | 14 | 11 | 14 | 0.35 |
| High | 1 | 1 | 4 | |
| TNM staging | | | | |
| 0–I–II | 11 | 6 | 7 | 0.13 |
| III–IV | 4 | 6 | 11 | |
| Anatomical location | | | | |
| Left | 8 | 4 | 8 | 0.58 |
| Right | 7 | 8 | 10 | |
| Histological subtype | | | | |
| Well differentiated | 5 | 0 | 1 | 0.02 |
| Moderately differentiated | 10 | 11 | 13 | |
| Poorly differentiated | 0 | 1 | 4 | |
| Mucinous component | | | | |
| No | 10 | 10 | 10 | 0.28 |
| Yes | 5 | 2 | 8 | |
| Inflammatory infiltrate | | | | |
| Low | 7 | 7 | 4 | 0.28 |
| Medium | 5 | 2 | 9 | |
| High | 3 | 3 | 5 | |
| Lymphatic invasion | | | | |
| No | 11 | 7 | 7 | 0.13 |
| Yes | 4 | 5 | 11 | |
| Perineural invasion | | | | |
| No | 10 | 5 | 10 | 0.43 |
| Yes | 5 | 7 | 8 | |
| Vascular invasion | | | | |
| Yes | 1 | 5 | 11 | 0.005 |
| No | 14 | 7 | 7 | |
| Distant metastasis | | | | |
| No | 14 | 10 | 12 | 0.05 |
| Yes | 0 | 3 | 6 | |
| Tumor size (cm, mean ± SD) | 4.50 ± 1.26 | 3.75 ± 0.91 | 4.25 ± 1.10 | 0.07 |
| Stromal component (%, mean ± SD) | 23.33 ± 19.88 | 26.67 ± 18.74 | 41.67 ± 19.47 | 0.02 |
| **PDX model's approach** | | | | |
| Engraftment rate (%, cases) | 80 (12/15) | 92 (11/12) | 83 (15/18) | 0.69 |
| Latency period (days, mean ± SD) | 32.08 ± 35.50 | 35.40 ± 25.52 | 28.20 ± 22.53 | 0.16 |

*BD1, budding grade 1; BD2, budding grade 2; BD3, budding grade 3.*

with BD3 compared to low-grade tumor budding (**Figure 7**). Notably, these distinct gene expression profiles of chemokine receptors and ligands depending on different budding statuses were in general, with some exceptions, preserved in the PDX models.

Despite the similar immune-related gene expression patterns found between primary tumors and PDXs with BD1 and BD3 grades, this correspondence was not as evident in PDXs with BD2 grade.

## DISCUSSION

Taking into account that tumor heterogeneity is one of the major obstacles in the success of the new personalized therapies for CRC, preclinical platforms which faithfully represent the complex tumor biology are urgently needed. Furthermore, the significance of tumor budding as an independent prognostic factor has now been well established, reinforcing the notion that may constitute a promising target for cancer therapy. However,

**TABLE 3 |** Multivariate analysis of clinicopathological data of the tumors.

| Variables | BD2 vs. BD1 | | | BD3 vs. BD1 | | |
|---|---|---|---|---|---|---|
| | Coef (SD) | *P*-value | OR 95% CI | Coef (SD) | *P*-value | OR 95% CI |
| Tumor size | −0.91 (0.46) | 0.046 | 0.40 [0.16-0.98] | −0.73 (0.44) | 0.097 | 0.48 [0.20–1.14] |
| Moderate vs. well diff. | 12.33 (0.92) | <0.001 | $2.27 \times 10^5$ [$3.73 \times 10^4$-$1.38 \times 10^6$] | 1.90 (1.43) | 0.184 | 6.72 [0.4–112.30] |
| Poorly vs. well diff. | 23.12 (0.80) | <0.001 | $1.10 \times 10^{10}$ [$2.28 \times 10^9$-$5.38 \times 10^{10}$] | 13.66 (0.80) | <0.001 | $8.57 \times 10^5$ [$2.28 \times 10^9$-$5.38 \times 10^{10}$] |
| Stromal component | 0.007 (0.02) | 0.772 | 1.007 [0.95–1.05] | 0.04 (0.02) | 0.055 | 1.04 [0.99–1.08] |

*Coef, coefficient; SD, standard deviation; OR, odds ratio; CI, confidence interval; BD1, budding grade 1; BD2, budding grade 2; BD3, budding grade 3.*

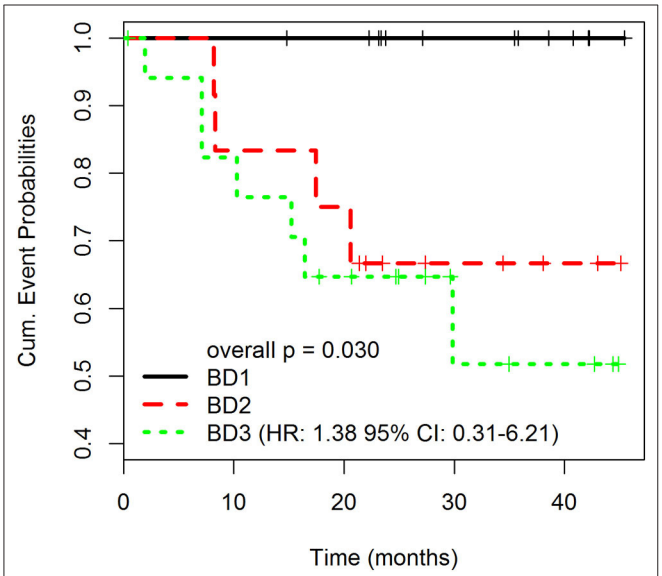


**FIGURE 3 |** Disease-free survival (DFS) rates according to different grades of tumor budding (BD1, BD2, BD3). Overall *p* is 0.030. The p-values for pairwise comparisons are BD1 vs. BD2 = 0.034; BD1 vs. BD3 = 0.022; BD2 vs. BD3 = 0.595. HR: 1.38 95% CI: 0.31–6.21).

the interaction between tumor budding and the immune tumor microenvironment still remains unclear. The present study demonstrates that tumor budding is reliably reproduced in early passages of PDXs of CRC. Moreover, our data support that high-grade tumor budding is intimately connected with poor-prognosis CMS4 subtype and with specific gene signatures related to tumor immune evasion.

Our data confirmed that tumor budding is associated with adverse clinicopathological characteristics, such as tumor size, poor histological differentiation, vascular invasion, and poor outcome, as previously reported in several type of cancers (2, 7, 10, 20). An interesting finding of the present study was the high level of correspondence between the budding score in clinical tumors and their corresponding PDX models. Intriguingly, the immune deficiency in host mice did not promote an increase in tumor budding. Pu et al. (21) demonstrated that patient-derived immune cells coexist in the first and second passages with a survival rate of 290 days in the mouse. Recently, tumor budding has also been demonstrated in both center and the invasion front in CRC cell-line xenografts (22). These findings strongly suggest that early passages of PDXs preserve the distinctive cross talk between cancer cells and the immune microenvironment and determine the suitability of this preclinical platform as a model of tumor budding in CRC.

Recently, Trihn et al. (10) reported the potential association of high-grade budding with the CMS4 subtype of CRC in a series of CMS2/3 and CMS4 patient tumors. In the present study, we found similar results with the CMS4 subtype enriched by high-grade tumor budding compared with CMS1 and CMS2/3 subtypes. The fact that tumor buds are well-established independent adverse prognostic factors in CRC (1, 2) as well as the correspondence of CMS subtypes and tumor budding grade between PDXs and their human counterparts observed in our study supports the use of PDX models as powerful tools for the development of targeted therapies against mechanisms involved in tumor budding.

We found that high-grade budding was also significantly associated with stroma-rich tumors. Earlier reports in CRC and breast cancer have suggested an association between tumor budding and the presence of a high density of stromal myofibroblasts (23, 24). Tumor-associated stroma has been shown to facilitate EMT by inducing growth factors, which has been linked with higher capacity of migration and invasion of bud cells (24, 25). Thus, these findings highlight the potential role of the stroma in establishing a microenvironment supportive of the formation of tumor buds. Taken together, the budding phenotype seems to be associated with the high stromal component, which is also accentuated in the mesenchymal CMS4 subtype of CRC.

It is important to note the remarkable overexpression of inhibitory immune checkpoint-related genes (PDL1, TIM-3, NOX2, and IDO1) in BD3 tumors in comparison to BD1 observed in this study. All these upregulated genes have been previously related with tumor invasion and metastasis. However, limited studies have analyzed the expression of immune checkpoint genes in relation with tumor budding (26, 27). In

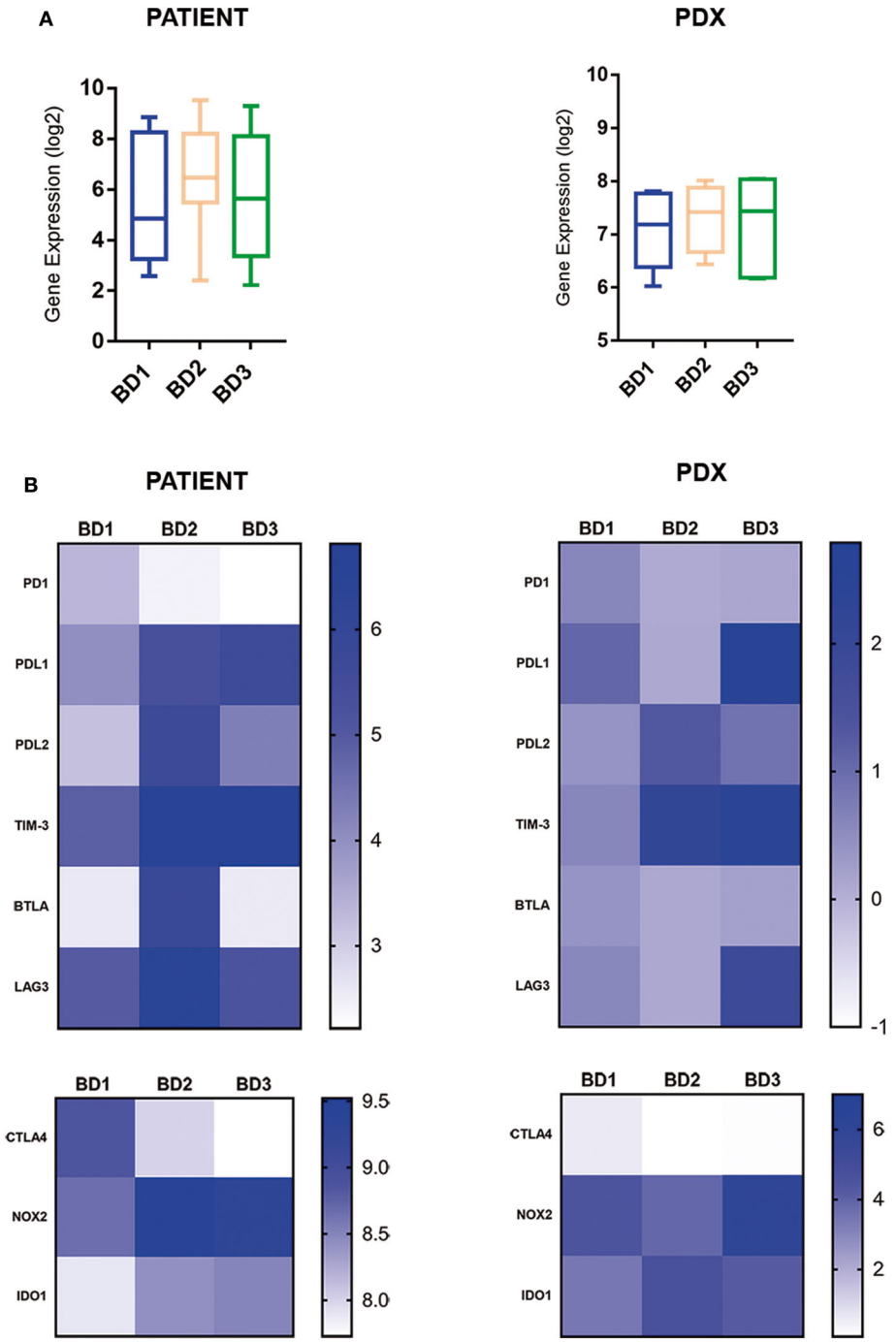


**FIGURE 4 |** Global **(A)** and single **(B)** gene expression levels of immune inhibitor checkpoints in patient tumors and their corresponding PDX models, according to different grades of tumor budding (BD1, BD2, BD3).

agreement with our data, an upregulation of PDL1 expression has been reported in high-grade tumor budding of CRC suggesting that PDL1 might be specifically overexpressed during EMT to allow invasion and immune escape (27–29). On the other hand, TIM-3, which has been shown to inhibit antitumor immunity by mediating CD8 T-cell exhaustion and pathways involved in metastasis, is an emerging immune checkpoint in several cancers including CRC (30–32). IDO1 and NOX2 are known to exert a potent immunosuppressive effect in a variety of human solid tumors by reducing both tumor-infiltrating T cells as well as B cells (33, 34). Recent studies suggest that NOX2 knockdown reduces metastasis via mechanisms involving

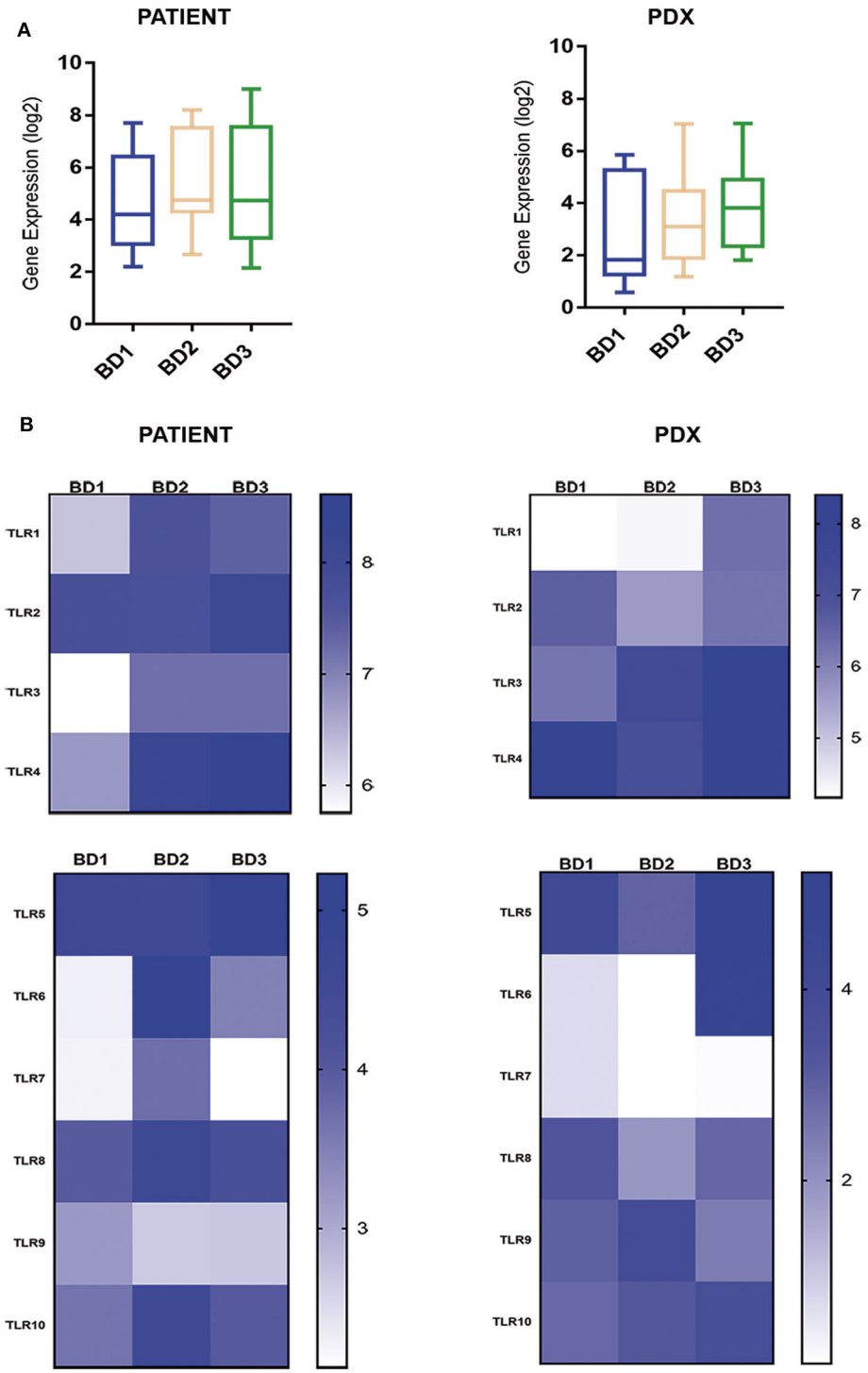


**FIGURE 5 |** Global **(A)** and single **(B)** gene expression levels of the TLR gene family in patient tumors and their corresponding PDX models, according to different grades of tumor budding (BD1, BD2, BD3).

amelioration of immune-mediated clearance of metastatic tumor cells (33, 35). The overexpression of these inhibitory immune checkpoints in BD3 tumors observed in our study could explain the immune-permissive microenvironment that facilitates tumor bud formation, invasion, and progression even in early passages of PDXs. Nevertheless, PD1 and CTLA4 genes were more expressed in low tumor budding grade in both patients and xenografts. The distinct expression of PD1 and CTLA4 in

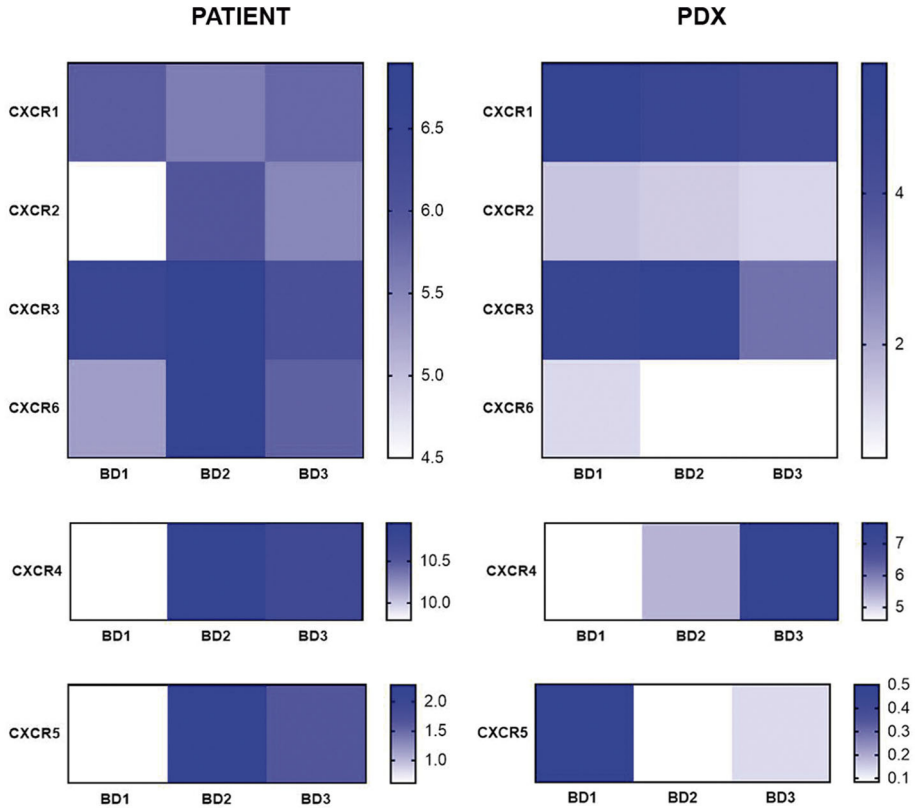


**FIGURE 6 |** Gene expression of CX chemokine receptors in patient tumors and their corresponding PDX models, according to different grades of tumor budding (BD1, BD2, BD3).

immune cells and PDL1 in tumor cells, respectively, would explain these apparent contradictory findings. Hence, the high expression of PDL1 in BD3 tumors would be associated with the immune evasion mechanisms deployed by cancer cells at the invasive front in these tumors, while the overexpression of PD1 and CTLA4 genes in BD1 tumors would reflect their comparative higher immunogenicity. In this regard, the overexpression of these immune checkpoints has been observed in tumors with high immunogenicity and with good clinical response to anti-PD1 and anti-CTLA4 therapy (36, 37). Moreover, high PD1 expression has been recently reported to be associated with a favorable outcome in CRC patients while high-level PDL1 expression, either alone or in combination with PD1, was associated with a worse recurrence-free survival (38). The prognostic value of PD1 expression in lymphocytes and tumor cells and its interaction with PDL1 expression for the prognosis impact in CRC remain to be more deeply investigated. In this context, it may be plausible that CRC patients with low-grade budding will most likely benefit from anti-PD1 and anti-CTLA4 therapies.

TLRs are a diverse family of receptors that regulate gut inflammation but also found to be aberrantly expressed and associated with poor survival and with invasive and metastatic phenotypes in tumors (39, 40). In our study, TLR family expression, specifically TLR1, TLR3, TLR4, and TLR6, was upregulated in BD3 tumors in comparison with low-grade budding tumors (both in patient and PDX tumors) suggesting the presence of TLR-mediated alterations in the tumor invasive front. Overexpression of these TLRs has been previously detected in CRC (39–44). Although the specific mechanisms of TLR-mediated immune escape are still unknown, the current evidences indicated that the high expression of TLRs in tumors can contribute to tumor-cell resistance to apoptosis, malignant transformation of epithelial cells, and tumor progression (40). Results from our study support that TLR upregulation is closely related to BD3 of CRC, which marks them as promising targets for tumor therapy. In addition, it has been previously reported that the activation of TLRs is also accompanied by the expression of PDL1 in tumor cells and other inhibitory molecules as we have observed in this study (41).

Many cancer types show altered chemokine secretion profiles, favoring the recruitment of pro-tumorigenic immune cells such as myeloid-derived suppressor cells (MDSCs), tumor-associated neutrophils (TAN), tumor-associated macrophages (TAM), and regulatory T cells. Particularly, CXCR2 and CXCR4 are chemokine receptors for T-cells implicated in cancer invasion and metastasis (45, 46). Interestingly, these chemokines were overexpressed in BD3 tumors in patients and xenografts in our study. These two chemokine receptors

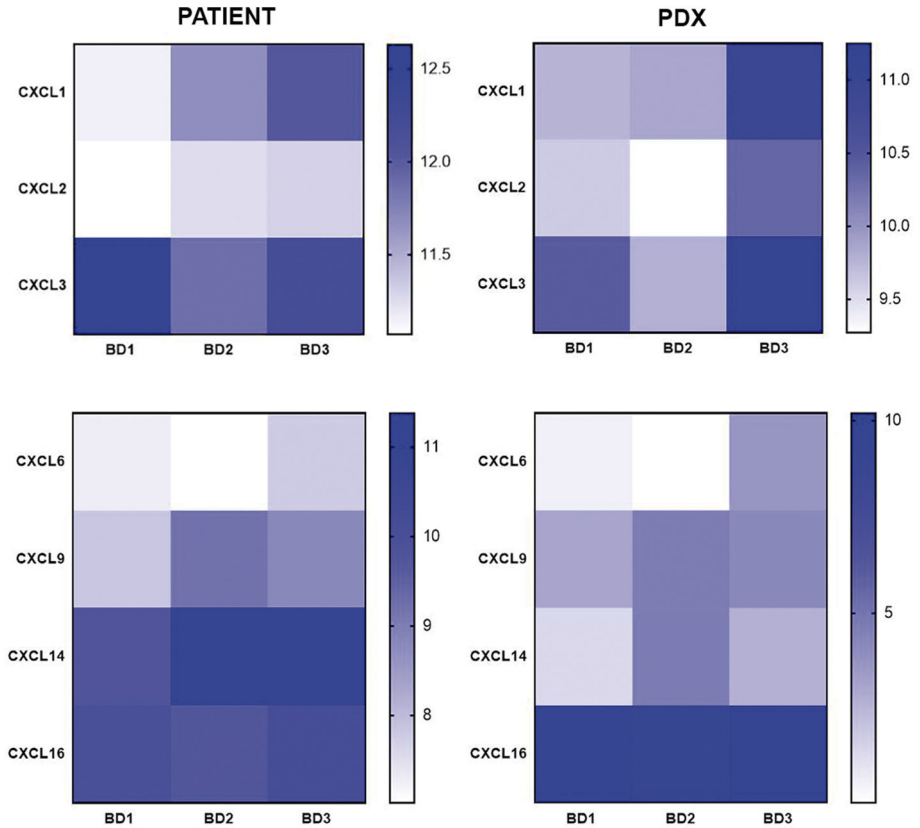


**FIGURE 7 |** Gene expression of CX chemokine ligands in patient tumors and their corresponding PDX models, according to different grades of tumor budding (BD1, BD2, BD3).

play a crucial role in establishing the "pre-metastatic niche" for tumor cells and are now emerging as key players in the regulation of antitumor immunity (41, 47–50). In addition to these chemokine receptors, chemokine ligands such as CXCL1, CXCL2, CXCL5, CXCL6, CXCL8, and CXCL9 have been also significantly correlated with poor survival and metastasis in several cancers by recruiting MDSCs and suppressing the antitumoral activity of CD8+ T effectors cells. In agreement with these reports, our study reinforces the notion that many different chemokines contribute to antitumoral T cell recruitment and likely some of them may be related to the establishment of a pro-metastatic niche for the tumor buds.

Taken together, our data support a close association between TLRs, chemokines, and tumor budding, raising the exciting hypothesis that the activation of these immune targets may have a determinant role in tumor budding, especially in the case of the CMS4 subtype.

In summary, our findings support that tumor budding in CRC is strongly associated with the mesenchymal poor-prognosis subtype and the presence of a combination of immunosuppressive mechanisms to evade antitumor immunity. Besides, our study suggests that PDXs constitute robust preclinical platforms for reproducing CMS subtypes and tumor budding, hence allowing the development of novel challenging therapies directed against tumor budding in CRC, with special focus in the most aggressive CMS4 subtype.

## DATA AVAILABILITY STATEMENT

The datasets have been uploaded to the repository, European Nucleotide Archive (ENA). The accession number is: PRJEB38274.

## ETHICS STATEMENT

The studies involving human participants were reviewed and approved by Reina Sofía Hospital ethical committee (Protocol number PI-0150-2017) in accordance with the Code of Ethics of the World Medical Association (Declaration of Helsinki). The patients/participants provided their written informed consent to participate in this study. The animal study was reviewed and approved by University of Córdoba Bioethics Committee and followed the regulations of the European Union normative (26/04/2016/066).

## AUTHOR CONTRIBUTIONS

SG-L and RM performed most of the experiments, analyzed the data, and wrote the manuscript. CN-S, AM, KK, and LL-S helped to perform the patient-derived xenograft experiments. KK and MT-H helped to perform the CRC molecular classification. IG analyzed the statistical data of the manuscript. CV, FM-F, CD, and JD contributed to the collection and clinical characterization of human samples. AR-A and EA conceived the project, designed the experiments, and revised the manuscript. All authors contributed to the article and approved the submitted version.

## FUNDING

This work was supported by funding from Instituto de Salud Carlos III through the project PI16/01508 (Plan Estatal de I+D+I, ISCIII-Subdirección General de Evaluación y Fomento de la Investigación, Spanish Government, and European fund for regional development) and Consejería de Salud de la Junta de Andalucía through the project PI-0150-2017. SG-L was funded with a researcher contract through the program Juan de la Cierva-Incorporación from the Spanish Ministry of Science, Innovation and Universities (IJCI-2016-29786). AM was funded through a predoctoral fellowship from the Asociación Española contra el cáncer (AECC). AR-A was funded with a researcher contract through the program Nicolás Monardes from Junta de Andalucía.

## ACKNOWLEDGMENTS

We would like to acknowledge the patients and the technical help of Alvaro Jiménez from the Genomics Units at the IMIBIC.

## SUPPLEMENTARY MATERIAL

The Supplementary Material for this article can be found online at: https://www.frontiersin.org/articles/10.3389/fmed.2020.00264/full#supplementary-material

## REFERENCES

1. Lugli A, Kirsch R, Ajioka Y, Bosman F, Cathomas G, Dawson H, et al. Recommendations for reporting tumor budding in colorectal cancer based on the international tumor budding consensus conference (ITBCC) 2016. *Mod Pathol.* (2017) 30:1299–311. doi: 10.1038/modpathol.2017.46
2. Dawson H, Galuppini F, Träger P, Berger MD, Studer P, Brügger L, et al. Validation of the international tumor budding consensus conference 2016 recommendations on tumor budding in stage i-IV colorectal cancer. *Hum Pathol.* (2019) 85:145–51. doi: 10.1016/j.humpath.2018.10.023
3. Mitrovic B, Schaeffer DF, Riddell RH, Kirsch R. Tumor budding in colorectal carcinoma: time to take notice. *Mod Pathol.* (2012) 25:1315–25. doi: 10.1038/modpathol.2012.94
4. Graham RP, Vierkant RA, Tillmans LS, Wang AH, Laird PW, Weisenberger DJ, et al. Tumor budding in colorectal carcinoma: confirmation of prognostic significance and histologic cutoff in a population-based cohort. *Am J Surg Pathol.* (2015) 39:1340–6. doi: 10.1097/PAS.0000000000000504
5. Grigore A, Jolly M, Jia D, Farach-Carson M, Levine H. Tumor budding: the name is eMT. *Partial EMT. J Clin Med.* (2016) 5:51. doi: 10.3390/jcm5050051
6. Li H, Xu F, Li S, Zhong A, Meng X, Lai M. The tumor microenvironment: an irreplaceable element of tumor budding and epithelial-mesenchymal transition-mediated cancer metastasis. *Cell Adhes Migr.* (2016) 10:434–446. doi: 10.1080/19336918.2015.1129481
7. De Smedt L, Palmans S, Andel D, Govaere O, Boeckx B, Smeets D, et al. Expression profiling of budding cells in colorectal cancer reveals an eMT-like phenotype and molecular subtype switching. *Br J Cancer.* (2017) 116:58–65. doi: 10.1038/bjc.2016.382
8. Galván JA, Zlobec I, Wartenberg M, Lugli A, Gloor B, Perren A, et al. Expression of e-cadherin repressors sNAIL, zEB1 and zEB2 by tumour and stromal cells influences tumour-budding phenotype and suggests heterogeneity of stromal cells in pancreatic cancer. *Br J Cancer.* (2015) 112:1944–50. doi: 10.1038/bjc.2015.177
9. Jensen DH, Dabelsteen E, Specht L, Fiehn AMK, Therkildsen MH, Jønson L, et al. Molecular profiling of tumour budding implicates tGFβ-mediated epithelial-mesenchymal transition as a therapeutic target in oral squamous cell carcinoma. *J Pathol.* (2015) 236:505–16. doi: 10.1002/path.4550
10. Trinh A, Lädrach C, Dawson HE, ten Hoorn S, Kuppen PJK, Reimers MS, et al. Tumour budding is associated with the mesenchymal colon cancer subtype and rAS/RAF mutations: a study of 1320 colorectal cancers with consensus molecular subgroup (CMS) data. *Br J Cancer.* (2018) 119:1244–51. doi: 10.1038/s41416-018-0230-7
11. Guinney J, Dienstmann R, Wang X, De Reyniès A, Schlicker A, Soneson C, et al. The consensus molecular subtypes of colorectal cancer. *Nat Med.* (2015) 21:1350–6. doi: 10.1038/nm.3967
12. Becht E, De Reyniès A, Giraldo NA, Pilati C, Buttard B, Lacroix L, et al. Immune and stromal classification of colorectal cancer is associated with molecular subtypes and relevant for precision immunotherapy. *Clin Cancer Res.* (2016) 22:4057–66. doi: 10.1158/1078-0432.CCR-15-2879
13. López-Sánchez LM, Jiménez-Izquierdo R, Peñarando J, Mena R, Guil-Luna S, Toledano M, et al. SWATH-based proteomics reveals processes associated with immune evasion and metastasis in poor prognosis colorectal tumours. *J Cell Mol Med.* (2019) 23:8219–32 doi: 10.1111/jcmm.14693
14. Bhimani J, Ball K, Stebbing J. Patient-derived xenograft models—the future of personalised cancer treatment. *Br J Cancer.* (2020) 122:601–2. doi: 10.1038/s41416-019-0678-0
15. Puig I, Chicote I, Tenbaum SP, Arqu es O, Ra ul Herance J, Gispert JD, et al. A personalized preclinical model to evaluate the metastatic potential of patient-Derived colon cancer initiating cells. *Clin Cancer Res.* (2013) 19:6787–801. doi: 10.1158/1078-0432.CCR-12-1740
16. Klintrup K, Mäkinen JM, Kauppila S, Väre PO, Melkko J, Tuominen H, et al. Inflammation and prognosis in colorectal cancer. *Eur J Cancer.* (2005) 41:2645–54. doi: 10.1016/j.ejca.2005.07.017
17. Gujam FJA, Edwards J, Mohammed ZMA, Going JJ, McMillan DC. The relationship between the tumour stroma percentage, clinicopathological characteristics and outcome in patients with operable ductal breast cancer. *Br J Cancer.* (2014) 111:157–65. doi: 10.1038/bjc.2014.279
18. Trinh A, Trumpi K, De Sousa E Melo F, Wang X, De Jong JH, Fessler E, et al. Practical and robust identification of molecular subtypes in colorectal cancer by immunohistochemistry. *Clin Cancer Res.* (2017) 23:387–98. doi: 10.1158/1078-0432.CCR-16-0680
19. Peñarando J, López-Sánchez LM, Mena R, Guil-Luna S, Conde F, Hernández V, et al. A role for endothelial nitric oxide synthase in intestinal stem cell proliferation and mesenchymal colorectal cancer. *BMC Biol.* (2018) 16:3. doi: 10.1186/s12915-017-0472-5
20. Giger OT, Comtesse SCM, Lugli A, Zlobec I, Kurrer MO. Intra-tumoral budding in preoperative biopsy specimens predicts lymph node and distant metastasis in patients with colorectal cancer. *Mod Pathol.* (2012) 25:1048–53. doi: 10.1038/modpathol.2012.56
21. Pu X, Zhang R, Wang L, Chen Y, Xu Y, Pataer A, et al. Patient-derived tumor immune microenvironments in patient-derived xenografts of lung cancer. *J Transl Med.* (2018) 16:1–2. doi: 10.1186/s12967-018-1704-3
22. Georges LMC, De Wever O, Galván JA, Dawson H, Lugli A, Demetter P, et al. Cell line derived xenograft mouse models are a suitable in vivo model

for studying tumor budding in colorectal cancer. *Front Med.* (2019) 6:139. doi: 10.3389/fmed.2019.00139
23. Gujam FJA, McMillan DC, Mohammed ZMA, Edwards J, Going JJ. The relationship between tumour budding, the tumour microenvironment and survival in patients with invasive ductal breast cancer. *Br J Cancer.* (2015) 113:1066–74. doi: 10.1038/bjc.2015.287
24. Van Wyk HC, Park JH, Edwards J, Horgan PG, McMillan DC, Going JJ. The relationship between tumour budding, the tumour microenvironment and survival in patients with primary operable colorectal cancer. *Br J Cancer.* (2016) 115:156–63. doi: 10.1038/bjc.2016.173
25. Masugi Y, Yamazaki K, Hibi T, Aiura K, Kitagawa Y, Sakamoto M. Solitary cell infiltration is a novel indicator of poor prognosis and epithelial-mesenchymal transition in pancreatic cancer. *Hum Pathol.* (2010) 41:1061–8. doi: 10.1016/j.humpath.2010.01.016
26. Prall F, Maletzki C, Hühns M, Krohn M, Linnebacher M. Colorectal carcinoma tumour budding and podia formation in the xenograft microenvironment. *PLoS ONE.* (2017) 12:1–2. doi: 10.1371/journal.pone.0186271
27. Martinez-Ciarpaglini C, Oltra S, Roselló S, Roda D, Mongort C, Carrasco F, et al. Low miR200c expression in tumor budding of invasive front predicts worse survival in patients with localized colon cancer and is related to pD-L1 overexpression. *Mod Pathol.* (2019) 32:306–13. doi: 10.1038/s41379-018-0124-5
28. Prall F, Hühns M. PD-L1 expression in tumour buds of colorectal carcinoma. *Histopathology.* (2016) 69:158–60. doi: 10.1111/his.12915
29. Korehisa S, Oki E, Iimori M, Nakaji Y, Shimokawa M, Saeki H, et al. Clinical significance of programmed cell death-ligand 1 expression and the immune microenvironment at the invasive front of colorectal cancers with high microsatellite instability. *Int J Cancer.* (2018) 142:822–32. doi: 10.1002/ijc.31107
30. Zhou E, Huang Q, Wang J, Fang C, Yang L, Zhu M, et al. Up-regulation of tim-3 is associated with poor prognosis of patients with colon cancer. *Int J Clin Exp Pathol.* (2015) 8:8018–27.
31. Nair VS, Toor SM, Taha RZ, Ahmed AA, Kurer MA, Murshed K, et al. Transcriptomic profiling of tumor-infiltrating cD4+ tIM-3+ t cells reveals their suppressive, exhausted, and metastatic characteristics in colorectal cancer patients. *Vaccines.* (2020) 8:71. doi: 10.3390/vaccines 8010071
32. Yu H, Borsotti C, Schickel JN, Zhu S, Strowig T, Eynon EE, et al. A novel humanized mouse model with significant improvement of class-switched, antigen-specific antibody production. *Blood.* (2017) 129:959–69. doi: 10.1182/blood-2016-04-709584
33. van der Weyden L, Speak AO, Swiatkowska A, Clare S, Schejtman A, Santilli G, et al. Pulmonary metastatic colonisation and granulomas in nOX2-deficient mice. *J Pathol.* (2018) 246:300–10. doi: 10.1002/path.5140
34. Zhang W, Zhang J, Zhang Z, Guo Y, Wu Y, Wang R, et al. Overexpression of indoleamine 2,3-Dioxygenase 1 promotes epithelial-Mesenchymal transition by activation of the iL-6/STAT3/PD-L1 pathway in bladder cancer. *Transl Oncol.* (2019) 12:485–92. doi: 10.1016/j.tranon.2018.11.012
35. Aydin E, Johansson J, Nazir FH, Hellstrand K, Martner A. Role of nOX2-derived reactive oxygen species in nK cell–mediated control of murine melanoma metastasis. *Cancer Immunol Res.* (2017) 5:804–11. doi: 10.1158/2326-6066.CIR-16-0382
36. Seidel JA, Otsuka A, Kabashima K. Anti-PD-1 and anti-CTLA-4 therapies in cancer: mechanisms of action, efficacy, and limitations. *Front Oncol.* (2018) 8:86. doi: 10.3389/fonc.2018.00086
37. Rotte A. Combination of cTLA-4 and pD-1 blockers for treatment of cancer. *J Exp Clin Cancer Res.* (2019) 38:1–12. doi: 10.1186/s13046-019-1259-z
38. Lee LH, Cavalcanti MS, Segal NH, Hechtman JF, Weiser MR, Smith JJ, et al. Patterns and prognostic relevance of pD-1 and pD-L1 expression in colorectal carcinoma. *Mod Pathol.* (2016) 29:1433–42. doi: 10.1038/modpathol.2016.139
39. Ridnour LA, Cheng RYS, Switzer CH, Heinecke JL, Ambs S, Glynn S, et al. Molecular pathways: toll-like receptors in the tumor microenvironment-poor prognosis or new therapeutic opportunity. *Clin Cancer Res.* (2013) 19:1340–6. doi: 10.1158/1078-0432.CCR-12-0408
40. Sato Y, Goto Y, Narita N, Hoon DSB. Cancer cells expressing toll-like receptors and the tumor microenvironment. *Cancer Microenviron.* (2009) 2:205–14. doi: 10.1007/s12307-009-0022-y
41. Wang K, Wang J, Wei F, Zhao N, Yang F, Ren X. Expression of tLR4 in non-small cell lung cancer is associated with pD-L1 and poor prognosis in patients receiving pulmonectomy. *Front Immunol.* (2017) 8:456. doi: 10.3389/fimmu.2017.00456
42. Lu C-C, Kuo H-C, Wang F-S, Jou M-H, Lee K-C, Chuang J-H. Upregulation of tLRs and iL-6 as a marker in human colorectal cancer. *Int J Mol Sci.* (2015) 16:159–77. doi: 10.3390/ijms16010159
43. Li Y, Chen S. Toll-like receptors expressed in tumor cells: targets for therapy. *Cancer Immunol Immunother.* (2008) 57:1271–8. doi: 10.1007/s00262-008-0459-8
44. Semlali A, Almutairi M, Pathan AAK, Azzi A, Parine NR, AlAmri A, et al. Toll-like receptor 6 expression, sequence variants, and their association with colorectal cancer risk. *J Cancer.* (2019) 10:2969–81. doi: 10.7150/jca.31011
45. Verbeke H, Struyf S, Laureys G, Van Damme J. The expression and role of cXC chemokines in colorectal cancer. *Cytokine Growth Factor Rev.* (2011) 22:345–58. doi: 10.1016/j.cytogfr.2011.09.002
46. Susek KH, Karvouni M, Alici E, Lundqvist A. The role of CXC chemokine receptors 1-4 on immune cells in the tumor microenvironment. *Front Immunol.* (2018) 9:2159. doi: 10.3389/fimmu.2018.02159
47. Kumar V, Donthireddy L, Marvel D, Condamine T, Wang F, Lavilla-Alonso S, et al. Cancer-Associated fibroblasts neutralize the anti-tumor effect of CSF1 receptor blockade by inducing PMN-MDSC infiltration of tumors. *Cancer Cell.* (2017) 32:654–68.e5. doi: 10.1016/j.ccell.2017.10.005
48. Yang J, Kumar A, Vilgelm AE, Chen SC, Ayers GD, Novitskiy S V., et al. Loss of cXCR4 in myeloid cells enhances antitumor immunity and reduces melanoma growth through nK cell and fASL mechanisms. *Cancer Immunol Res.* (2018) 6:1186–98. doi: 10.1158/2326-6066.CIR-18-0045
49. Yang L, Huang J, Ren X, Gorska AE, Chytil A, Aakre M, et al. Abrogation of tGFβ signaling in mammary carcinomas recruits gr-1+CD11b+ myeloid cells that promote metastasis. *Cancer Cell.* (2008) 13:23–35. doi: 10.1016/j.ccr.2007.12.004
50. Yu M, Lu B, Liu Y, Me Y, Wang L, Zhang P. Tim-3 is upregulated in human colorectal carcinoma and associated with tumor progression. *Mol Med Rep.* (2017) 15:689–95. doi: 10.3892/mmr.2016.6065

**Conflict of Interest:** The authors declare that the research was conducted in the absence of any commercial or financial relationships that could be construed as a potential conflict of interest.